AD-A066 062 AIR FORCE MATERIALS LAB WRIGHT-PATTERSON AFB OHIO F/G 11/6
EFFECTS OF ISOTHERMAL FORGING CONDITIONS ON THE PROPERTIES AND --ETC(U)
DEC 78 I A MARTORELL
UNCLASSIFIED AFML-TR-78-114 NL

1 OF 3
AD
A066062

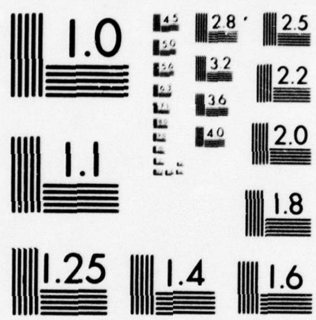
1.0
1.1
1.25
1.4
1.6
1.8
2.0
2.2
2.5
2.8
3.2
3.6
4.0

AFML-TR-78-114

LEVEL II

4

SC

AD A0 66062

DDC FILE COPY

EFFECTS OF ISOTHERMAL FORGING CONDITIONS ON THE PROPERTIES AND MICROSTRUCTURES OF Ti10V-2Fe-3Al

Processing and High Temperature Materials Branch
Metals and Ceramics Division

December 1978

TECHNICAL REPORT AFML-TR-78-114

Final Report for Period March 1975 to May 1978

79 03 19 028

AIR FORCE MATERIALS LABORATORY
AIR FORCE WRIGHT AERONAUTICAL LABORATORIES
AIR FORCE SYSTEMS COMMAND
WRIGHT-PATTERSON AIR FORCE BASE, OHIO 45433

NOTICE

When Government drawings, specifications, or other data are used for any purpose other than in connection with a definitely related Government procurement operation, the United States Government thereby incurs no responsibility nor any obligation whatsoever; and the fact that the government may have formulated, furnished, or in any way supplied the said drawings, specifications, or other data, is not to be regarded by implication or otherwise as in any manner licensing the holder or any other person or corporation, or conveying any rights or permission to manufacture, use, or sell any patented invention that may in any way be related thereto.

This report has been reviewed by the Information Office (OI) and is releasable to the National Technical Information Service (NTIS). At NTIS, it will be available to the general public, including foreign nations.

This technical report has been reviewed and is approved for publication.

Ivan Antonio Martorell

IVAN ANTONIO MARTORELL, Capt., USAF
Project Engineer

Attwell M. Adair

ATTWELL M. ADAIR
Group Leader

FOR THE COMMANDER

Henry C. Graham

HENRY M. GRAHAM
Acting Chief, Processing and High
Temperature Materials Branch
Metals and Ceramics Division
Air Force Materials Laboratory

"If your address has changed, if you wish to be removed from our mailing list, or if the addressee is no longer employed by your organization please notify AFML/LLM *,W-PAFB, OH 45433 to help us maintain a current mailing list".*

Copies of this report should not be returned unless return is required by security considerations, contractual obligations, or notice on a specific document.

UNCLASSIFIED
SECURITY CLASSIFICATION OF THIS PAGE (When Data Entered)

REPORT DOCUMENTATION PAGE		READ INSTRUCTIONS BEFORE COMPLETING FORM
1. REPORT NUMBER 14 AFML-TR-78-114	2. GOVT ACCESSION NO.	3. RECIPIENT'S CATALOG NUMBER 9
4. TITLE (and Subtitle) 6 Effects of Isothermal Forging Conditions on the Properties and Microstructures of Ti-10V-2Fe-3Al		5. TYPE OF REPORT & PERIOD COVERED Final Rep[redacted]t Marc[redacted]975 [redacted] May [redacted]978 6. PERFORMING ORG. REPORT NUMBER
7. AUTHOR(s) 10 Ivan Antonio Martorell, Capt, USAF		8. CONTRACT OR GRANT NUMBER(s)
9. PERFORMING ORGANIZATION NAME AND ADDRESS Air Force Materials Laboratory (AFML/LLM) Air Force Wright Aeronautical Laboratories Air Force Systems Command Wright-Patterson AFB, Ohio 45433		10. PROGRAM ELEMENT, PROJECT, TASK AREA & WORK UNIT NUMBERS 16 Project No. 2418 Task No. 2418 02 17
11. CONTROLLING OFFICE NAME AND ADDRESS Air Force Wright Aeronautical Laboratories Air Force Materials Laboratory Wright-Patterson AFB Ohio 45433		12. REPORT DATE 11 Dec[redacted]978 13. NUMBER OF PAGES 197 12 197p.
14. MONITORING AGENCY NAME & ADDRESS(if different from Controlling Office)		15. SECURITY CLASS. (of this report) UNCLASSIFIED 15a. DECLASSIFICATION/DOWNGRADING SCHEDULE

16. DISTRIBUTION STATEMENT (of this Report)

Approved for public release; distribution unlimited.

62102F

17. DISTRIBUTION STATEMENT (of the abstract entered in Block 20, if different from Report)

18. SUPPLEMENTARY NOTES

19. KEY WORDS (Continue on reverse side if necessary and identify by block number)

Titanium
Processing
Isothermal Forging
Properties

20. ABSTRACT (Continue on reverse side if necessary and identify by block number)

The effects of isothermal forging conditions on the properties and microstructures of Ti-10V-2Fe-3Al were investigated. Ring specimens with two different grain sizes were forged isothermally on a hydraulic press at two different speeds (0.03 and 3.0 ipm). The ring specimens with the smaller grains (8μm) were forged at three temperatures 1250°F(677°C), 1350°F(732°C) and 1450°F(788°C); the rings with the larger grains (255μm) were forged at eight temperatures in the range 1190°F(643°C) to 1750°F(954°C). After forging, the rings were quenched in water to (Continued on back of DD Form 1473).

microns

DD FORM 1 JAN 73 1473 EDITION OF 1 NOV 65 IS OBSOLETE

UNCLASSIFIED
SECURITY CLASSIFICATION OF THIS PAGE (When Data Entered)

012 320 79 03 19 028 TOB

20. ABSTRACT (Continued)

retain the as-forged structure. The resulting microstructures were determined using a light microscope and a Transmission Electron Microscope. The room temperature mechanical properties (tensile properties, fracture toughness, W/A, and hardness) resulting from forging at selected conditions were also determined.

The stress-strain curves were determined from the forging of the rings at the temperatures and speeds indicated, using the ring compression test. The stress-strain curves showed work softening at subtransus temperatures. This work softening is believed to result from a rearrangement of the microstructure. The stress-strain data is shown to obey an equation of the form

$$\dot{\varepsilon} = A\sigma^n \exp(-Q/RT)$$

The parameters A and n are strain and grain size dependent. The apparent activation energy, Q, is strain, stress and grain size dependent. These parameters are constant with temperature in two regions over and below the beta transformation temperature.

The flow stress and the resulting microstructures and mechanical properties depend on the forging conditions used, which can be characterized by the value of the flow stress. It is proposed that if the flow stress (forging conditions) is known, the room temperature mechanical properties (tensile, fracture toughness, W/A) may be closely estimated. Furthermore, a long-term relation is shown to exist between room temperature Rockwell C hardness and flow stress and room temperature properties, which could be used for a rough estimate of the properties of the as-forged material.

FOREWORD

This report was prepared by Captain Ivan Antonio Martorell of the Processing and High Temperature Materials Branch, Metals and Ceramics Division, Wright-Patterson Air Force Base, Ohio 45433, under Project 2418, "Metallic Structural Materials," Task Number 241802, "Metals and Alloys Technology."

This research was performed during the period March 1975 to May 1978 by the author, project engineer, Air Force Materials Laboratory.

In the course of this work many individuals made their contribution in the areas of discussion, encouragement, extrusion, forging, photography, electron microscopy, light microscopy, mechanical testing, reading of the manuscript, and typing. To each and everyone of the individuals that contributed, my sincere appreciation. I would like to recognize, in particular the following individuals:

Mr. Attwell Adair	Mr. Richard Klinger
Mr. Walter Griffith	Mr. Marion Myers
Mr. Ferdinand J. Gurney	Mr. Ralph Omlor
Ms. Faye Hichman	Mr. Robert Sweeney
Mr. Tom Jones	Mr. Vincent Vidoni

I would like to acknowledge the contributions of Dr. John Moteff and very specially the contributions of the late Mr. Vincent DePierre.

TABLE OF CONTENTS

TABLE OF CONTENTS (CONTINUED)

TABLE OF CONTENTS (CONTINUED)

LIST OF TABLES

LIST OF TABLES (CONTINUED)

LIST OF TABLES (CONTINUED)

LIST OF ILLUSTRATIONS

LIST OF ILLUSTRATIONS (CONTINUED)

LIST OF ILLUSTRATIONS (CONTINUED)

LIST OF ILLUSTRATIONS (CONTINUED)

LIST OF ILLUSTRATIONS (CONTINUED)

LIST OF ILLUSTRATIONS (CONTINUED)

LIST OF ILLUSTRATIONS (CONTINUED)

LIST OF ILLUSTRATIONS (CONTINUED)

SECTION I

INTRODUCTION

Increasing demand for improved system performance, specially in the aerospace industry, has increased the emphasis on more efficient system design with lower safety factors, on materials with improved mechanical properties and on advanced manufacturing techniques. The demand for improved performance coupled with higher cost for materials, manpower, equipment, and for higher cost of no longer so plentiful energy sources are responsible for increasing product cost.

Technological advances in every field (material, design, processing) are needed to produce cost effective, long-life systems. One area that offers a potential for reduced cost with no deterioration or with improved mechanical properties is material processing, in particular, isothermal forging.

The potential advantages of isothermal forging are numerous and could result in lower cost of parts with more uniform and improved mechanical properties (References 1, 2, 15, 16). The lack of popularity of the process is purely economical. The cost of dies needed for forging of the alpha + beta type titanium alloys traditionally used are prohibitive. The high forging temperatures imposed by the alpha + beta transus of these alloys, require more creep resistant die materials at competitive cost (Reference 1).

The lower transus temperature of the newly developed beta or near beta titanium alloys offer broader selection of lubricants and a broader selection of less expensive die materials, an increased die life, and a lower energy necessary to heat the billet. A significant advantage of isothermal forging is the possibility of producing net shape parts, eliminating the need for extensive post processing machining (Reference

1). All these factors contribute to the potential lower cost of isothermal forgings of beta/near beta titanium alloys. For these reasons primarily, isothermal forging of beta/near beta titanium alloys is of interest to the Air Force for production of parts for advanced weapon systems. The selection and utilization of an alloy for production of parts for a given application depends on the choice of the optimum processing parameters and/or heat treatment necessary to obtain the desired geometrical mechanical and metallurgical properties in the most economical manner. A sound selection requires a good understanding of the effects of isothermal forging on the properties and microstructure of all the alloys being considered. The work presented here provides guidelines of such effects for Ti-alloy 10V-2Fe-3Al.

1. TITANIUM: GENERAL INFORMATION (REFERENCES 3, 4, 5)

Titanium is a relatively light element, with a density of 0.163 lb/ in^3 (4.5gm/cm^3), an excellent corrosion resistance up to about 400°C and a relatively high strength to weight ratio (see Table 1 for properties of titanium). For these reasons, titanium and its alloys have an important industrial application.

Titanium is an allotopic element. It exists as hexagonal close pack (α) from room temperature up to 882°C. At this temperature it transforms to a body center cubic (β). Alloying elements affect this transformation temperature. Some elements like Al, Sn, C, O, and N raise the temperature at which the transformation occurs. These elements are called alpha stabilizers. Oxygen and nitrogen tend to increase hardness and reduce ductility making titanium brittle and more difficult to form. Other elements such as Fe, Mn, Cr, Mo, Cu, V, Nb, and Ta stabilize the transformation temperature at lower temperatures. These elements are called beta stabilizers.

Titanium is very seldom utilized in its more pure elemental form. Most commonly it is used as an alloy and very seldom of the binary type. Titanium alloys commonly have two or more alloying elements, nevertheless phase diagrams for other than binary alloys are not readily available. (See References 6-8 for phase diagram of titanium alloys).

Titanium alloys are divided into three major categories according to the predominant phase at room temperature, alpha alloys, alpha + beta alloys, and beta alloys.

The alpha stabilized alloys have a high $(\alpha + \beta)/\beta$ transformation temperature. Alloys of this type usually have good ductility at low temperatures, good high temperature creep strength, and relatively weak dependency of stress on temperature. They are considered weldable but not heat treatable and their mechanical properties are not too sensitive to changes in microstructure.

Alpha + beta alloys are heat treatable, their strength levels are medium to high, they possess good forming qualities, and lower creep strength than alpha alloys.

The beta alloys have the best response to heat treatment, have high strength, good formability, are generally weldable and have lower $(\alpha + \beta)/\beta$ transformation temperatures. Most beta alloys are considered to have higher hardenability than the alpha or alpha + beta alloys.

The structures that can be found in titanium alloys depend largely on the type alloy being considered and the thermal history, heat treat temperature, and cooling rate. Excellent treatments on titanium structures are available in the literature (References 4, 9, 10) and an exhaustive treatment will not be presented here. A summary of the structures is shown in Table 2.

2. TITANIUM ALLOY 10V-2Fe-3Al

Titanium alloy 10V-2Fe-3Al is a near beta alloy with a nominal composition of 10 w/o vanadium, 2 w/o iron, and 3 w/o aluminum. This alloy was developed by Titanium Metals Corporation of America as a highly hardenable, high fracture toughness alloy. Being a beta alloy it has a marked dependency of stress on temperature, it is, nevertheless, recommended for use up to about 310°C. At this temperature 10V-2Fe-3Al retains about 80% of its room temperature strength (Reference 11).

Ti-10V-2Fe-3Al is heat treatable. The resulting high strength that can be achieved during heat treatment is due to a fine dispersion of alpha particles in a beta matrix.

Evidence exists, strongly suggesting, that Ti-10V-2Fe-3Al exhibits stress induced transformations (Reference 14). This phenomenon has not been fully documented and characterized.

Little work has been published on the stress-strain rate-temperature relation for Ti-10V-2Fe-3Al. The only such relation known was reported by Rosenberg (Reference 13) on work by Chen (Reference 8):

$$\dot{\varepsilon} = 0.451\ \sigma^{2.72} \exp\left(\frac{-36600}{RT}\right) \qquad (1)$$

where the strain rate ($\dot{\varepsilon}$) is in sec.$^{-1}$, the flow stress (σ) is in MPa and T is the absolute temperature in degree Kelvin. Equation 1 is applicable in the temperature range 704°C to 982°C and in the strain rate range 1.67×10^{-3} sec.$^{-1}$ to 8.33×10^{-5} sec.$^{-1}$.

Rosenberg (Reference 13) also reported on the findings of Paton and Hamilton on the effects of strain rate on the inverse of the stress exponent n. Paton and Hamilton found that the value of m in

$$\sigma = \sigma_0 \dot{\varepsilon}^m \quad (2)$$

is not a constant for Ti-10V-2Fe-3Al. The inverse of the stress exponent has a maximum value of m = 0.37 at about $\dot{\varepsilon} = 10^{-4}$ sec.$^{-1}$ (n = 2.70). This value of m is in good agreement with Chen's value of n.

TABLE 1

PROPERTIES OF COMMERCIALLY PURE TITANIUM

Density	4.5 gm/cm^3
Atomic Number	22
Atomic Weight	48.90 gm/gm Mole
Melting Point	1668°C
Allotropic Change	α(HCP)below 882°C β(BCC)above 882°C
Modulus of Elasticity	16 x 10^6 psi
Room Temperature Ultimate Tensile Strength	40000 psi
Yield Strength (0.2 % Offset)	30000 psi
Elongation in 2 inch Gage Length (%)	25
Coefficient Thermal Expansion (0 - 100°C)	4.8 x 10^{-6} in/in/F

TABLE 2

STRUCTURES IN TITANIUM (REFERENCES 4, 9, 10)

STRUCTURE	CHARACTERISTICS	PRODUCED BY/PRODUCED IN
Serrated Alpha	Jagged boundaries, nonuniform grain size.	Rapid cooling from above beta transus, alpha alloy and pure titanium.
Primary Alpha	Equiaxed, untransformed alpha.	Holding at temperature in alpha + beta region, by slow cooling.
Alpha Prime	Nonequilibrium product, supersaturated, alpha produced by diffusionless decomposition from beta.	Rapid cooling, beta lean alloys.
Acicular Alpha	Fine needle-like alpha.	Cooling from beta field, nucleation and growth process, alpha or alpha-beta alloys.
Widmanstatten	Acicular or plate-like, fine or coarse, interchangeable with acicular, term acicular generally limited to fine structure.	Cooling from beta field, nucleation and growth process, alpha or alpha-beta alloys, cooling rate affects primarily the plate width.
Intergranular Beta	Beta precipitate in boundaries of alpha grains.	
Omega	Nonequilibrium phase, submicroscopic, brittle and hard.	Occurs upon aging beta alloys with relatively lean beta stabilizers.

TABLE 3

PROPERTIES AND CHARACTERISTICS OF Ti-10V-2Fe-3Al

Density (Reference 11)	0.168 lbs/in^3
Beta Transus	799 $\pm$ 6C (1470 $\pm$ 10F)
Modulus of Elasticity at Room Temperature	12 to 15 x 10^6 psi (as forged, depending on conditions)
Forgeability	The flow stress of Ti-6Al-4V is better than 2.5 times that of Ti-10V-2Fe-3Al up to a strain of approximately 0.65 in/in for a forging temperature of 1500°F and a forging speed of 0.030 ipm (Reference 12). The flow of Ti-10V-2Fe-3Al at 1089K is comparable to that of Ti-6Al-4V at 1200K (as reported by Rosenberg (Reference 13) on work by Chen (Reference 8).
Recommended Heat Treatment (STA) (Reference 11)	1400°F/1 Hr/WQ 950°F/8 Hrs/AC
Resulting Properties (Reference 11) (c)	155 - 180 ksi UTS 145 - 170 ksi YS 8 - 10% El 15 - 20% RA
Fatigue Strength (Reference 11)	Notched (K_T = 3.5) 30 ksi, unnotched 70 ksi for 10^7 cycles and YS = 150 ksi
Fracture Toughness (Reference 14)	78 ksi$\sqrt{in}$ with a yield strength of 132 ksi and ultimate strength of 142 ksi. Thermomechanical treatment: forged at 1500°F/AC plus aged at 1200°F/8 hrs/AC. 24 ksi $\sqrt{in}$ with a yield strength of 147 ksi and ultimate strength of 180 ksi. Thermomechanical treatment: forged at 1400°F plus heat treated at 1400°F/1 hr/WQ and aged at 900°F/8 hrs/AC.
Phases and Structures Reported for the Alloy	Alpha, beta, omega, alpha prime or titanium martensite, twinning.
Lattice Parameters (d)	Alpha Phase a = 2.93595 Å b = 2.93595 Å c = 4.67454 Å Beta Phase a = b = c = 3.23809 Å

(b) From present work unless otherwise indicated.

(c) Properties obtained, depend on section thickness.

(d) Determined by X-Ray diffraction.

SECTION II

LITERATURE REVIEW

1. FORGING

Thermomechanical processing is the shaping of a metal using mechanical deformation and temperature. In a broad sense, thermomechanical processing includes not only geometrical changes, but also the development of the required mechanical and metallurgical properties. Forging is only one of many deformation processes, other processes include: extrusion, swaging, rolling, and drawing.

Forging is the deformation of a metal to obtain a desired geometry by hammering or pressing. It can be used as a massive deformation process or as a final operation. Forging by hammering produces deformation primarily on the surface of the workpiece, whereas the pressing operation results in a deeper and more uniform deformation. Forging can be accomplished with the workpiece and dies at different temperatures or at the same temperatures. The former is conventional, the latter is termed isothermal.

Conventional forging of titanium alloys is usually carried out with the dies at about 425°C (Reference 15) regardless of workpiece temperature, which depends on the alloy. The forging speeds employed are usually very fast in order to limit workpiece chilling to a minimum, and in order to control the temperature between the narrow limits required to obtain the desired microstructure and properties. Since the flow stress of titanium is very sensitive to strain rate, high forging speeds result in high flow stresses. The complexity of the part and the degree of detail in the final forging also contributes to higher forging loads. The high loads and the chilling of the workpiece limit the deformation before reheating is necessary. It is not uncommon to use multiple forging steps

TABLE 3

PROPERTIES AND CHARACTERISTICS OF Ti-10V-2Fe-3Al

Density (Reference 11)	0.168 lbs/in^3
Beta Transus	799 $\pm$ 6C (1470 $\pm$ 10F)
Modulus of Elasticity at Room Temperature	12 to 15 x 10^6 psi (as forged, depending on conditions)
Forgeability	The flow stress of Ti-6Al-4V is better than 2.5 times that of Ti-10V-2Fe-3Al up to a strain of approximately 0.65 in/in for a forging temperature of 1500°F and a forging speed of 0.030 ipm (Reference 12). The flow of Ti-10V-2Fe-3Al at 1089K is comparable to that of Ti-6Al-4V at 1200K (as reported by Rosenberg (Reference 13) on work by Chen (Reference 8).
Recommended Heat Treatment (STA) (Reference 11)	1400°F/1 Hr/WQ 950°F/8 Hrs/AC
Resulting Properties (Reference 11) (c)	155 - 180 ksi UTS 145 - 170 ksi YS 8 - 10% El 15 - 20% RA
Fatigue Strength (Reference 11)	Notched (K_T = 3.5) 30 ksi, unnotched 70 ksi for 10^7 cycles and YS = 150 ksi
Fracture Toughness (Reference 14)	78 ksi$\sqrt{in}$ with a yield strength of 132 ksi and ultimate strength of 142 ksi. Thermomechanical treatment: forged at 1500°F/AC plus aged at 1200°F/8 hrs/AC. 24 ksi $\sqrt{in}$ with a yield strength of 147 ksi and ultimate strength of 180 ksi. Thermomechanical treatment: forged at 1400°F plus heat treated at 1400°F/1 hr/WQ and aged at 900°F/8 hrs/AC.
Phases and Structures Reported for the Alloy	Alpha, beta, omega, alpha prime or titanium martensite, twinning.
Lattice Parameters (d)	Alpha Phase a = 2.93595 Å b = 2.93595 Å c = 4.67454 Å Beta Phase a = b = c = 3.23809 Å

(b) From present work unless otherwise indicated.

(c) Properties obtained, depend on section thickness.

(d) Determined by X-Ray diffraction.

with reheating of the workpiece between steps. Since the cost of the dies is high, it is common practice to reduce the number of forging dies and produce parts with dimensions larger than the final desired part. Costly machining of the part is necessary: the material removed can be of the order of 80% of the volume of the forging (Reference 15).

Since the workpiece and the dies are at the same temperature, isothermal forging has certain advantages (References 2, 15, 16) over conventional forging. Chilling of the workpiece is eliminated, therefore slower speeds can be used, and consequently this results in lower loads. Better control of the speed and temperature results in more uniform properties. The lower loads needed for isothermal forging compared to conventional forging allow more complex and/or larger forging with the same equipment. Other advantages include reduction of the number of dies needed to produce a forging and closer tolerances which translate into less material used and little or no machining necessary.

2. EFFECT OF FORGING ON PROPERTIES

The effect of forging on the properties of titanium alloys has received considerable attention in the past (References 1, 2, 13-26, 30-31). The alloys studied cover a wide range including alpha, alpha-beta, and beta type alloys. The properties investigated include tensile strength, fracture toughness, time-stress rupture, and fatigue. A summary is shown in Table 3 relating the properties considered, the alloys, references, and other information considered pertinent.

The majority of the work on the effect of forging on properties deals with conventional forging. During conventional beta forging the workpiece is initially heated in the beta region, but since the process is not isothermal, as the deformation proceeds, the temperature of the workpiece changes. Even considering the heat developed due to the high strain rates used, some investigators believe that as much as 75% of the deformation may occur in alpha + beta region (Reference 31). Many of the investigations comparing the effects of alpha + beta and beta forging included post forging heat treatments. These heat treatments used may themselves emphasize or de-emphasize the effect of the forging operation.

a. Effects on Tensile Properties

Forging titanium alloys in the alpha + beta region results in improved tensile properties compared to forging in the beta region (References 14, 17, 18, 20, 21, 22, 26, 31). Only Chen and Gure (Reference 22) investigated the effects of isothermal forging on tensile properties of Ti-10V-2Fe-3Al. All others investigated conventional forging.

The work of Bohanek (Reference 14) is an exception of the effects of forging on tensile properties. Bohanek measured the tensile properties of Ti-10V-2Fe-3Al after forging at three different temperatures, one in the alpha + beta region (1400°F) and two in the beta region (1550°F, 1700°F). The forgings were air-cooled and given two aging treatments. After processing, tensile properties were determined for all six conditions. The yield strength (0.2% offset) and ultimate strength of the beta forged (1550°F, 1700°F) material was higher than that of the alpha + beta forged material for both aging treatments. The beta forging (1550°F) resulted in an improvement in ductility (%El) over alpha + beta (1400°F) forging. The material forged at 1700°F showed no significant change in ductility compared to the alpha + beta forged. The reduction in area showed a similar trend. Changing the post forging heat treatment to a water quenched, followed by various aging treatments, shows the same trends on yield and ultimate strength as for the air-cooled heat treatment. The ductility nevertheless did not change with forging temperature. The trend in reduction in area changed with forging temperature, depending on the aging treatment used.

Gurney and Male (Reference 32) also reported improved yield and ultimate strength for certain beta processed conditions over alpha + beta processed in their work on the effects of extrusion variables on the properties of titanium alloys.

b. Effects on Fracture Toughness

Forging titanium alloys in the beta region results in an improvement in fracture toughness over that resulting from forging in the alpha + beta region (References 14, 17, 18, 20, 21, 24-27, 30-31).

Besides investigating the effects of beta and alpha + beta forging on the fracture toughness of Ti-10V-2Fe-3Al, Bohanek (Reference 14) also considered two rates of cooling after forging, air-cooled and water quenched, followed by various aging treatments. The air-cooled plus aging treatments resulted in better fracture toughness than the water quenched plus aging. For all the forging and cooling conditions the fracture toughness increased as the yield strength decreased. These results are in agreement with other investigators (Reference 18). An exception is noted. An increase in aging temperature, over about 1100°F, results in a decrease in yield strength and no significant increase or decrease in fracture toughness. The best combination of yield strength and toughness reported by Bohanek (Reference 14) for Ti-10V-2Fe-3Al is 156 ksi and 68 ksi$\sqrt{in}$, respectively. These properties resulted from forging at 1700°F followed by AC plus 1000°F/8 hrs/AC. The values reported by Chen and Gure (Reference 22) were somewhat lower in toughness, 161 ksi and 54 ksi$\sqrt{in}$, for as forged 1550°F followed by air-cool. Two reasons can be cited for the differences: (1) different forging temperatures and (2) different heat treatment.

c. Effects on Other Properties

The effect of forging on other properties beside tensile and fracture toughness have not received as much attention in the past.

Information on the effects of forging on creep properties, (References 20, 21, 31), fatigue (References 19, 20, 21, 18, 26) and post creep tensile strength (Reference 21) is more limited. A review of the available literature shows that forging in the beta region results in better notch fatigue and no significant difference in smooth fatigue properties over material forged in the alpha + beta region.

Petrak (Reference 20) reported an improvement in fatigue life at room temperature (an improvement at 350°F) which he considered not significant, and no change at 600°F for beta over alpha + beta forged material.

In reference to creep properties, Petrak (Reference 20) reported no significant difference for beta over alpha + beta forged material. But Coyne (Reference 21) reported an improvement in creep properties for beta forging. According to Coyne (Reference 21) better post creep tensile properties are possible through alpha + beta forging than through beta forging.

Data exists on the effect of a particular forging condition and in aging treatment on the mechanical properties of titanium alloys, with no comparable results from other forging conditions. The purpose of most of these investigations was not to compare the resulting properties from various forging conditions, but to show that a particular process results in properties that meet certain working specifications or standards, to study the process feasibility or to determine if it was an economical process.

d. Microstructural Characteristics

The propagation of a crack in an equiaxed alpha + beta structure is controlled by void formation ahead of the crack tip (Reference 27). As the void forms, the crack tip radius increases and the crack is temporarily arrested. In this type of microstructure, the yield strength and fracture toughness increases with a decrease in mean free path between primary alpha particles. Based on these results Rogers (Reference 27) suggested that although the voids formed in very fine structures may be less effective arresting the crack, further improvement in yield strength and fracture toughness may be possible by refinement of the microstructure, such as might be achieved by powder metallurgy.

The crack path through the acicular alpha structures, resulting from beta working or heat treating shows frequent changes in direction (Reference 27). Rogers (Reference 27) found that crack arrest in the Widmanstatten structure, although less frequent, was more severe than in the equiaxed alpha + beta structures.

Increased fracture toughness with refinement of the structure for equiaxed alpha in aged beta agrees with results from Greenfield and Margolin (Reference 28). They found that fracture toughness of this structure increases with decreasing beta matrix grain size. For the structure with Widmanstatten plus grain boundary alpha in aged beta, the fracture toughness depends on beta grain boundary area per unit volume and on grain boundary alpha thickness.

According to Hall et al., (Reference 24) the microstructure resulting in the best combination of tensile strength and fracture toughness contains about 10% primary alpha with relatively coarse acicular alpha and aged beta. These results are in general agreement with results from Ashton and Chambers (Reference 33). They recommend that at least 20% primary alpha should be present in microstructures for two British alloys, (IMI 679, 2.25Al-11Sn-1Mo-5Zr-0.25Si, and Hylite 50, 2.06Sn-4.32Al-3.90Mo-0.46Si) (Reference 33), in order to obtain acceptable properties.

The work of Eylon et al., (Reference 30) is of particular interest. They found good correlation between properties and microstructure for forged and heat treated titanium alloy Ti-11. The properties were grouped according to four microstructural categories, I to IV.

Category I is characterized by large colonies of similarly aligned alpha needles, separated by continuous beta, resulting from alpha + beta or beta forged and beta heat treatment. Category II consists of equiaxed alpha grains with transformed beta at grain boundaries. This type structure results from alpha + beta forged plus alpha + beta heat treatment. Category III, acicular alpha separated by discontinuous beta films, results form beta forged and alpha + beta heat treatment + AC. The last type, IV is similar to III, acicular alpha separated by discontinuous beta films in a criss-cross arrangement, produced by beta forged and alpha + beta heat treatment + WQ. As expected and in agreement with results previously outlined (Section 2b), category III and IV results in the best fracture toughness. What is surprising is that category IV microstructure also results in the best yield strength and ultimate strength with acceptable ductility (slightly less than for category II). These results are in general agreement with Bohanek's (Reference 14) work on Ti-10V-2Fe-3Al. The alpha + beta forged plus alpha + beta heat treatments results in the best overall tensile properties and the lowest fracture toughness, as would generally be expected (Section 2a and 2b).

3. STRESS-STRAIN RATE-TEMPERATURE RELATIONS

Numerous equations have been proposed in the past for the strain rate of metals and alloys, in terms of appropriate variables such as temperature, stress, shear modulus, activation energy, and other parameters. Some of these equations have been empirical and some theoretical. The validity of these equations is limited by restrictions in the range of applicability of the variables. In many instances these equations show disagreement between the strain rate they predict (Figure 1) as well as disagreement with experimental results. These disagreements, as well as the limited applicability of the equations, reflect the complex interaction of the factors affecting the strain rate. The extreme theoretical complexity and/or experimental difficulties, make the consideration of all factors contributing to the strain rate impractical, if not impossible. An equation of universal applicability, one that applies for unlimited conditions of the variables, would be of extreme complexity in theoretical formulation, mathematical manipulation and applicability.

Most theoretical strain rate equations are based on motion of dislocation and on the calculations of dislocation velocities. Some are based on the balance between recovery and strain hardening. This type also depends on dislocation motion in one way or another. Few strain rate equations, both of theoretical and experimental origin, claim to apply to transient conditions. The great majority are limited to prediction of steady state strain rates. All the equations, almost without exception, consider the deformation phenomenon to be a diffusion controlled and thermally activated process.

a. Diffusion

A great deal of information exists indicating that steady state creep is diffusion controlled. Some of the most convincing evidence is (shown in Figure 2) the near equality between activation energy for self-diffusion and the activation energy for creep. According to this data, steady state creep is proportional to the self-diffusion coefficient, $D = D_o \exp(-Q/RT)$. Data available on creep and self-diffusion shows that the activation volumes of these two processes are approximately equal, pointing again to creep being diffusion controlled. Still further evidence that creep is a diffusion controlled process, at least at high temperature, comes from the observation that creep is more pronounced at temperatures higher than about $0.4T_m$, where diffusion is significant also.

b. Thermal Activation

Plastic deformation of crystalline solids is considered a thermally activated process, because thermal fluctuations assist the applied stress in overcoming the obstacles to the deformation. The concept of thermal activation was introduced in 1925 when Becker applied the Bolztmann's principle to the nucleation of the slip region (Reference 34). Later in 1938 Kauzmann (Reference 35) applied Eyring's rate reaction theory (identical to Becker's) to crystalline solids and developed a theory of thermally activated plastic deformation process.

This concept of thermal activation is intimately related to the atomic structure and its defects, both point defects (vacancies and interstitials) and line defects (dislocations). For example, an edge dislocation moves on its slip plane by rearranging the atomic structure at its core. Due to the periodicity of the atomic structure, as the dislocation moves it passes from one equilibrium position to another, through a position of maximum energy. This energy represents the basic resistance of the structure to dislocation motion. A minimum stress is required to move the dislocation past this energy barrier. This energy barrier is known as the Peierls-Nabarro energy and can be affected by thermal fluctuations. For this reason, the Peierls-Nabarro energy is considered a short-range or thermal obstacle. Other short-range obstacles exist such as other dislocations in their slip plane, climb of edge dislocation, and motion of jogs on screw dislocations.

Obstacles that cannot be affected by thermal fluctuations are known as long-range or athermal obstacles. Examples of athermal obstacles are precipitates and second phase particles, and other dislocation on parallel slip planes.

The stress field seen by a dislocation is the algebraic sum of all stress. Hence, the effective stress field is a superposition of all the short-term stresses (those resulting from the thermal obstacles) on the long-term stress field (athermal obstacles). The process that controls the rate of deformation will be the thermally activated process that will overcome the short-range obstacles at the top of the long-range field.

The general equation for thermally activated strain rate can be written as (Reference 36).

$$\dot{\varepsilon} = \dot{\varepsilon}_o \exp(-\Delta G/KT) \tag{3}$$

where $\dot{\varepsilon}_o$ is a pre-exponential term and depends on the particular model. The pre-exponential term, in general, includes the strain per successful deformation, frequency of vibration, number of units involved in the deformation, and a stress dependent term. ΔG is the free energy of activation, K is the Bolztmann's constant and T is the absolute temperature. The activation free energy, ΔG, in Equation 3 is equal to

$$\Delta G = \Delta H - T\Delta S \tag{4}$$

Equation 3 becomes

$$\dot{\varepsilon} = \dot{\varepsilon}_o \exp(-\Delta H/RT) \tag{5}$$

where ΔS is the activation entropy

ΔH is the activation enthalpy

T is the absolute temperature

The activation enthalpy can be calculated by taking the natural logarithm of both sides of Equation 5 and taking the derivative with respect to T:

$$\ln\dot{\varepsilon} = \ln \dot{\varepsilon}_o - \Delta H/RT \tag{6}$$

where $\dot{\varepsilon}_o = NAb\nu \exp(\Delta S/R)$ and $\ln\dot{\varepsilon}_o = \ln NAb\nu + \Delta S/R$

$$\frac{\partial \ln\dot{\varepsilon}}{\partial T} = \frac{\partial}{\partial T} (\ln NAb\nu + \Delta S/R) - \frac{1}{R}\frac{\partial}{\partial T} (\Delta H/T)$$

$$\frac{\partial \ln\dot{\varepsilon}}{\partial T} = \frac{\partial}{\partial T} (\ln NAb\nu) + \frac{1}{R} \frac{\partial \Delta S}{\partial T} - \frac{1}{R} \left(\frac{1}{T}\frac{\partial \Delta H}{\partial T} - \frac{\Delta H}{T^2}\right)$$

Assuming that lnNAbν does not depend on temperature and at constant structure

$$\frac{\partial \ln\dot{\varepsilon}}{\partial T} = \frac{1}{R}\frac{\partial \Delta S}{\partial T} - \frac{1}{RT}\frac{\partial \Delta H}{\partial T} + \frac{\Delta H}{RT^2}$$

$$\Delta H = RT^2\left[\frac{\partial \ln\dot{\varepsilon}}{\partial T} - \frac{1}{R}\frac{\partial \Delta S}{\partial T} + \frac{1}{RT}\frac{\partial \Delta H}{\partial T}\right] \qquad (7)$$

using Equation 4 and since the crystal will adopt the condition of lowest free energy (Reference 37), then at constant temperature and constant structure, *that is for NAbν = constant*

$$\Delta H = T\Delta S$$

Equation 7 becomes

$$\Delta H = RT^2\left[\frac{\partial \ln\dot{\varepsilon}}{\partial T} - \frac{1}{R}\frac{\partial \Delta S}{\partial T} + \frac{T}{RT}\frac{\partial \Delta S}{\partial T}\right]$$

$$Q_c = \Delta H = RT^2\,\frac{\partial \ln\dot{\varepsilon}}{\partial T}$$

The activation enthalpy is generally identified in the literature as the apparent activation energy, Q_c.

Since $\Delta H = \Delta U - \sigma\Delta V$, for a constant stress test

$$Q_c = \Delta H = RT^2\,\frac{\partial \ln\dot{\varepsilon}}{\partial T} = \Delta U - \sigma\Delta V \quad \text{(a)} \qquad (8)$$

where ΔV is the activation volume (the volume such that $\bar{\sigma}\Delta V$ is the total work done by the effective stress $\bar{\sigma}$). When $\bar{\sigma}\Delta V \ll \Delta U$ the apparent activation energy $Q_c \approx \Delta U$, the energy of self-diffusion.

(a) From the second law of thermodynamics $\Delta E = \Delta Q - \Delta W$ (Reference 38)

c. Experimental Strain Rate Equations

The secondary strain rate for a large number of metals and alloys has been successfully correlated at constant temperatures and low stress levels (Reference 39) by

$$\dot{\varepsilon}_s = A\sigma^n \tag{9}$$

and at high stress levels (Reference 39) by

$$\dot{\varepsilon}_s = A' \exp(\beta\sigma) \tag{10}$$

The values of A, n, A' and β are generally temperature dependent, but independent of stress.

Under conditions of constant structure and constant strain, the strain rate of some metals and alloys at low stresses is given by Equation 9 with $A = S \exp(-\Delta H/RT)$ and at high stresses by Equation 10 with $A' = S' \exp(-\Delta H/RT)$, where S and S' are structure parameters. The value of S, S', n, β and ΔH are independent of temperature for some temperature range around $0.5T_m$.

$$\dot{\varepsilon}_s = S \exp(-\Delta H/RT) \quad \sigma^n \tag{11}$$

$$\dot{\varepsilon}_s = S' \exp(-\Delta H/RT) \quad \exp(\beta\sigma) \tag{12}$$

The strain rate for single crystals and polycrystalline annealed metals and alloys, at both low and high stress, can be correlated by a single equation

$$\dot{\varepsilon}_s = A'' (\text{Sinh } \alpha\sigma)^n \tag{13}$$

Both A'' and α are constant at constant temperature. For $\alpha\sigma<0.8$ Equation 13 becomes Equation 9 and $A''\alpha^n = A'$. For $\alpha\sigma<1.2$ Equation 13 becomes Equation 10 and $A''/2^n = A'$ and $n\alpha = \beta$.

Table 2 shows a list of metals and alloys whose strain rate have been correlated using Equation 9 to 13. The conditions for the equations applicability are indicated.

d. Theoretical Strain Rate Equations

(1) Nabarro-Herring Creep (Reference 50)

Nabarro-Herring Creep involves the mass transport of atoms from one boundary to another. This type of creep is also known as diffusional creep (Reference 50), and is significant in very fine grained materials. The Nabarro-Herring strain rate equation is

$$\dot{\varepsilon}_{NH} = \frac{C_1 \Omega N_o D_v \sigma}{L^2 kT} \tag{14}$$

C_1 is a constant dependent on grain geometry.

Ω is the atomic volume = cb^3.

b is the Burger vector.

c. is a constant ≈ 0.7 for fcc, hcp, and bcc structures.

N_o is the equilibrium vacancy concentration.

D_v is the diffusion coefficient of vacancies.

σ is the applied tensile stress.

k is the Boltzmann's constant.

T is the absolute temperature.

L is the grain size.

In the derivation (Reference 50) of Equation 14 the large angle grain boundaries of the grain were assumed to be good sources and sinks of vacancies, and self-diffusion was assumed to be the controlled mechanism. The grain was loaded in compression in the horizontal and in tension in the vertical direction. This loading configuration results in higher equilibrium vacancy concentration at the horizontal boundaries. The vacancies flow from the horizontal to the vertical boundary is driven by a concentration gradient of $4\sigma\Omega N_o/kTL$. This gradient results in a vacancy flow of $4\sigma\Omega N_o D_v/kTL$.

The grain size at which Equation 14 will dominate over Equation 9 can be determined by solving for L in the inequality $\dot{\varepsilon}_{NH} > \dot{\varepsilon}_s$. When Equation 14 is applied to materials with subgrains, L becomes the subgrain size.

(2) Nabarro Creep (Reference 50)

Nabarro calculated the creep rate resulting when the spacing between the dislocations becomes of the same order of magnitude as the subgrain size. Nabarro's strain rate is given by

$$\varepsilon_n = \alpha\rho bV \qquad (15)$$

ρ is the dislocation density

b is the Burger vector

V is the dislocation velocity

α is a constant, approximately equal to 1/2

In the derivation of the Nabarro equation, it was assumed that creep strain results only by dislocation climb.

The dislocation density is equal (Reference 50) to

$$N(r) = N\left\{1 - \left[1-\exp(\sigma\Omega/kT)\right]\frac{\log(d/2r)}{\log(d/2b)}\right\} \qquad (17)$$

The dislocation velocity (Reference 50) is given by

$$V = b^2F \tag{18}$$

where F is the vacancy flux and b the Burger vector. From an analogy with the heat transfer through a cylinder of radius d/2, the vacancy flux (Reference 51) is

$$F = -AD_v dN/dr \tag{19}$$

where A is the surface area of the cylinder and is equal to $2\Pi rL$.

$$F = -2\Pi rLD_vN_o \left\{ - \left[\frac{1-\exp(\sigma\Omega/kT)}{\log(d/2b)}\right]\left[\frac{r(d/2)(-1)}{(d/2)(r)(r)}\right]\right\} \tag{20}$$

The velocity becomes

$$V = b^2F = [2\Pi b^2 D_v N_o/\log(d/2b)] \quad [\exp(\sigma\Omega/kT)-1] \tag{21}$$

and since $D_vN_o = D/\Omega = D/b^3$ the dislocation climb velocity is

$$V = [2\Pi D/b\log(d/2b)] \quad [\exp(\sigma\Omega/kT)-1] \tag{22}$$

Since $\log(d/2b) \sim 10$ and assuming that $\sigma\Omega << 1$, then the climb velocity becomes

$$V = \frac{2\Pi D}{10b}\left(\frac{\sigma\Omega}{kT}\right) \tag{23}$$

The creep strain rate is then given by Equation 15 with $\alpha \sim 1/2$

$$\dot{\varepsilon}_n = \frac{\Pi D\beta^2}{10b^2} \; (\sigma/\mu)^2 \quad (\sigma\Omega/kT) \tag{24}$$

(3) Weertman's Glide Produced Strain, Climb Controlled Strain Rate Equation (References 50, 52)

Weertman (References 50, 52) derived a strain rate equation based on the premise that the creep strain is produced by dislocation glide and the strain rate is controlled by dislocation climb. Weertman's model consisted of a density M of active dislocation sources per unit volume of material, which would produce dislocations to glide on their slip planes until they form dipoles with dislocations on adjacent slip planes produced by other sources. The dislocations would climb and annilhilate decreasing the back stress on the sources. More dislocations could now be produced to glide, climb, and annihilate.

The strain rate for Weertman's model is given by Equation 15 and the velocity is the average glide velocity

$$V = (L/d)\overline{V} \tag{25}$$

Where L is the mean diameter of the dislocation loop and d is the spacing between two parallel slip planes. The factor L/d results because the dislocation glides a distance L/2 before climbing a distance d/2.

The average climb velocity is

$$V = (d)/\left[\int_b^d \frac{dy}{V(\sigma^*)}\right] = \frac{d}{t} \tag{26}$$

$$\text{where } t = \int_b^d (1/V)dy \tag{26a}$$

is the climb time and V the climb velocity given by Equation 23, for

$$\sigma^* = \mu b/4y$$

$$t = \int_b^d \frac{dy}{\frac{2\Pi D}{10b}\left(\frac{\mu b}{4y}\ \frac{\Omega}{kT}\right)} \tag{26b}$$

$$t = \left[\frac{1}{\frac{2\Pi D}{10b} \frac{\mu b}{4} \frac{\Omega}{kT}} \right] \frac{y^2}{2} \Bigg|_b^d \qquad (26c)$$

$$t = \frac{(d^2 - b^2)}{\frac{\Pi D}{10b}(\mu b)\ (\Omega kT)} \qquad (26d)$$

but since b<<d

$$t \sim \frac{d^2}{\frac{\Pi D}{10b}\ (\mu b)\ (\Omega/kT)} \qquad (26e)$$

$$\overline{V} = \frac{d}{d^2}\ \frac{(\Pi D)}{10b}\ \ (\mu b)\ \ \frac{\Omega}{kT} \qquad (26f)$$

since (Reference 50)

$$d = \frac{\mu b}{\beta^* \sigma} \qquad (27)$$

$$\overline{V} = \frac{\beta^* \Pi D}{10b}\ \frac{\sigma\,\Omega}{kT} \qquad (28)$$

Since there can only be one active dislocation source in a volume $\Pi L^2 d$, then

$$1 = M\Pi d\ L^2 \qquad (29)$$

$$L^2 = \frac{1}{\Pi M d} \qquad (30)$$

The dislocation density, ρ is equal to the number of dipoles per source $(1/\gamma^*d)$ times the product of the density of dislocation sources (M) and the average length of dislocation loop $\frac{(2\Pi L)}{2}$

$$\rho = \frac{LM\ (2\Pi L)}{\gamma^* d} = \frac{L^2 M\Pi}{\gamma^* d} \tag{31}$$

Substituting Equation 29 into 30

$$\rho = \frac{M\Pi}{\Pi M d\gamma^* d} = \frac{1}{\gamma^* d^2} \tag{32}$$

Substituting Equations 25, 28, 30, and 32 into Equation 15

$$\dot{\varepsilon}_{gc} = \frac{\alpha\beta^* D}{(10)\gamma^* d^{3.5}}\left(\frac{\Pi}{M}\right)^{0.5}\left(\frac{\sigma\Omega}{kT}\right) \tag{33}$$

Substituting Equation 27 into 33 the strain rate becomes

$$\dot{\varepsilon}_{gc} = \frac{\alpha\beta^{*4.5} D}{\gamma^* b^{3.5}\log(d/b)}\left(\frac{\Pi}{M}\right)^{1/2}\left(\frac{\sigma}{\mu}\right)^{4.5}\left(\frac{\mu\Omega}{kT}\right) \tag{34}$$

Provided the dislocation source density is not a function of the stress and that it is a constant, then Equation 34 can be written as

$$\dot{\varepsilon}_{gc} = \alpha_{gc}\ D(\sigma/\mu)^{4.5}\left(\frac{\mu\Omega}{kT}\right) \tag{35}$$

$$\alpha_{gc} = \text{const.} = (\Pi/M)^{0.5}\ \alpha\beta^{*4.5}/\ \ [\gamma^* b^{3.5}\log(d/b)]$$

Nevertheless, if the source density is assumed to be a function of the dislocation density, ρ, and the spacing between dislocation, d, then

$$M = \rho / d \tag{36a}$$

from Equation 32

$$M = \frac{1}{\gamma^* d^2} \quad \frac{1}{d} = \frac{1}{\gamma^* d^3} \tag{36b}$$

from Equation 27

$$M = \frac{\beta^{*3}}{\gamma^*} \left(\frac{\sigma}{\mu b}\right)^3 \tag{36}$$

and the strain rate becomes

$$\dot{\varepsilon}_{gc} = \alpha'_{gc} \quad D \left(\frac{\sigma}{\mu}\right)^3 \left(\frac{\mu\Omega}{kT}\right) \tag{37}$$

$$\alpha'_{gc} = \frac{\alpha \Pi^{.5} \beta^{*3}}{\gamma^{*0.5} b^2 \log(d/b)}$$

(4) The Jogged Screw Dislocation Model (Reference 53)

This theory of creep is based on a diffusion controlled motion of jogs on screw dislocations. The strain rate equation developed by Barrett and Nix (Reference 53) is applicable to steady state conditions:

$$\dot{\varepsilon}_s = 2\Pi \rho_s D \gamma \left(\frac{b}{a_o}\right)^3 \text{Sinh} \frac{(\alpha b^2 \lambda)}{2kT} \tag{38}$$

ρ_s = mobile screw dislocation density

D = coefficient of self-diffusion

γ = number of atoms per unit cell

b = Burger vector

a_o = lattice parameter

λ = average spacing between jogs

In their derivation of Equation 38 Barrett and Nix considered the vacancy concentration about the jogged screw dislocation controlled by either vacancy bulk diffusion or dislocation core diffusion, and calculated the strain rate resulting from each. In addition they also considered a screw dislocation containing both vacancy producing and vacancy absorbing jogs. The cases of screw dislocations containing interstitial producing and/or absorbing jogs was dismissed, since the interstitial concentration in thermodynamic equilibrium is negligible compared to the concentration.

The derivation by Barrett and Nix proceeded essentially as follows: The chemical force (Reference 54) on a screw dislocation by a vacancy producing jog is

$$F_p = \frac{kT}{b} \ln(C'_p/C_o) \tag{39}$$

and by a vacancy absorbing jog is

$$F_a = \frac{kT}{b} \ln(C'_p/C'_a) \tag{40}$$

C'_p/C'_a are the steady state vacancy concentration about a vacancy producing and vacancy absorbing jog, respectively

C_o is the equilibrium vacancy concentration

b,k and T have the usual meaning

The steady state vacancy concentrations near a jog can be calculated by making an analogy to heat transfer (References 51, 53). For bulk diffusion controlled vacancy concentration, the analogy is made with the moving point source heat flow. The vacancy concentrations C'p and C'a are

$$C'_a = C_o + v_p/(4\Pi D_v b^2) \tag{41}$$

$$C'_a = C_o - v_a/(4\Pi D_v b^2) \tag{42}$$

D_v is the lattice diffusion coefficient

v_p, v_a are the steady state velocities of the vacancy producing jogs, and of the vacancy absorbing respectively.

The steady state velocities, v_p and v_a, can be calculated since under steady state the net force on the dislocation is zero

$$F_p = \alpha\sigma b\lambda \qquad (43)$$

α is a constant $\approx 1/2$ since $\tau = \sigma/2$

from Equations 41 and 43

$$v_p = \Delta\Pi D_v b^2 C b_o \quad [\exp(\alpha\sigma b^2\lambda/kT) \; -1] \qquad (44)$$

likewise

$$v_a = \Delta\Pi D_v b^2 C_o \quad [1-\exp(-\alpha\sigma b^2\lambda/kT)] \qquad (45)$$

It would be an over-simplification to assume that a screw dislocation contains jogs of only one type. Then the average velocity should be produced by a combination of both vacancy absorbing and vacancy producing jogs.

$$v = B_a v_a + B_p v_p \qquad (46)$$

B_a and B_p are constants and represents the fraction of vacancy absorbing and vacancy producing jogs in the screw dislocation, respectively.

The strain rate equation when bulk diffusion controls the vacancy concentration is obtained by substituting Equations 44, 45, 46 and the product.

$$D_v C_o = D\gamma/a_o^3 \tag{47}$$

into Equation 15 and assuming that vacancy producing and vacancy absorbing jogs are equally possible $B_o = B_a = 0.5$

$$\dot{\varepsilon}_s = \Delta\Pi\alpha\gamma\left(\frac{b}{a_o}\right)^3 \rho_s D \,\mathrm{Sinh}\left(\frac{\alpha\sigma b^2\lambda}{kT}\right) \tag{48}$$

When the vacancy movement is controlled by dislocation core diffusion, the steady state vacancy concentrations, C'_p and C'_a are obtained from the heat transfer analogy to the moving line heat source flow (Reference 53).

$$C'_p = \left| \; C_o + \frac{v_p}{2\Pi D_v b\lambda} \exp\left(\frac{-v_p b}{2D_v}\right) k_o \left(\frac{v_p b}{2D_v}\right) \right. \tag{49}$$

$$C'_a = \left| \; C_o - \frac{v_a}{2\Pi D_v b\lambda} \exp\left(\frac{-v_a b}{2D_v}\right) k_o \left(\frac{v_a b}{2D_v}\right) \right. \tag{50}$$

The modified Bessel function of the second kind and order zero in Equations 49 and 50 can be approximated by

$$k_o(vb/2D_v) \approx \ln(4D_v/\gamma vb) \tag{51}$$

Since usually $vb/2D_v \ll 1$ then $\exp(vb/2D_v) \sim 1$.

Assuming that the vacancy producing and vacancy absorbing jogs are equally possible ($B_a = B_p = 0.5$) and that $\ln(4D_v/\gamma v_p b) \approx \ln(4D_v/\gamma v_p b) \approx$ constant $= W$, the strain rate equation for dislocation core diffusion becomes

$$\dot{\varepsilon}_s \sim \frac{2\Pi\alpha}{b}\left|\left(\frac{b}{a_o}\right)^3 \left(\frac{D\lambda\rho_s}{W}\right)\left[\mathrm{Sinh}\left(\frac{\alpha\sigma b^2\lambda}{kT}\right)\right]\right. \tag{52}$$

The strain rate equation for the jogged screw dislocation model can be generalized as follows

$$\dot{\varepsilon}_s = \Psi\sigma^n \ \mathrm{Sinh}(C\sigma) \qquad (53)$$

where

$\Psi = 4\Pi\alpha\gamma(b/a_o)^3 \ ABD_b$ for bulk diffusion controlled vacancy movement

$\Psi = \dfrac{2\Pi\alpha\gamma(b/a_o)^3 ABD_c}{b\ W}$ for dislocation core diffusion controlled vacancy movement

$C = \dfrac{\alpha b^2\lambda}{kT}$

D_b and D_c are the lattice and dislocation core diffusion coefficients, respectively

A and B are constants (Reference 53) in the equation below

$\rho_s = A\rho = A(B\sigma^n)$

(5) Subgrain Creep: Ivanov and Yanushkevich's Equation (Reference 52)

The model used by Ivanov and Yanushkevich consisted of dislocations of different signs meeting at the subgrain boundary where they would climb and annihilate. In their equation, the strain rate is controlled by dislocation climb velocity.

The average time required for a dislocation to be annihilated at the boundary is given by

$$t = d/V \qquad (54)$$

where d is the dislocation separation at the sub-boundary Equation 25 and V the climb velocity Equation 23.

The strain rate is given by

$$\dot{\varepsilon}_{iy} = \frac{\alpha ABCb}{t} \tag{55}$$

α is the orientation factor between τ and σ.

A is the area swept by a dislocation loop = L^2

B is the number of dislocations annihilated per length L of boundary = L/d,' d' = $\mu b/\gamma'\sigma$ the separation of the annihilating dislocations within the boundary

C is the subgrain density = $1/L^3$

t is the time required to annihilate a dislocation of length L in a subgrain boundary = d/V, with d = $\mu b/\gamma\sigma$

$$\dot{\varepsilon}_{iy} = \frac{\alpha bV}{d'd} \tag{56}$$

Using the average velocity from Equation 28, the strain rate becomes

$$\dot{\varepsilon}_{iy} = \frac{\alpha B^{*}\gamma}{10} \frac{\gamma'\pi D}{b^2} \left(\frac{\sigma}{\mu}\right)^3 \left(\frac{\mu\Omega}{kT}\right) \tag{57}$$

The Ivanov Yanushkevich strain rate equation is essentially equal to Weertman's glide-climb equation (Equation 37) when the dislocation source density (M) is a function of the stress.

(6) Sub-Grain-Pile Up Creep Strain Rate Equation (Reference 52)

Weertman's glide-climb equations and Ivanov-Yanushkevich's equation do not account for the possibility of a dislocation pile-up at the sub-grain boundary. If the pile-up is introduced into these equations it is equivalent to replacing σ by $N\sigma$, the stress due to a pile-up of N dislocations. The factor N is given by (Reference 54).

$$N = \frac{\gamma'' L\sigma}{\mu b} \tag{58}$$

where L is the sub-grain size and is (Reference 52)

$$L = L\sigma\mu/\sigma \tag{59}$$

$$N = \frac{\gamma'' L_p}{b}$$

Then the Ivanov-Yanushkevich strain rate equation with dislocation pile-up at the sub-grain boundary becomes

$$\dot{\varepsilon}_{iy,p} = \frac{B^*D}{b^2}\left(\frac{\gamma L_o}{b}\right)^3\left(\frac{\sigma}{\mu}\right)^3\left(\frac{\mu\Omega}{kT}\right) \tag{60}$$

and Weertman's glide and climb equations become

M = constant

$$\dot{\varepsilon}_{gc,p} = \alpha_{gc}\left(\frac{\gamma'' L_o}{b}\right)^{4.5} D\left(\frac{\sigma}{\mu}\right)^{4.5}\left(\frac{\mu\Omega}{kT}\right) \tag{61}$$

M = f (σ)

$$\dot{\varepsilon}_{gc,p} = \alpha'_{gc}\left(\frac{\gamma'' L_o}{b}\right)^{3} D\left(\frac{\sigma}{\mu}\right)^{3}\left(\frac{\mu\Omega}{kT}\right) \tag{62}$$

This presentation of the strain rate equations, both of empirical and theoretical origins was not intended to be an exhaustive treatment. Such a treatment is beyond the scope of this work. It was intended as a quick review to point out some of the equations available in the literature.

Examination of these equations will show that regardless whether the equation was derived under rigorous theoretical considerations or if it was obtained based only on experimental results, most strain rate equations have the general form:

$$\dot{\varepsilon} = A\sigma^n \exp(-Q/RT) \tag{63}$$

where the pre-exponential includes a diffusion term, Burger's vector, lattice vibration, and elastic modulus term.

TABLE 4

SUMMARY OF DATA ON EFFECTS OF PROCESSING MODE ON PROPERTIES FOR VARIOUS TITANIUM ALLOYS.

Ti-Alloy	Reference	Processing	Properties Investigated	Comments
6Al-4V	17	Conv. Forging α+β vs β	Tensile Fracture Toughness Notch Tensile Strength	Post Forging Heat Treatment (PFHT), α+β/WQ + α+β/AC; Valid K_{IC}
	18	Conv. Forging α+β vs β	Tensile Fracture Toughness Notch Fatigue	Hammer Forging, Three PFHT, two α+β/WQ + α+β/AC, one α+β/FC + α+β/AC; Valid K_{IC}; Processability also considered.
	19	Conv. Forging α+β vs β	Tension-Compression Fatigue, Notch and Un-notched Pulsating Tension Fatigue	Two PFHT, α+β/AC and α+β/WQ + α+β/AC.
	20	Conv. Forging α+β vs β	Tensile, RT and 600 F Fracture Toughness Fatigue, 350 F and 600 F Time-Stress Rupture, 600 F	Valid K_{IC}.
	21	Conv. Forging α+β vs β	Tensile Fracture Toughness Time-Stress Rupture Post Creep Tensile Fatigue	Valid K_{IC}; two PFHT, α+β/AC
	26	Conv. Forging α+β vs β	Tensile Fracture Toughness Charpy V Notch Impact	Savings Results From Beta Forging
6Al-5Zr-4Mo-1Cu-0.5Si, 6Al-5Zr-0.5Mo-0.25Si, 4Al-4Mo-2Sn-0.5Si, 6Al-4V, 4Al-4Mo-4Sn-0.5Si, 15Mo	27	Heat Treatment α+β vs β	Fracture Toughness	Microstructural Characterization
5.2Al-5.5V-0.9Fe-0.5Cu	28	Heat Treatment	Fracture Toughness	Microstructural Characterization K_Q Charpy V notch 3 point slow bend

TABLE 4 (CONTINUED)

SUMMARY OF DATA ON EFFECTS OF PROCESSING MODE ON PROPERTIES FOR VARIOUS TITANIUM ALLOYS.

Ti-Alloy	Reference	Processing	Properties Investigated	Comments
6Al-5Zr-1Cu-0.2Si, 6Al-5Zr-1W-0.3Si, 4Al-4MN, 11Sn-2.25Al-4Mo-0.2Si, 11Sn-2.25Al-5Zr-1Mo-0.2Si	18	Conv. Forging $\alpha+\beta$ vs β	Tensile Fracture Toughness Fatigue	Hammer Forging; Three PFHT, Two $\alpha+\beta$/WQ + $\alpha+\beta$/AC, One $\alpha+\beta$/FC + $\alpha+\beta$/AC; Valid K_{IC}
6Al-2Mo-4Zr-2Sn, 6Al-6V-2Sn-3.5Zr, 11Sn-2.25Al-5Zr-1Mo-0.2Si, 4Al-3Mo-1V, 13V-11Cr-3Al	17	Conv. Forging $\alpha+\beta$ vs β	Tensile Fracture Toughness Notch Tensile Strength	PFHT $\alpha+\beta$/WQ + $\alpha+\beta$/AC; Valid K_{IC}
	25	Aging Response Heat Treatment	Tensile	Hardenability Investigated.
6Al-2Sn-4Zr-6Mo	24	Forging and Heat Treatment	Tensile Fracture Toughness	Microstructural Characaterization; Valid K_{IC}.
6Al-2Sn-4Zr-2Mo, 6Al-2Sn-1.5Zr-1Mo-0.35Bi-0.15Si	21	Conv. Forging $\alpha+\beta$ vs β	Tensile Fracture Toughness Time-Stress Rupture	Valid K_{IC}; Two PFHT $\alpha+\beta$/AC.
8Al-1Mo-1V	17	Conv. Forging $\alpha+\beta$ vs β	Tensile Fracture Toughness Notch Tensile Strength	PFHT $\alpha+\beta$/WQ + $\alpha+\beta$/AC; Valid K_{IC}
	29	Heat Treatment	Tensile Hardness Fracture Toughness (W/A)	
6Al-6V-2Sn	21	Conv. Forging $\alpha+\beta$ vs β	Tensile Fracture Toughness Time-Stress Rupture	Valid K_{IC}; Two PFHT $\alpha+\beta$/AC.
	17	Conv. Forging $\alpha+\beta$ vs β	Tensile Fracture Toughness Notch Tensile Strength	Valid K_{IC}; PFHT $\alpha+\beta$/WQ + $\alpha+\beta$/AC.
10V-2Fe-3Al	14	Conv. Forging $\alpha+\beta$ vs β	Tensile, RT, 600 F Fracture Toughness	Hardenability Investigated; Heat Treatment of As-Forged AC + Aging, Tensile Properties Heat Treatment Response; Valid K_{IC}.

TABLE 4 (CONTINUED)

SUMMARY OF DATA ON EFFECTS OF PROCESSING MODE ON PROPERTIES FOR VARIOUS TITANIUM ALLOYS.

Ti-Alloy	Reference	Processing	Properties Investigated	Comments
	22	Isothermal Forging $\alpha+\beta$ vs β	Tensile, RT, 400 F, 600 F Time-Stress Rupture, 600 F Post Creep Tensile Fracture Toughness	Valid K_{IC}, Some K_Q; Tensile Data Only For $\alpha+\beta$ Forging.
7Al-4Mo	17	Conv. Forging $\alpha+\beta$ vs β	Tensile Fracture Toughness Notch Tensile Strength	PFHT $\alpha+\beta$/WQ + $\alpha+\beta$/AC; Valid K_{IC}.
7Al-4Mo , 8Al-1Mo-1V	21	Conv. Forging $\alpha+\beta$ vs β	Tensile Fracture Toughness Time-Stress Rupture	Valid K_{IC}; Two PFHT $\alpha+\beta$/AC.
10V-2Fe-3Al	23	Isothermal and Conv. Forging	Hot Tensile Property	Processability As-Received Condition.
	25	Heat Treatment	Tensile Fracture Toughness Hardenability	Machinability.
10V-8Cr-3Al	25	Aging Response and Heat Treatment	Tensile	
8Mo-8V-2Fe-3Al	25	Heat Treatment	Tensile	Hardenability, Limited Forging Data

TABLE 5

METALS AND ALLOYS THAT OBEY THE STRAIN RATE EQUATION 9 TO 13.

MATERIAL	EQUATION(b)	TEMPERATURE RANGE (K)	STRESS RANGE (KSI)	STRAIN RATE RANGE ($SECS^{-1}$)	STRESS MULTIPLIER	ACTIVATION ENERGY (KCAL/MOL)	STRESS EXPONENT	COMMENTS	REF
Al(99.99)	2.9	295 to 873	1 to 19	0.4 to 311				Constant $\dot{\varepsilon}$ Compression	40
Al-4.2%Cu	2.9	573 to 773	6 to 24	0.4 to 311				Constant $\dot{\varepsilon}$ Compression	40
Al-5.7%Zn	2.9	673 to 823	4 to 23	0.4 to 311				Constant $\dot{\varepsilon}$ Compression	40
Pb(99.98)	2.9	295 to 573	0.4 to 7	0.4 to 311				Constant $\dot{\varepsilon}$ Compression	40
Al (c)	2.9	463 to 823	2 to 28	1 to 40				Plastometer	41
Cu (d)	2.9	291 to 1173	5 to 58	1 to 40				Plastometer	41
Fe-0.17%C	2.9	1203 to 1473	10 to 30	1 to 40				Plastometer	41
Al (c)	2.9	593 to 889	----	0.1 to 10				Extrusion	42
Ti-10V-2Fe-3Al	2.9	977 to 1255	1.5 to 21.0	1.67×10^{-3} to 8.33×10^{-5}		36.6	2.72	Tension	13
Al (c)	2.10	223 to 673	4 to 24	0.11 to 227				Cam plastometer	43
Mg(99.99)	2.11	747 to 802	0.3 to 0.5			52	4.0	Compression creep at const. stress	44
Mg(99.99)	2.11	459 to 557	2 to 4			28	5.5	Compression creep at const. stress	44
Al-2.1%Mg	2.11	873 and 923	0.5 to 4.5			36	3.54	Const. stress creep test	45
Ag-33%Al	2.11	440 to 700	0.2 to 20			33	3.6	Creep test	46
Ag-33%Al-1%Zn	2.11	440 to 700	0.2 to 20			33	4.0	Creep test	46
Fe-22%Al	2.11	851	20 to 38			73	5.5	Creep test	47
Fe-23.5%Al	2.11	853	22 to 36			78	5.9	Creep test	47

TABLE 5 (CONTINUED)

METALS AND ALLOYS THAT OBEY THE STRAIN RATE EQUATION 9 TO 13.

MATERIAL	EQUATION(b)	TEMPERATURE RANGE (K)	STRESS RANGE (KSI)	STRAIN RATE RANGE ($SECS^{-1}$)	STRESS MULTIPLIER	ACTIVATION ENERGY (KCAL/MOL)	STRESS EXPONENT	COMMENTS	REF
Fe-24.8%Al	2.11	912 to 962	8 to 16			86	6.0	Creep test	47
α Thallium	2.11	335 to 488	0.025 to [illegible].6			22.7	5.2	Creep test	48
β Thallium	2.11	507 to 553	0.025 to 0.08			20	5.2	Creep test	40
Al-2.1%Mg	2.12	478, 531, 600	3 to 14		1/1860	36		Creep test	45(e)
Al (c)	2.13	593 to 889		0.1 to 10	$3x10^{-3}$	37.4	4	Extrusion	42(f)
Aust. SS	2.13	977		$3x10^{-6}$ to $2x10^{-1}$	$7.8x10^{-5}$		3.64	Extrusion	49
Al-3.1%Mg	2.13	531			$2.08x10^{-4}$		2.26	Extrusion	49
Al	2.13	920			$1.25x10^{-1}$		1.24	Extrusion	49

(b) When Eq. 2.9 is applicable factors A & n are temperature dependent and constant at constant temperature and strain. When Eq. 2.10 is applicable A' and B are temperature dependent and constant at constant temperature and strain.
(c) Commercially pure.
(d) Phosphorus deoxidized.
(e) B is temperature independent.
(f) With $A''=A_1 \exp(-\Delta h/RT)$ and the values of α and n independent of temperature.

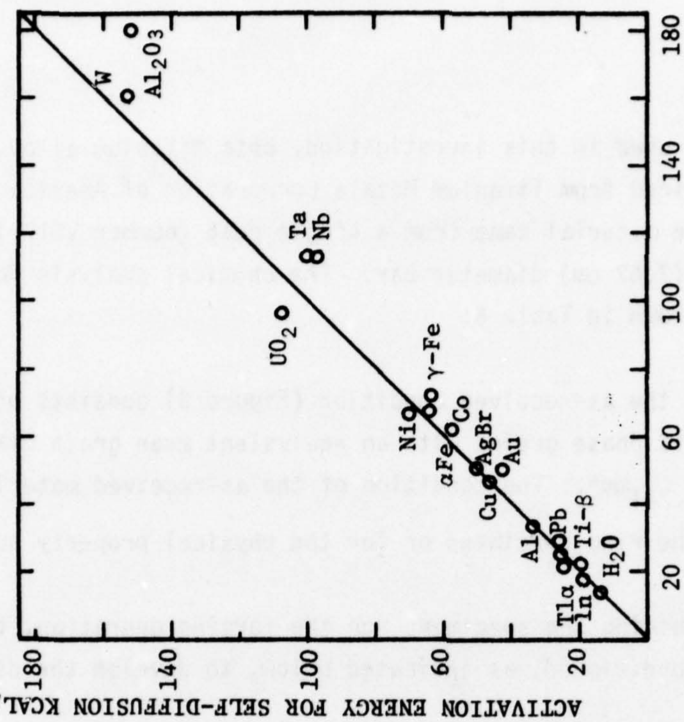

Figure 2. Creep Activation Energy Versus Self-Diffusion Activation Energy for Various Materials (After Weertman, 50)

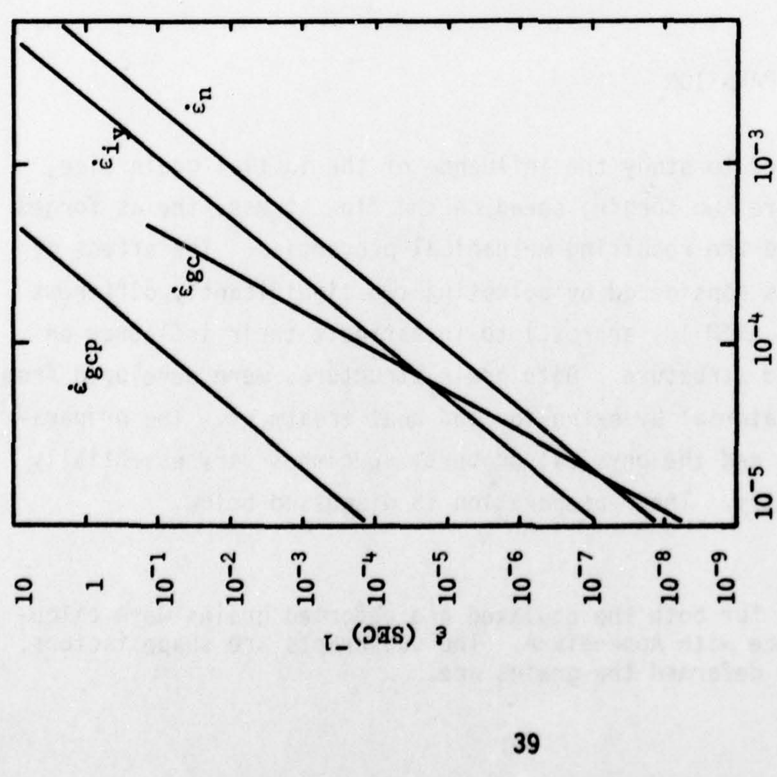

Figure 1. Log-log Plot Comparing Creep Rate Vs. Normalized Stress for Various Strain Rate Equations. (After Weertman, 52)

SECTION III

EXPERIMENTAL PROCEDURE

1. MATERIAL

The material used in this investigation, beta titanium alloy 10V-2Fe-3Al, was obtained from Titanium Metals Corporation of America, Toronto, Ohio. All the material came from a single heat (number V5171) in the form of 3 inches (7.62 cm) diameter bar. The chemical analysis for heat number V5171 is shown in Table 6.

The alloy in the as-received condition (Figure 3) consists of deformed alpha + beta phase grains with an equivalent mean grain diameter, MGD = $1.10_{0.799,2.741}$mm*. The condition of the as-received material was not desired for the ring specimens or for the physical property specimens.

Prior to machining the specimens for the forging operation, the material was preconditioned, as indicated below, to develop the desired structure.

2. MATERIAL PREPARATION

It was desired to study the influence of the initial grain size, forging temperature and forging speed on the flow stress, the as forged microstructure and the resulting mechanical properties. The effect of the grain size was considered by selecting two significantly different sizes (ASTM 2 and ASTM 10, approx.) to investigate their influence on the properties and structure. Both grain structures were developed from the as-received material by extrusion and heat treatment. The preparation of the rings and the physical property specimens vary essentially only in the geometry. Their preparation is discussed below.

* The grain sizes for both the equiaxed and deformed grains were calculated in accordance with Appendix A. The subscripts are shape factors. They indicate how deformed the grains are.

a. Ring Specimens

The alloy was extruded from billets 2.950 $\pm$ 0.005 inch (7.43 $\pm$ 0.0127 cm) inch diameter and 6 inch (15.24 cm) long at an extrusion ratio of 5.76:1 and a temperature of 1000°F(538°C). The extruded bars were quenched in water to retain the worked structure. The extrusion ratio of 5.76:1 was chosen to obtain the best balance between work stored in the material and a diameter of the extruded product of approximately 1.250 inch (3.175 cm) desired for the ring specimens. The extrusion temperature of 1000°F(538°C) was chosen in order to extrude the alloy below the beta transus temperature and obtain an unrecrystallized wrought structure. This type of grain structure was required to develop the small grain size by heat treatment. A wrought structure, with no recrystallization and some previous beta grain boundaries, was obtained by extrusion of 1000°F (538°C)/5.76:1/WQ. A photomicrograph of the as-extruded structure is shown in Figure 4.

Various time-temperature combinations were considered in the selection of the heat treating conditions most suitable to develop the two desired grain structures. Some of the heat treating conditions tested, particularly at 1450°F(788°C), resulted in specimens with a banded grain structure (Figure 5), the grains in the bands being larger than the grains in the remaining of the specimen. Segregation of alloying elements was suspected because of the effects of the type and amounts of alloying elements on the beta transus temperatures and because of the changes in grain growth rate above and below this temperature.

Some elements, like aluminum, dissolves preferentially in the alpha phase and stablizes this phase at higher temperatures, therefore raising both the alpha and beta transus temperatures. Other elements, like iron and vanadium, are beta stabilizers. These elements lower both the alpha and beta transus temperatures. The rate of grain growth is faster above the transus. Consequently, small changes in the concentration of a heavy beta stabilizer, like iron, would cause changes in the beta transus temperature and increase grain growth rate in the beta enriched regions. These changes in concentration would result in bands of varying grain sizes when the material is heat treated at temperatures above the transus of the beta enriched portions. Heat treating at a relatively high temperature [over 150°F(66°C) to 200°F(93°C) above the beta transus of the bulk material] will probably reduce the grain size variation to an insignificant difference, perhaps explaining why the effect was most noticeable at about 1450°F(788°C).

Samples of the alloy showing the banding phenomenon were tested for any evidence of segregation of alloying elements. The microprobe traces showed (Figure 6) an increase in iron in the large grain band regions. Point count measurement in the banded region and in the bulk revealed an estimated 15% higher concentration of iron in the bands than in the rest of the specimen. This difference of 15% in the concentration of iron is considered significant and responsible for the banding phenomenon. No significant difference was detected in the concentration of vanadium or aluminum.

A sample of the banded material was vacuum annealed at 2200°F (1204°C) for ten hours to homogenize the alloying elements and to eliminate the banding phenomenon. No evidence of segregation of aluminum, vanadium or iron was detected by microprobe analysis (Figure 7) of the homogenized material.

The machined billets required for the specimens were vacuum annealed (homogenized) at 2200°F(1204°C)/10 hrs/VC prior to extrusion. Billets before and after the homogenization are shown in Figure 9.

The extrusion of the homogenized billets was attempted unsuccessfully through a 90°*, 5.76:1 extrusion ratio die at 1000°F(538°C). The maximum load delivered by the extrusion press was not sufficient to push the billet through the die. The increase in extrusion load from approximately 650 tons before the homogenization to over 730 tons after the

* The walls of the die make 45° angles with the direction of extrusion.

vacuum anneal treatment was attributed to the latter's large grain size, MGD = 1.45 mm. It was necessary to raise the extrusion temperature to reduce the forging load. The billets were extruded at 1150°F(621°C)/ 5.76:1/WQ with a resulting peak extrusion load of 650 tons. The microstructure of the extruded material, shown in Figure 10, showed some signs of recrystallization but was considered acceptable.

The selection of the heat treatment conditions suitable for development of the two grain sizes was then completed. The larger grain size was developed by heat treating the extrusions at 1750°F(954°C) for one hour followed by a water quench to retain the structure. Prior to the heat treatment the extrusion was coated with glass lubricant to minimize contamination. The heat treating temperature, 1750°F(954°C), was chosen to develop a grain size stable in the entire forging temperature range, from 1190°F(643°C) ($0.43T_m$) to 1750°F(954°C) ($0.58T_m$). The grain structure developed, MGD = 255μm, is shown in Figure 11a.

The smaller grain size was produced by heat treating at 1450°F (788°C) for six hours followed by water quenching. Two additional temperatures were considered to develop the smaller grain structure, 1425°F (774°C) and 1475°F(802°C). The lower temperature resulted in a somewhat wrought grain structure, with nonuniform grain sizes. The higher temperature produced grains larger in diameter than desired, MGD = 45.1 mm. The structure developed at 1450°F(788°C)/6 hrs/WQ (Figure 11b) resulted in equiaxed grains with MGD = 8.0μm.

b. Mechanical Property Specimens

The material required for the Charpy blanks was extruded and heat treated the same way as the ring specimens. The microstructure for these specimens is identical as that of the ring specimens, and is shown in Figure 11a for the larger grain size and in Figure 11b for the smaller grains. The specifications for the Charpy forging blanks is shown in Figure 12.

The forging blanks for the tensile specimens were obtained from material extruded at 1150°F(621°C) through a 60^{o} angle die and a 10:1 extrusion ratio. The higher extrusion ratio was used to obtain a product of smaller diameter more suitable for the tensile forging blanks. The material was water quenched after extrusion and heat treated as before. The microstructures are shown in Figures 13 and 14 for the small and large grain size respectively. The specifications for the forging blanks are shown in Figure 12.

3. SPECIMEN IDENTIFICATION

A system was adopted (Figure 15) to identify each specimen in their relative location in the bars of as-received material. Each of the two bars was identified with a letter, A or B. Each billet machined was identified with the bar letter and an additional number starting with one at one end of the bar and running sequentially towards the other end. After the billets were extruded, the extrusion number was cross-referenced with the billet number and the former utilized from then on as identification. An arrow was used to identify the head of the extrusion. The bars were then heat treated to develop the microstructure. An L or S was added to the extrusion number to identify the material with large or small grains. Each specimen was machined to specifications (Figure 16 for the ring specimens and Figure 12 for the physical properties forging blanks) and identified with the extrusion number, including the grain size identifier, and an additional number starting with one at the extrusion head and running sequentially toward the tail. With this system it was possible to locate relative position of each specimen in the original bars of as-received material. This identification system was utilized for both the ring specimens and the physical property specimens.

4. THE FORGING OPERATION

a. The Equipment

All of the specimens were forged isothermally on a 500-ton Lombard Hydraulic Forging Press at the Metals Processing Facility of the

Air Force Materials Laboratory, Wright-Patterson Air Force Base, Ohio. The press had been previously fitted with an electrical servovalve system to ensure constant ram motion ($\pm$ 5% in the range 0.03 ipm (0.00127 cm/sec) to 3.0 ipm (0.127 cm/sec) and modified with an auxiliary hydraulic system for slow control of the ram movement. In addition, the die area had been enclosed with sheet metal and insulated with Fiberfrax Lo-Con blanket, creating a furnace (Figure 17) suitable for isothermal forging up to approximately 1750°F(954°C).

The furnace is heated by 14 SCR controlled heating elements. Two of these are rectangular (8.5" X 11") radiant Kanthol coil wound heaters, one located on each side panel of the furnace. The remaining 12 elements are rod cartridge heaters, six embedded in each of the two dies (Figure 18a). The temperature in the furnace is controlled by a thermocouple embedded just below the working surface of each die, and monitored at a control panel by a second set of thermocouples located just below the working die surface diametrally opposed to the control thermocouples. One of the two flat dies in the furnace is connected to the press ram; the other die is floating on a tubular strain gage load cell (Figure 18b). The load cell is connected to a high speed response Honeywell 906B Visicorder. This system was used to record the load continuously during forging.

Prior to the forging operation, the specimens were heat treated at the forging temperature for 30 minutes in a Harrop Electric Furnace model NMR BH18. After the forging operation the specimens were quenched in water to preserve the as forged structure.

b. The Ring Specimens

The ring specimens were forged at conditions indicated in Table 7, quenched in water and measured. The thickness was measured using a micrometer. The contact inside ($2B_1$), the contact outside ($2B_0$), the inside diameter at mid-height ($2A_1$), and the outside maximum diameter ($2A_o$) were measured using a Quantimet 720 Image Analyzing Computer. The Quantimet senses the difference in light intensities resulting from the interference of a coherent light beam by the sample. Calibration of the Quantimet with samples of different areas permit conversion of the Quantimet readings to unit of area. The ring diameters (Figure 19) were then computed from the area measurements.

The ring dimensions ($2B_o$, $2B_1$, $2A_o$, $2A_1$, and T_r) (Figure 19) together with the forging load were used to calculate the flow stress of the alloy using the mathematical analysis of the ring by Avitzur (Reference 57) (Appendix C). The flow stress calculated corresponds to the true strain at which both the forging load and the dimensions were determined.

c. Forging of Mechanical Property Blanks and Measurement of Properties

The blanks (Figure 12) used to machine the mechanical property specimens (Figure 20) were forged in the same manner as the ring specimens. The forging conditions (temperature and speed) were selected (Table 9) to emphasize the dependency of the resulting properties on the forging conditions. In all cases the specimens were forged to a nominal strain of 0.50 in/in. The properties (tensile, fracture toughness) were measured at room temperature using methods outlined in Figure 20.

d. Hardness Measurements

The hardness was determined for each of the large grain size ring specimens forged to 0.50 in/in (nominal) at each temperature and speed. The measurements were made to investigate a possible correlation between the hardness and strength. The Rockwell C scale was chosen for the hardness determination. The measurements were made on a Wilson Hardness Tester at random locations with at least ten measurements per specimen. The surface was prepared by grinding and etching. Final polishing was done with 400 grit silicon carbide paper.

5. MICROSTRUCTURAL CHARACTERIZATION

The specimens identified in Table 8 were chosen for determination of characteristic structure using both a light microscope and a transmission electron microscope. These particular specimens were selected to establish the general trend in microstructural changes due to a wide range of processing conditions.

a. Light Metallography

A Leitz Metallograph was used for determination of the microstructures at low magnification (light microscopy). The samples were prepared by cutting a pie section from the ring specimen with an Isomet Low Speed Diamond Saw. The pie sections were then mounted in bakelite and mechanically polished using successively finer grit of silicone carbide grinding paper starting with 180 grit. The samples were rotated 90° for each finer grit used. After grinding on 600 grit, the samples were etched lightly with Kroll's Reagent (1%HF, 10%HNO_3, and 89%H_2O) and polished on 600 grit soft paper. The samples were again etched lightly and polished on 6μ diamond compound, re-etched and polished on a slow speed 0.05μ alumina impregnated wheel. This procedure, etching and polishing on 0.05μ alumina, was repeated until the samples were scratch free. Finally the samples were etched, inspected under the Leitz Metallograph, and photographed as required.

b. Transmission Electron Metallography (TEM)

The TEM samples were prepared from the same rings used for inspection under the Leitz Metallograph. The procedure used was as follows: Thin slices approximately 0.008 inch to 0.010 inch thick, were cut from the rings using an Isomet Low Speed Diamond Saw. The slices were thinned to approximately 0.006 inch using silicone carbide grinding paper. A disc, 1/8 inch in diameter, was punched out of the thin slice using a Ladd, Inc. Specimen Grid Punch P/N 1178. The samples were then thinned and polished to approximately 0.004 inch thick using 400 and 600 grit silicone carbide grinding paper.

The samples were electro-thinned in a Fishione Twin Jet Electro-Thinning Machine using an electrolytic solution of 250 ml methanol, 150 ml butylcelosolve and 13 ml perchloric acid at -33°C to -35°C. The methanol bath surrounding the electrolyte container was cooled with a Cryocool cooling unit. The temperature of the electrolyte was monitored with a Weston Dial Thermometer and the operation of the cooling unit adjusted, as necessary to maintain the desired temperature in the electrolyte. The samples were electro-thinned until a pinhole was detected, at the center of the sample, by the light-photocell system of the Fishione. A current density of 2.61 amp/in^2 (0.4 amp/cm^2) or 25 volts at 10 to 12 ma was used in the electro-thinning of the samples. The samples were inspected under the TEM at various magnifications and photographed as required.

TABLE 6

CHEMICAL ANALYSIS FOR HEAT NUMBER V5171 OF TI ALLOY 10V-2Fe-3Al*

V - 10.10	Fe - 1.90	Al - 2.95
C - 0.008	N - 0.020	O - 0.116
H - 0.0051	Si - 0.050	Ca - 0.015
Ta < 0.030	Mg - 0.006	Cr - 0.0045
Mn - 0.003	Ni - 0.003	Cu - 0.003
Mo - 0.003	Zr < 0.003	W < 0.003
Nb < 0.003	Sn < 0.003	B - 0.0015
Pb - 0.0015	Ti - Balance	

* Values are in weight per cent.

TABLE 7

FORGING MATRIX *

TEMPERATURE (F (C))	NOMINAL STRAIN (ϵ, IN/IN) 0.10	0.20	0.30	0.40	0.50
1190(643) ($0.43T_m$)			FOUR RINGS FORGED		
1250(677) ($0.45T_m$)			AT EACH STRAIN-TEMPERATURE CONDITION		
1300(704) ($0.46T_m$)			$V_1 - S_1$** $V_1 - S_2$		
1350(732) ($0.48T_m$)			$V_2 - S_1$ $V_2 - S_2$		
1400(760) ($0.490T_m$)					
1450(788) ($0.50T_m$)					
1600(871) ($0.54T_m$)			TWO RINGS FORGED		
1750(954) ($0.58T_m$)			AT EACH STRAIN-TEMPERATURE CONDITION $V_1 - S_2$ $V_1 - S_2$		

* Ring specimens were forged at the temperature, total strain, and strain rate (determined by the true ram speed) indicated.

** V_1 = 0.03 ipm(0.0762 cm/min), V_2 = 3.0 ipm(7.62 cm/min). S_1 = Structure with MGD = 8.0μm, S_2 = Structure with MGD = 255μm.

TABLE 8

INSPECTION MATRIX*

TEMPERATURE (F (C))	NOMINAL STRAIN (ε, IN/IN) 0.10: INSPECTION UNDER LIGHT MICROSCOPE		0.50: INSPECTION UNDER LIGHT MICROSCOPE		0.50: INSPECTION UNDER TRANSMISSION ELECTRON MICROSCOPE	
1190(643) ($0.43T_m$)				S_2-V_1,V_2		S_2-V_1,V_2
1250(677) ($0.45T_m$)	S_1-V_1,V_2	S_2-V_1,V_2	S_1-V_1,V_2	S_2-V_1,V_2	S_1-V_1,V_2	S_2-V_1,V_2
1300(704) ($0.46T_m$)						
1350(732) ($0.48T_m$)	S_1-V_1,V_2	S_2-V_1,V_2	S_1-V_1,V_2	S_2-V_1,V_2		
1400(760) ($0.49T_m$)						
1450(788) ($0.50T_m$)	S_1-V_1,V_2	S_2-V_1,V_2	S_1-V_1,V_2	S_2-V_1,V_2	S_1-V_1,V_2	S_2-V_1
1600(871) ($0.54T_m$)		S_2-V_1,V_2		S_2-V_1,V_2		S_2-V_1
1750(954) ($0.58T_m$)		S_2-V_1,V_2		S_2-V_1,V_2		S_2-V_1

* Hardness measurements were made on every sample with MGD = 255μm forged to 0.50 in/in (nominal).

TABLE 9

FORGING CONDITIONS FOR MECHANICAL PROPERTY MEASUREMENT*

TEMPERATURE (F (C))	NOMINAL SPEED (V, IPM(CM/MIN)) 0.03(0.0762)	3.0(7.62)
1250(677) ($0.45T_m$)	S_1 S_2	S_1 S_2
1350(732) ($0.48T_m$)		S_1
1450(788) ($0.50T_m$)	S_1 S_2	
1600(871) ($0.54T_m$)	S_2	
1750(954) ($0.58T_m$)	S_2	

* Four specimens were forged to a total strain of 0.50 in/in (nominal) at each speed and temperature indicated, two charpy specimens and two tensile specimens for each condition .

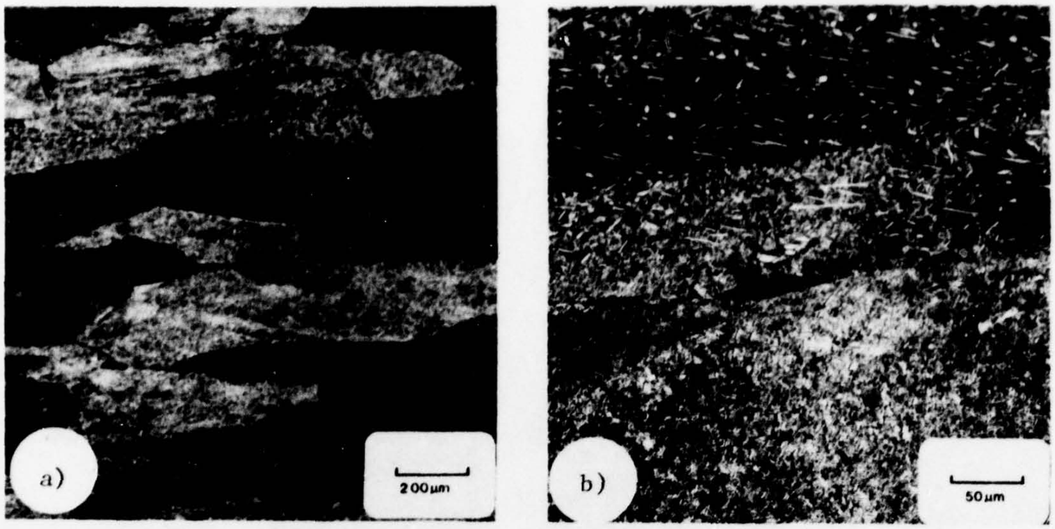

Figure 3. Ti-10V-2Fe-3Al in the As-Received Condition (MGD = $1.10_{0.799,2.741}$mm) ($^{t\uparrow}\!\rightarrow e$). Kroll's Reagent

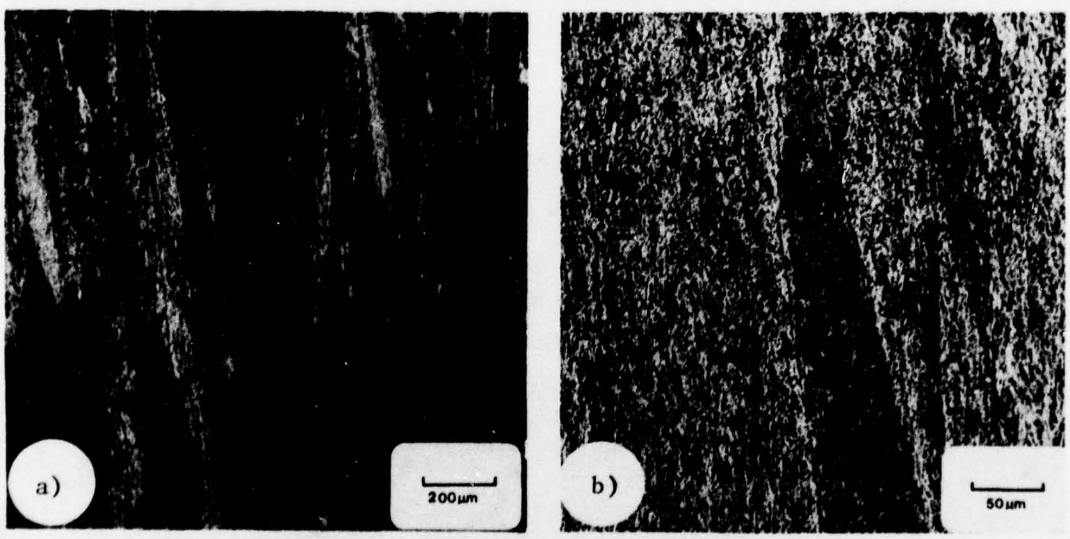

Figure 4. Ti-10V-2Fe-3Al Extruded at 1000°F(538°C)/5.76:1/WQ ($^{e\uparrow}\!\rightarrow r$). Kroll's Reagent

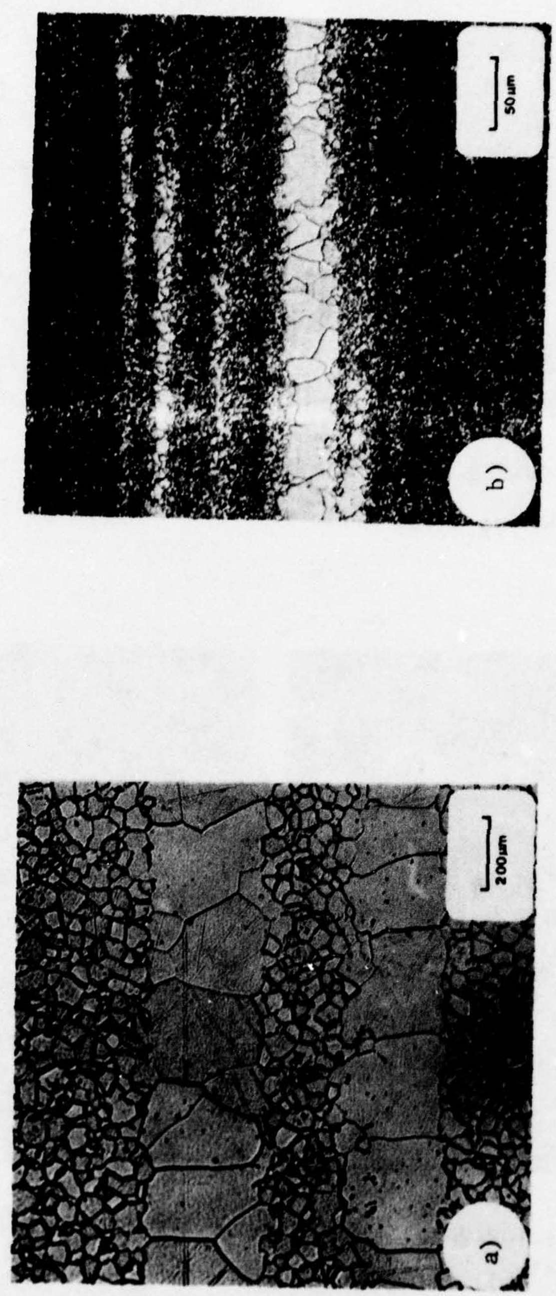

Figure 5. Banding in Ti-10V-2Fe-3Al Extruded at 1000°F(538°C)/ 5.76:1/WQ and Heat Treated at 1450°F(788°C)/45 min/ WQ($e^{+}\rightarrow r$). Kroll's Reagent

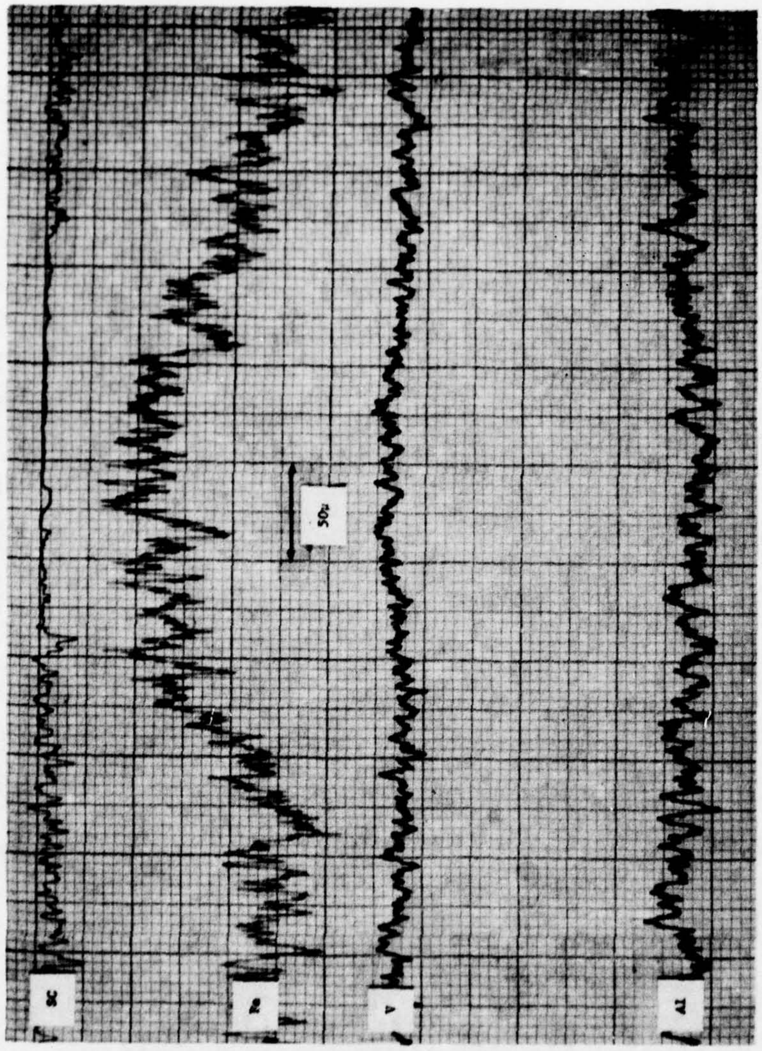

Figure 6. Microprobe Trace of Aluminum, Vanadium and Iron Across a Band in Ti-10V-2Fe-3Al Extruded at 1000°F(538°C)/5.76:1/WQ and Heat Treated at 1450°F(788°C)/45 min/WQ. The Microstructure is Similar to Figure 5.

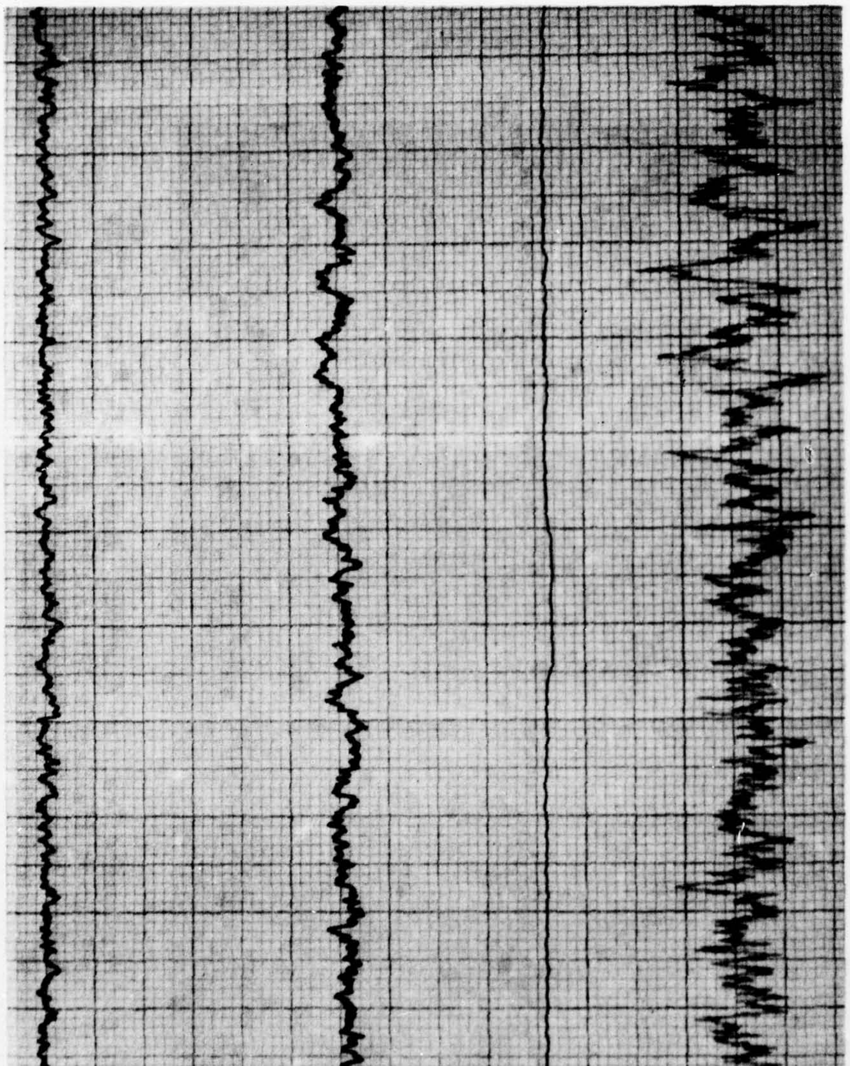

Figure 7. Microprobe Trace of Iron, Aluminum and Vanadium for Ti-10V-2Fe-3Al after Vacuum Annealed at 2200°F(1204°C)/ 10 hrs/VC. The microstructure is shown in Figure 8.

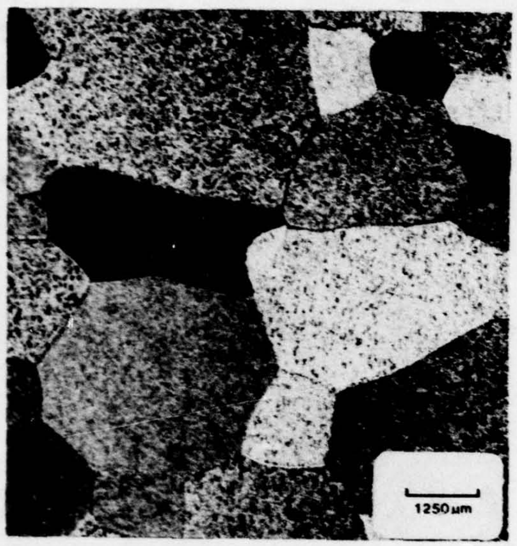

Figure 8. Ti-10V-2Fe-3Al Vacuum Annealed at 2200°F(1204°C)/10 hrs/VC (MGD = 1.45mm). Kroll's Reagent.

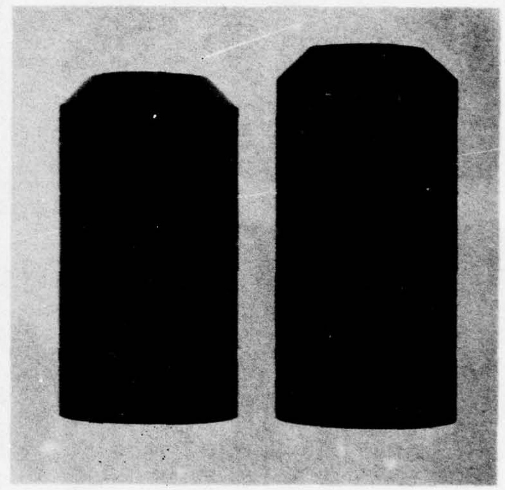

Figure 9. Billets of Ti-10V-2Fe-3Al Used for Extrusion, Shown as Machined (Left) and Vacuum Annealed (Right).

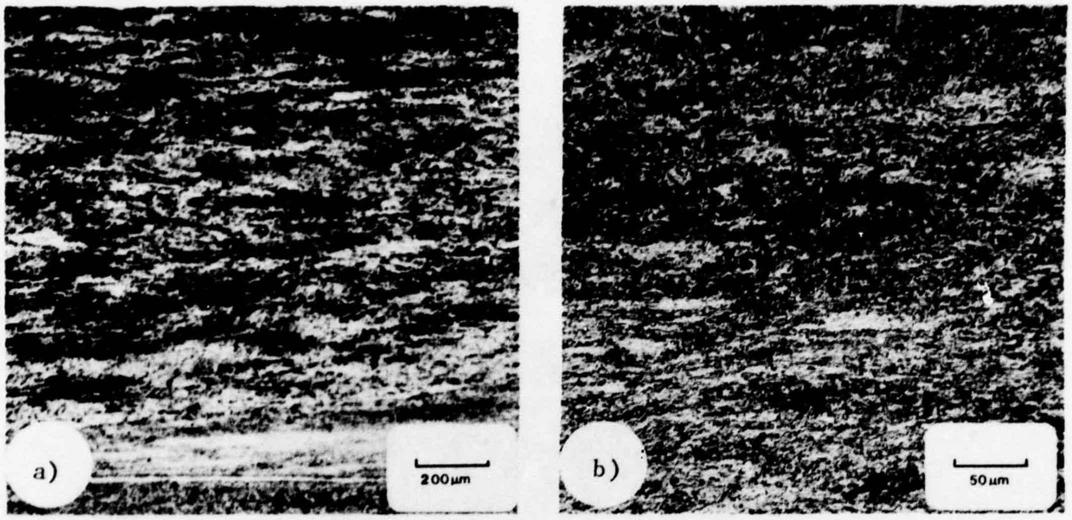

Figure 10. Ti-10V-2Fe-3Al Extruded at 1150°F(621°C)/5.76:1 WQ($^{r\uparrow}\rightarrow$e). Kroll's Reagent

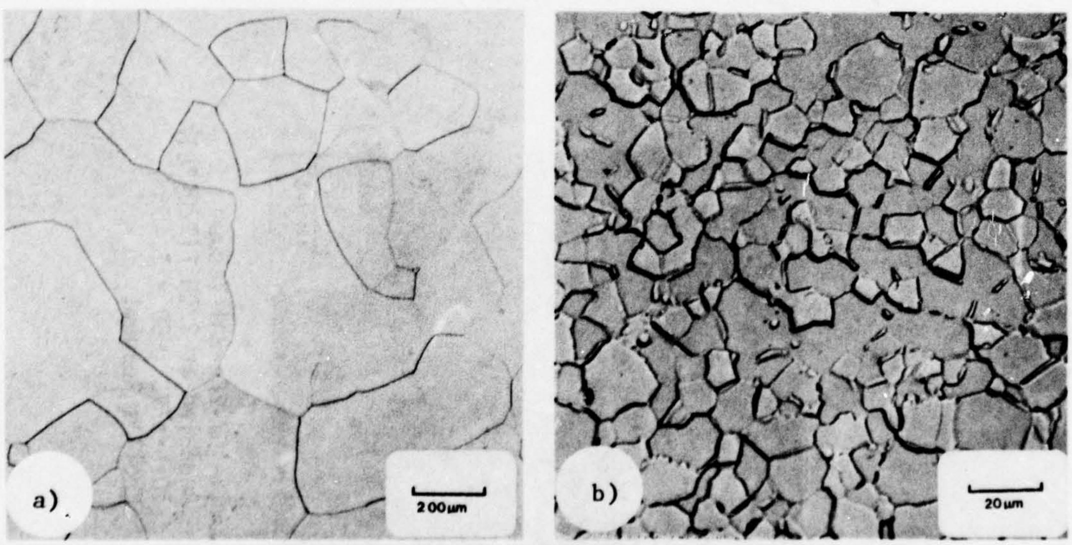

Figure 11. Ti-10V-2Fe-3Al Extruded at 1150°F(621°C)/5.76:1/ WQ. a) Heat Treated at 1750°F(954°C)/1hr/WQ (MGD = 255μm), b) Heat Treated at 1450°F(788°C)/6 hrs/ WQ (MGD = 8μm). Kroll's Reagent

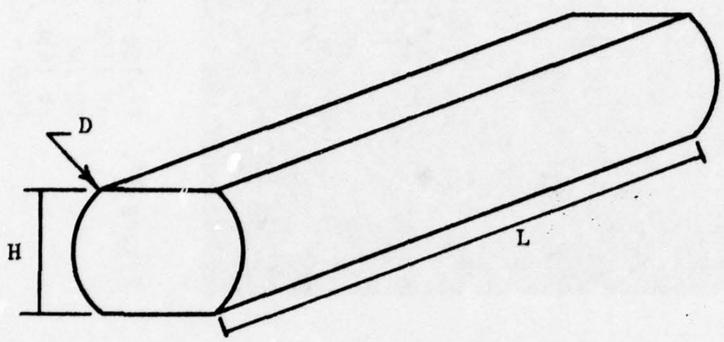

Figure 12. Specifications for the Forging Blanks Used for Determination of Mechanical Properties.
Charpy Blanks, D = 1.280, H = 1.120 ± 0.004, L = 2.30, Surface Finish on Flats: 64 RMS
Tensile Blanks, D = 1.00, H = 0.860 ± 0.005, L = 3.10, Surface Finish on Flats: 64 RMS
(All Dimensions in Inches)

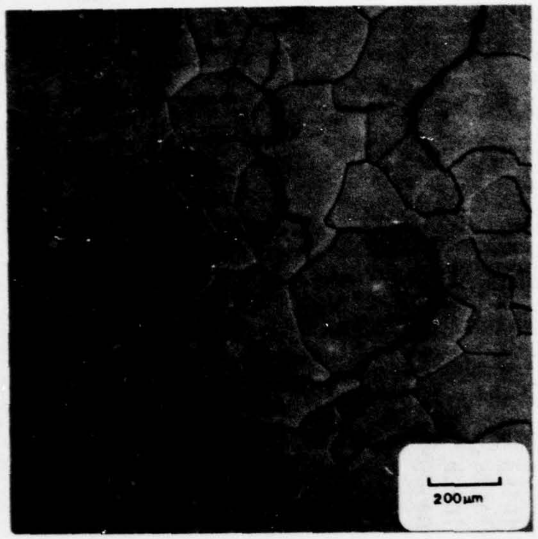

Figure 13. Ti-10V-2Fe-3Al Extruded at 1250°F(677°C)/10:1, 60°/WQ and Heat Treated at 1750°F(954°C)/1 hr/WQ (MGD = 255µm). Kroll's Reagent

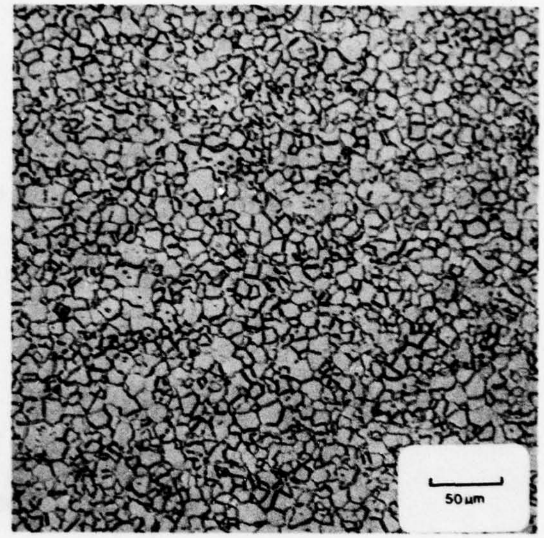

Figure 14. Ti-10V-2Fe-3Al Extruded at 1150°F(621°C)/10:1, 60°/WQ and Heat Treated at 1450°F(788°C)/6 hrs/WQ (MGD = 8µm). Kroll's Reagent

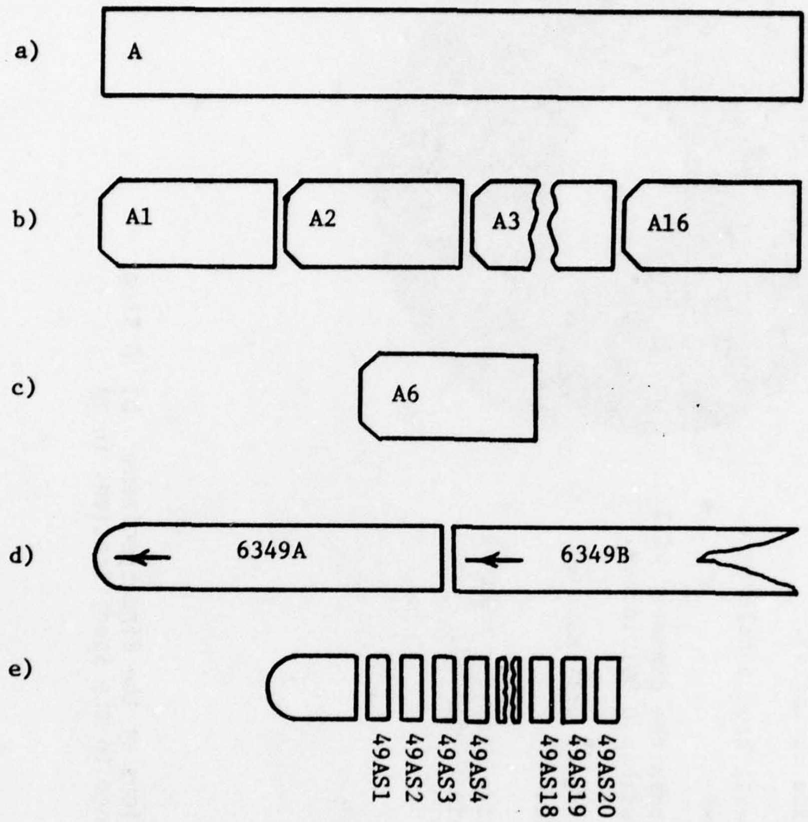

Figure 15. The System Used for Identification of Specimens: a) The Two Bars of the As-Received Material Were Identified as A and B. b) Sixteen Billets Were Machined for Bar A. Each Billet Was Identified as Shown Above. c) Billet A6 Was Extruded Through a Round Die (Extrusion Number 6349) and Heat Treated to Develop the Small Grain Size. d) The Extrusion Was Cut in Half to Facilitate the Heat Treatment and Identified as Indicated. e) The Ring Specimens Were Machined and Identified as Indicated

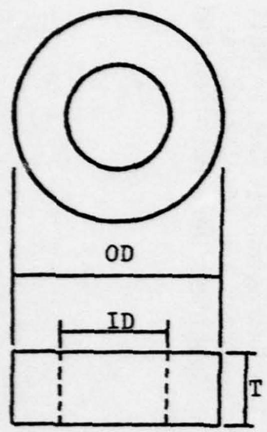

RING SPECIFICATIONS

1) All dimensions are in inches.

2) All dimensions will have a tolerance of $\pm$ 0.001 inches.

3) Edge to edge across the diameter will be parallel to within 0.001 inches.

4) Lathe turned surfaces will have a finish of 32 RMS.

5) Inside and outside diameter will be concentric within 0.001 "R".

6) OD = 1.200
ID = 0.600
T = 0.400

Figure 16. a) Specifications of the Ring Specimens. b) A Ring Specimen Machined to the Specifications in a)

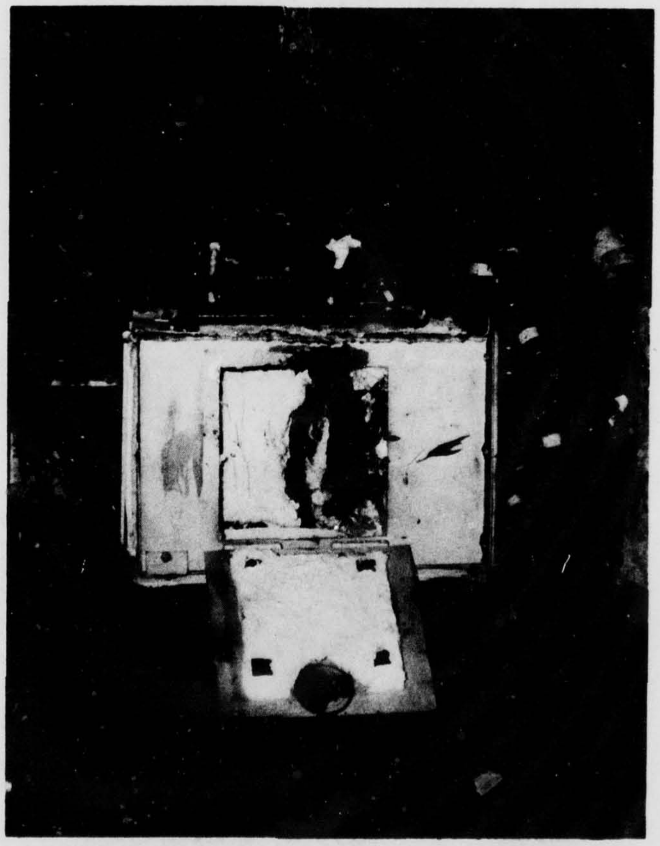

Figure 17. The Furnace and Die Section (See Figure 18) of the 500-Ton Lombard Hydraulic Forging Press

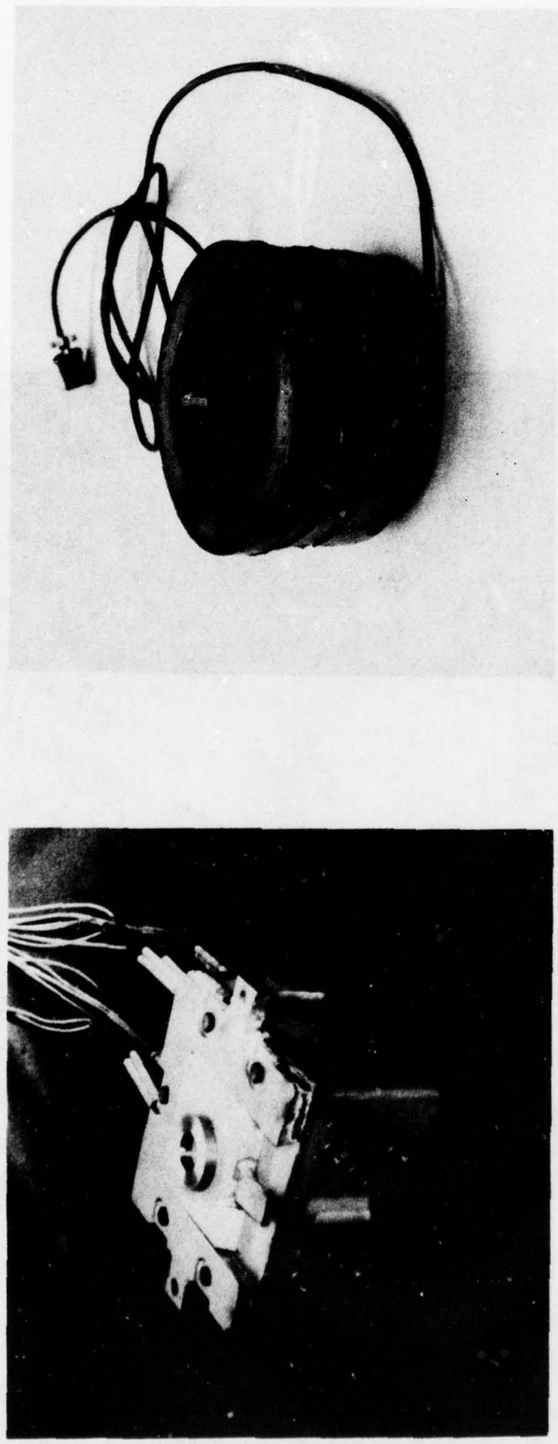

Figure 18. The Lower Die Assembly Shown in a) Rests on a Water Jacket Over the Load Cell. a) Ring Specimen on Lower Die of the Forging Press. The Cartridge Heaters Can Be Seen Protruding from the Back of the Die. b) Load Cell Used to Measure Forging Loads

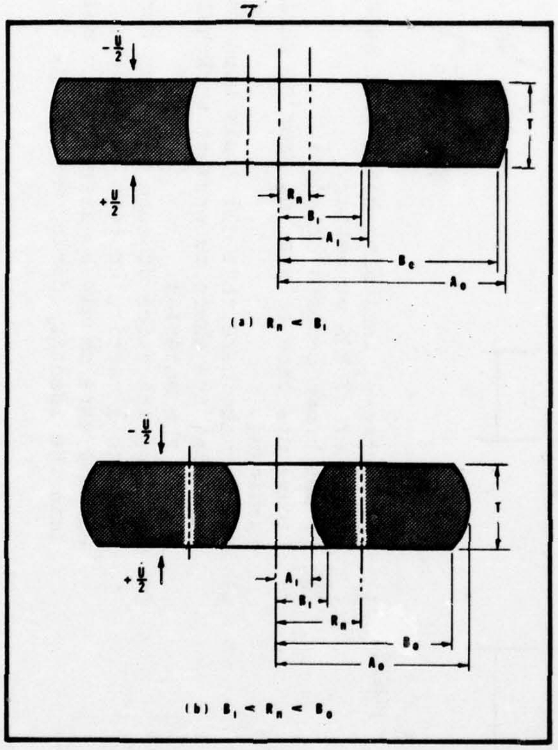

Figure 19. Schematic of Forged Ring. Top Ring Shows Low Friction Conditions, Bottom Ring Shows High Friction Conditions. (Reference 58)

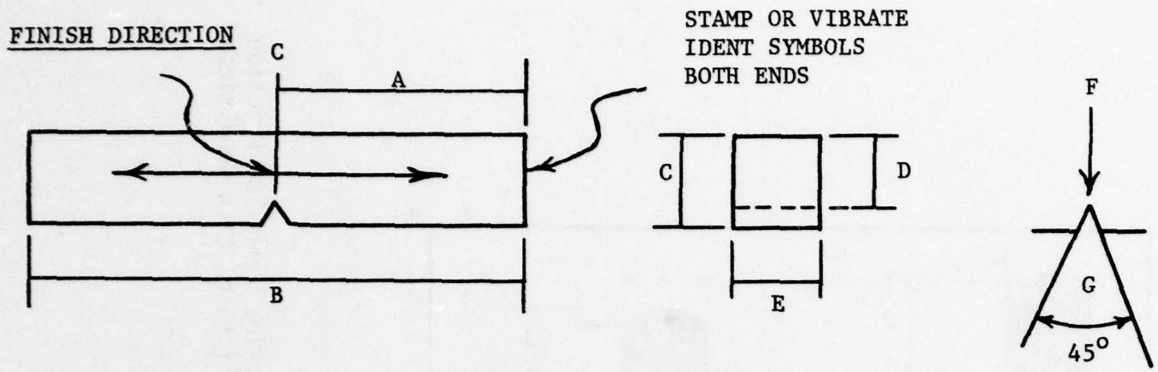

$A = 1.083 \pm 0.065$
$B = 2.165 \pm 0.010$
$C = 0.394 \pm 0.001$
$D = 0.315 \pm 0.001$
$E = 0.394 \pm 0.001$
$F = 0.010 \pm 0.001$
$G = 45^{\circ} \pm 1^{\circ}$

NOTES:

1) All surfaces, including notch will have a finish of 32 RMS or better.
2) Do not break corners or edges.
3) Please use care to prevent heating during machining.
4) Please make sure that all tools used for machining are sharp to prevent work hardening of the material.
5) The identification of each specimen corresponds to a particular test condition; extreme care should be exercised to maintain the identity during machining.

Figure 20a. Charpy Specimen for Determination of Fracture Toughness (Energy Per Unit Area, W/A) Using Slow Bend Method (Reference 60)

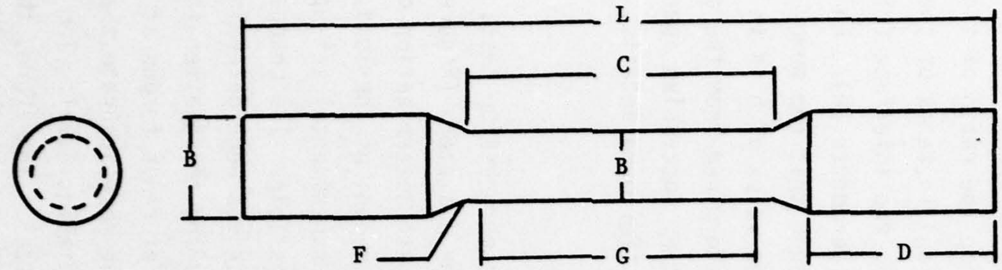

A = 0.252 ± 0.005 - gage section diameter
B = 3/8-24 thds. - grip end diameter
C = 1 1/4, min. - length of reduced section
D = 5/8, approx. - grip length
F = 0.18, min. - fillet radius
G = 1.000 ± 0.005 - gage length
L = 3, approx. - total length

Please exercise extreme care in maintaining each specimen's identity. Each specimen represents a different test condition.

All dimensions are in inches.
The material is forged Ti-10V-2Fe-3Al.

SPECIMENS: T3, T4, T7, T8, T13, T14, T15, T16, T17, T18, T21 and T22.

Figure 20b. Tensile Specimen for Determination of Yield Strength, Ultimate Strength and Uniform Elongation. The Tensile Properties Were Determined at 0.05 in/min and Room Temperature. The Yield Strength is Defined as .2% Offset (Reference 61)

SECTION IV

DATA REDUCTION AND ANALYSIS

The flow stress of the titanium alloy under investigation was determined using the ring compression test (Appendix C). This method is based on the mathematical analysis of a hollow disk made by Avitzur (References 56, 57) and on the solution of Avitzur's equation by DePierre and Gurney (Reference 58). Avitzur developed an equation for the ratio of the forging pressure (P) to the material's flow stress (σ_0) in terms of the neutral radius (R_n), the ring geometry (R_i, R_o, T_r), the interface friction (m) between the die and the ring, and the bulge parameter (b). An expression for the bulge parameter (b) is determined such that the power of deformation is minimized. The expression for the value of b is in terms of R_n, R_o, R_i, T_r, and m. The value of R_n is determined from the change in the geometry. The friction (m) is determined by successive approximations such that the value of P/σ is minimized. (For more details, see Appendix C).

To determine the flow stress using the ring compression test, it is necessary to obtain the forging load and the ring diameters (Figure 19) as a function of ring thickness. The most accurate determination of the flow stress can be made using a continuous measurement of the load, the thickness, and the diameters. With the present experimental set-up, a continuous measurement of the geometry is not possible. The changes in inside diameter, outside diameter, and ring thickness were determined by forging rings to different thicknesses and measuring these after the rings had been quenched. The larger the number of rings forged at each temperature-strain rate-grain size condition, the more accurate the determination of the flow stress, all others variables equal. Too large a number of specimens is, nevertheless, impractical. Therefore, the flow stress was determined at each temperature-strain rate-grain size condition using five rings deformed at 10% strain intervals (nominal).

1. FORGING LOADS

The forging records represent the output voltage of the load cell on the ordinate and the forging time on the abscissa. The ordinate was converted to forging load using the load cell calibration from Reference 62.

$$L = 1.953MV - 0.537: \quad MV \leq 8.366MV \tag{64}$$

$$L = 2.475MV - 4.905; \quad MV \leq 8.366MV \tag{65}$$

The load is in thousands of pounds when the voltage is in millivolts.

The abscissa, x, was converted to apparent ring thickness, $T_r(x)$, from knowledge of the true ram speed of the forge press, TS (Appendix B) and the original ring thickness, 0.400 inches:

$$T_r(x) = 0.40 - x(TS). \tag{66}$$

The forging load, corresponding to the room temperature ring thickness, precedes a marked drop in load cell output and a sharp increase in hydraulic pressure to the forge press. This marked drop in cell output indicates that the ram has contacted the side columns. At this point, the deformation of the ring is assumed to have stopped. The forging load curves obtained from the forging records are shown in Figures 21 to 24.

2. DETERMINATION OF RING DIAMETERS USING THE QUANTIMET 720 IMAGE ANALYZING COMPUTER

In general, areas are determined with the Quantimet by sensing differences in light intensities when a sample interrupts a beam of coherent light. The Quantimet reading (R) obtained is converted to units of area by applying a conversion factor (F). This conversion factor is determined by calibration: relating known areas to Quantimet readings.

The conversion factor was found to have a slight dependency on area and a slight variation from day to day. A relationship for F as a function of R was determined for each group of rings measured by alternating standard rings with forged rings. Four different area measurements (R1, R2, R3, R4) were necessary to determine the ring diameters ($2A_o$, $2A_1$, $2B_o$, $2B_1$, Figure 19).

In terms of the areas illustrated in Figure 25 the four measurements represent the following areas:

$$R1 = A1 + A2 + A3 \tag{67}$$

$$R2 = A2$$

$$R3 = A4$$

$$R4 = A3 + A4$$

The four diameters (Figure 19) are given by the formulas below:

$$\begin{aligned}
2A_o &= \left[\frac{4}{\Pi}\left(\frac{R3}{F3} + \frac{R1}{F1}\right)\right]^{1/2} \\
2A_1 &= \left[\frac{4}{\Pi}\left(\frac{R3}{F3}\right)\right]^{1/2} \\
2B_o &= \left[\frac{4}{\Pi}\left(\frac{R4}{F4} + \frac{R2}{F2}\right)\right]^{1/2} \\
2B_1 &= \left[\frac{4}{\Pi}\left(\frac{R4}{F4}\right)\right]^{1/2}
\end{aligned} \tag{68}$$

3. STRESS-STRAIN CURVES (*)

The ring geometry (T_r, $2A_0$, $2A_1$, $2B_0$, $2B_1$, Figure 19) before and after the forging operation, together with the forging loads were used to calculate flow stress using the equations in Appendix C. The strains were calculated using Equation 69.

$$\varepsilon = \ln (T_{ro}/T_{rc}) \tag{69}$$

where T_{ro} is the original ring thickness

T_{rc} is the as-forged ring thickness corrected for constant ring volume

The stress-strain curve for isothermally forged Ti-10V-2Fe-3Al are shown in Figures 26 and 27 for the small grain size (8μm) material and in Figures 28 and 29 for the large grain size (255μm) material. The data used for Figures 26 to 29 is tabulated in Appendix D.

4. STRAIN-RATE EQUATION

The strain-rate for a large number of pure metals and alloys has been shown (Section II) to obey a relation such as:

$$\dot{\varepsilon} = A\sigma^n \exp(-Q/RT) \tag{70}$$

where

$\dot{\varepsilon}$ is the strain rate, sec^{-1}

A is a constant which depends on structure and which may have a slight temperature dependence. This constant includes a diffusion term (D_0), a Burger's vector term (b), and a lattice vibration term (kT).

* Stress will be used interchangeably with flow stress unless otherwise Indicated.

σ is the stress, ksi

Q is the apparent activation energy, cal/mol

R is the universal gas constant, 1.987 cal/[(mol)(T)]

T is the temperature in degrees Kelvin

In order to determine if this equation applies to the stress-strain rate-temperature data for Ti-10V-2Fe-3Al, it is necessary to determine the values of A, n and Q.

a. Determination of Activation Energy (MGD = 255μm)

Under conditions of constant stress and constant structure, Equation 70 becomes

$$\dot{\varepsilon} = A' \exp(-Q/RT) \tag{71}$$

Taking the logarithm of each side of Equation 71, results in

$$\ln\dot{\varepsilon} = \ln A' - \frac{Q}{RT} \tag{72}$$

Equation 72 is recognized as a straight line with intercept

$$b = \ln A' = \ln(A\sigma^{n}) \tag{73}$$

and with slope

$$m = -Q/R \tag{74}$$

The activation energy can be determined from the slope of a $\ln\dot{\varepsilon}$ - 1/T line at conditions of constant stress and strain. The slope was obtained by fitting a least mean square line through the $\ln\dot{\varepsilon}$ - 1/T data.

The conditions of constant strain were satisfied by replotting the stresses from Figures 28 and 29 at constant strain and temperature as $\ln\dot{\varepsilon} - \ln\sigma$. The data from this plot ($\ln\dot{\varepsilon} - \ln\sigma$) was again replotted at constant stress as $\ln\dot{\varepsilon} - 1/T$. This plot of $\ln\dot{\varepsilon} - 1/T$ satisfies both requirements, namely constant stress and constant strain. The strain rates were calculated from

$$\dot{\varepsilon} = TS/T_r \tag{75}$$

$$TS = (1.0912)\,(V)^{1.0208} \tag{76}$$

T_r is the ring thickness, $T_r = T_{ro}\exp(-\varepsilon)$

TS is the true ram speed in ipm from Appendix B

V is the nominal ram speed,

$V_1 = 0.03$ ipm, $V_2 = 3.00$ ipm

T_{ro} is the original ring thickness, 0.400 in.

ε is the true strain, in/in

The activation energy was originally calculated at two strains, 0.10 in/in and 0.50 in/in. At each strain the activation energy was independent of temperature in two regions

$$643 \leq C < 799$$

and

$$799 < C \leq 954$$

below and above the beta transformation temperature, respectively. The activation energy was, nevertheless stress dependent. The stress dependency was of the form

$$Q = B - C\ln\sigma \tag{77}$$

Variations in B and C with strain were observed, suggesting that the activation energy might be strain dependent as well.

In an attempt to establish the strain dependence, the activation energy, and hence the constants B and C were determined as a function of strain for each temperature region.

The stress-strain rate-temperature data was read from Figures 28 and 29 for five strains ranging from 0.10 in/in to 0.50 in/in in 0.10 in/in intervals. The data for 0.50 in/in strain is shown in Table 10. The corresponding data for 0.10, 0.20, 0.30, and 0.40 in/in is shown in Appendix D, Tables D.3a, D.4a, D.5a and D.6a respectively. The $\ln\dot{\varepsilon}$-$\ln\sigma$ data for each strain was fitted with a straight line. With the equation of the $\ln\dot{\varepsilon}$-$\ln\sigma$ line the ordinate ($\ln\dot{\varepsilon}$) corresponding to a given abscissa ($\ln\sigma$) value was easily determined. The $\ln\dot{\varepsilon}$-$\ln\sigma$ lines at constant temperature are shown in Figure 30a for 0.50 in/in strain (and in Appendix D, Figures D.a to D.4a for the remaining strains). The $\ln\dot{\varepsilon}$-1/T data was fitted with a straight line at each strain-stress condition to obtain the slope for determination of apparent activation energy. The temperature-strain rate-stress data for Ti-10V-2Fe-3Al forged to a strain of 0.50 in/in is shown plotted in Figure 30b and listed in Table 10b. The corresponding activation energy is also included. The corresponding data for the remaining strains is included in Appendix D (Figures D.1b to D.4b and Tables D.3b to D.6b).

The Q-$\ln\sigma$ data for each strain was fitted with a line to determine the stress dependency of the activation energy. The Q-$\ln\sigma$ equation for each strain is listed in Table 11. The equations are also plotted in Figures 31 and 32 for the temperature region below and above the beta transformation temperature, respectively. The activation energy depends on strain through the strain dependency of the constants B and C in Equation 77. These constants are plotted as a function of strain in Figures 33 and 34 for the two temperature regions below and above the beta transformation temperature. The strain dependency for B and C is included in Table 11.

The activation energy can now be written in terms of both strain and stress for each temperature region:

Below the beta transformation temperature

$$Q = B - C \ln\sigma$$

$$B = 118140 + 78250\varepsilon \quad (78a)$$

$$C = 12590 + 36180\varepsilon \quad (78b)$$

$$Q = 118140 + 78250\varepsilon - (36180\varepsilon) \ln\sigma - 12590 \ln\sigma \quad (79)$$

Above the beta transformation temperature

$$B = 61880 + 13920\varepsilon$$

$$C = 3810 + 9580\varepsilon$$

$$Q = 61880 + 13920\varepsilon - (9580\varepsilon) \ln\sigma - 3810 \ln\sigma \quad (80)$$

b. Determination of the Pre-Exponential A and Stress Exponent n in Equation 70 (MGD = 255μm)

For each temperature region, the activation energy is constant with temperature but is stress dependent. Substituting Equation 77 into Equation 70 results in

$$\dot{\varepsilon} = A\sigma^{(n+C/RT)}\exp(-B/RT) \quad (81)$$

Taking the logarithm of each side of Equation 81

$$\ln\dot{\varepsilon} = (\ln A - B/RT) + (n + C/RT) \ln\sigma \quad (82)$$

At conditions of constant temperature and constant strain both B/RT and C/RT are constants. Equation 82 becomes the equation of a straight line

$$\ln\dot{\varepsilon} = b + m \ln\sigma \tag{83}$$

The values of A and n can be calculated from the intercept and slope of the $\ln\dot{\varepsilon}$-$\ln\sigma$ lines

$$\ln A = b + B/RT \tag{84}$$

$$n = m - C/RT \tag{85}$$

The slope and intercept of the $\ln\dot{\varepsilon}$-$\ln\sigma$ lines are shown in Table 16 together with the determined value for the pre-exponential and stress exponent. The stress exponent and pre-exponential are summarized in Table 12 as a function of strain for both temperature regions. The values of A and n are plotted as a function of strain in Figures 35 and 36 respectively. The strain dependency of A and n is given below:

For the temperature region: $643 \leq C < 799$

$$\ln A = 41.973 + 41.41\varepsilon \tag{86a}$$

$$n = -2.358 - 17.32\varepsilon \tag{86b}$$

For the temperature region: $799 < C \leq 954$

$$\ln A = 14.432 + 8.92\varepsilon \tag{87a}$$

$$n = 2.225 - 4.86\varepsilon \tag{87b}$$

AD-A066 062 AIR FORCE MATERIALS LAB WRIGHT-PATTERSON AFB OHIO F/G 11/6
EFFECTS OF ISOTHERMAL FORGING CONDITIONS ON THE PROPERTIES AND --ETC(U)
DEC 78 I A MARTORELL
UNCLASSIFIED AFML-TR-78-114 NL

2 OF 3
AD
A066062

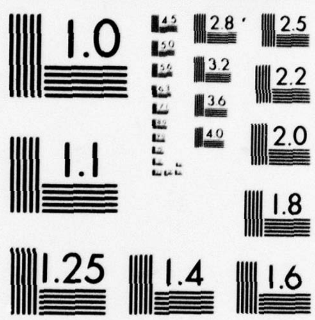

MICROCOPY RESOLUTION TEST CHART

NATIONAL BUREAU OF STANDARDS-1963-A

c. Stress-Strain Rate-Temperature Relationship (MGD = 255μm)

The relationship between stress-strain rate and temperature for Ti-10V-2Fe-3Al is given by Equation 81

$$\dot{\varepsilon} = A\sigma^{(n+C/RT)}\exp(-B/RT) \tag{81}$$

the parameters A, n, C and B are strain dependent and constant with temperature in two regions:

Below the beta transus temperature $643 \leq C < 799$

$$B = 118140 + 78250\varepsilon \tag{88a}$$

$$C = 12590 + 36180\varepsilon \tag{88b}$$

$$n = 2.358 - 17.32\varepsilon \tag{88c}$$

$$\ln A = 41.973 + 41.41\varepsilon \tag{88d}$$

Above the beta transus temperature $799 \leq C < 954$

$$B = 61880 + 13920\varepsilon \tag{89a}$$

$$C = 3810 + 9580\varepsilon \tag{89b}$$

$$n = 2.225 - 4.86\varepsilon \tag{89c}$$

$$\ln A = 14.432 + 8.92\varepsilon \tag{89d}$$

Equation 81 can be expressed in a more convenient form by solving for the stress

$$\sigma = \left[\frac{\dot{\varepsilon}}{A}\exp(B/RT)\right]^{1/(n+C/RT)} \tag{81a}$$

The stress can be calculated if the strain rate, strain and temperature are known. Since the strain rate, strain and forging speed are related by Equations 75 and 76 the flow stress can be expressed in terms of strain, temperature, and forging speed:

$$\sigma = \left[\frac{0.0455}{A} \quad V^{1.0208} \quad \exp(\varepsilon + B/RT)\right]^{1/(n + C/RT)} \tag{81b}$$

The stresses calculated from Equation 81 are compared to the measured stresses in Figure 37 and Table 13. The various forging conditions are identified with a number to facilitate future reference. The 45^{o} line drawn in Figure 37 represents a perfect correlation between the measured and the calculated stress values.

d. Stress-Strain Rate - Temperature Relationship (MGD = 8μm)

The stress-strain rate-temperature relation for Ti-10V-2Fe-3Al with MGD = 8μm is given by Equation 81

$$\dot{\varepsilon} = A\sigma^{(n + C/RT} \exp(-B/RT) \tag{81}$$

The parameters A, n, C, and B were determined following the same procedure used for the material with larger grains, 255μm (previous sections). The data used for the determination of these parameters was obtained from Figure 15 and 16 and is shown in Tables D.8a, D.8b, D.9, and D.10. The values of the parameters are summarized below for the temperature range used:

$$677 \leq C \leq 788$$

$$B = 170109 - 204084\varepsilon \tag{90a}$$

$$C = 24611 - 44961\varepsilon \tag{90b}$$

$$\ln A = 67.293 - 99.211\varepsilon \qquad (90c)$$

$$n = -7.99 + 23.015\varepsilon \qquad (90d)$$

The stresses calculated from Equation 81b and 90 are compared in Table 14 and in Figure 38 for a strain of 0.50 in/in.

5. MECHANICAL PROPERTIES

The tensile properties and the fracture toughness were determined for Ti-10V-2Fe-3Al forged isothermally at various temperatures and speeds. The specimen geometry and test conditions for the determination of the properties are shown in Figure 20. The forging conditions and the resulting properties are listed in Table 15 for both grain sizes. The properties have also been plotted as a function of the calculated flow stress in Figure 39 for the material with MGD = 255μm and in Figure 40 for the material with MGD = 8μm.

6. HARDNESS DETERMINATION

The hardness measurements made on the rings with MGD = 255μm are listed in Table 16 and plotted in Figure 39 as a function of σ_c. All the measurements were made on ring forged isothermally to a nominal strain of 0.50 in/in. Each harness value represents the average of ten measurements on the Rockwell C Scale.

7. MICROSTRUCTURE

a. Light Microscopy

The microstructure for Ti-10V-2Fe-3Al with MGD = 8μm forged isothermally to nominal strains of 0.10 in/in and 0.50 in/in are shown in Figures 41 and 42, respectively. The microstructures corresponding to the MGD = 255μm are shown in Figures 43 and 44. Each microstructure is identified with a forging condition number for easy reference to the forging conditions listed in Tables 13 and 14.

b. Transmission Electron Microscopy

The TEM microstructures for Ti-10V-2Fe-3Al forged isothermally at various conditions are shown in Figures 45 and 46 for MGD = 8μm and MGD = 255μm, respectively. Each microstructure is identified with the forging condition number, which can be referenced to Tables 13 and 14 and to Figures 41 to 44.

TABLE 10a

STRESS-STRAIN RATE-TEMPERATURE DATA FOR TI-10V-2Fe-3Al
FORGED ISOTHERMALLY TO 0.50 IN/IN. DATA FROM
FIGURES 28 and 29, MGD = 255μm

Temperature (C)	Forging Speed (V, imp)	Strain Rate ($\dot{\varepsilon}$, sec^{-1})	Stress (σ, ksi)	($\ln\sigma$, $\ln\dot{\varepsilon}$)	Intercept (b)	Slope (m)
643	0.03 3.00	2.091×10^{-3} 2.301×10^{-1}	21.0 46.8	(3.045,-6.17) (3.846,-1.47)	-24.026	5.865
677	0.03 3.00	2.091×10^{-3} 2.301×10^{-1}	16.8 38.2	(2.821,-6.17) (2.643,-1.47)	-22.313	5.722
704	0.03 3.00	2.091×10^{-3} 2.301×10^{-1}	11.6 32.0	(2.451,-6.17) (3.463,-1.47)	-17.522	4.632
732	0.03 3.00	2.091×10^{-3} 2.301×10^{-1}	9.6 28.4	(2.262,-6.17) (3.366,-1.47)	-15.973	4.334
760	0.03 3.00	2.091×10^{-3} 2.301×10^{-1}	7.4 24.6	(2.001,-6.17) (3.203,-1.47)	-14.001	3.913
788	0.03 3.00	2.091×10^{-3} 2.301×10^{-1}	6.0 21.2	(1.792,-6.17) (3.054,-1.47)	-12.843	3.724
871	0.03 3.00	2.091×10^{-3} 2.301×10^{-1}	4.3 16.0	(1.459,-6.17) (2.773,-1.47)	-11.387	3.577
954	0.03 3.00	2.091×10^{-3} 2.301×10^{-1}	2.6 10.7	(0.956,-6.17) (2.370,-1.47)	-9.344	3.322

TABLE 10b

STRAIN RATES FOR VARIOUS STRESS LEVELS AND TEMPERATURES FOR Ti-10V-2Fe-3Al FORGED ISOTHERMALLY TO 0.50 IN/IN. DATA FROM TABLE 10a, MGD = 255μm

Temperature (C)	Reciprocal Absolute Temperature ($1/K \times 10^{-4}$)	$\ln\dot{\epsilon}$ (sec^{-1}) for stress (ksi) indicated							
		10	20	30	40	50	60	70	80
643	10.91	-10.521	-6.456	-4.078	-2.391	-1.082	-0.013	-0.891	1.674
677	10.53	-9.138	-5.172	-2.853	-1.207	0.070	1.113	1.995	2.759
704	10.23	-6.858	-3.647	-1.768	-0.435	0.598	1.443	2.157	2.776
732	9.95	-5.993	-2.989	-1.232	0.015	0.982	1.772	2.441	3.019
760	9.68	-4.992	-2.280	-0.694	0.432	1.305	2.018	2.622	3.144
788	9.43	-4.268	-1.686	-0.176	0.895	1.726	2.405	2.979	3.477
	Intercept	37.372	29.368	24.682	21.357	18.776	16.672	14.892	13.353
	Slope	-43801	-32675	-26163	-21544	-17758	-15033	-12558	-10418
	Activation Energy	87032	64925	51986	42807	35682	29870	24952	20700

871	8.74	-3.151	-0.672	0.778	1.808	2.605	3.258	3.809	4.287
954	8.15	-1.695	0.608	1.955	2.911	3.652	4.258	4.770	5.214
	Intercept	18.418	18.284	18.214	18.147	18.101	18.072	18.045	18.019
	Slope	-24678	-21695	-19949	-18695	-17729	-16949	-16288	-15712
	Activation Energy	49035	43108	39639	37147	35227	33673	32365	31219

TABLE 11

STRESS AND STRAIN DEPENDENCY OF THE APPARENT ACTIVATION ENERGY FOR ISOTHERMALLY FORGED Ti-10V-2Fe-3Al, MGD = 255μm*

STRAIN (ε, in/in)	APPARENT ACTIVATION ENERGY (Q, CAL/MOLE) FOR TEMPERATURE REGION BELOW TRANSUS	APPARENT ACTIVATION ENERGY (Q, CAL/MOLE FOR TEMPERATURE REGION ABOVE TRANSUS
	$643 \leq C < 799$	$799 < C \leq 954$
0.10	$Q = 128130 - 17060 \ln\sigma$	$Q = 63210 - 4740 \ln\sigma$
0.20	$Q = 133010 - 19500 \ln\sigma$	$Q = 64700 - 5740 \ln\sigma$
0.30	$Q = 139900 - 22740 \ln\sigma$	$Q = 66110 - 6710 \ln\sigma$
0.40	$Q = 146540 - 26000 \ln\sigma$	$Q = 67480 - 7660 \ln\sigma$
0.50	$Q = 160490 - 31900 \ln\sigma$	$Q = 68780 - 8570 \ln\sigma$
	$B = 118140 + 72250\varepsilon$	$B = 61880 + 13920\varepsilon$
	$C = 12590 + 36180\varepsilon$	$C = 3810 + 9580\varepsilon$

* THE STRESS IS IN KSI

TABLE 12

STRAIN DEPENDENCY OF THE PRE-EXPONENTIAL AND STRESS EXPONENT FOR ISOTHERMALLY FORGED Ti-10V-2Fe-3Al, MGD = 255μm*

	$643 \leq C < 799$		$799 \leq C \leq 954$	
STRAIN (ε, in/in)	n	lnA	n	lnA
0.10	-4.01	45.81	1.74	15.32
0.20	-5.85	50.38	1.25	16.22
0.30	-7.64	54.71	0.77	17.11
0.40	-9.35	58.75	0.28	18.00
0.50	-10.92	62.33	-0.205	18.89

* SEE APPENDIX D, TABLE D.7 FOR THE COMPLETE SET OF DATA USED TO CALCULATE ABOVE VALUES

TABLE 13

MEASURED AND CALCULATED FLOW STRESSES FOR Ti-10V-2Fe-3Al FORGED ISOTHERMALLY TO 0.50 IN/IN, MGD = 255μm*

FORGING CONDITIONS				CALCULATED STRESS	MEASURED STRESS
	TEMPERATURE		SPEED		
	(C)	(K)	(V, IPM)	(σ_c, KSI)	(σ_m, KSI)
1	954	1227.4	0.03	2.59	2.6
2	871	1144.1	0.03	4.30	4.3
3	788	1060.8	0.03	5.10	6.0
4	760	1033.2	0.03	7.23	7.4
5	732	1005.2	0.03	9.75	9.6
6	954	1227.4	3.00	10.68	10.7
7	704	977.4	0.03	12.65	11.6
8	871	1144.1	3.00	16.00	16.0
9	677	949.7	0.03	15.89	16.8
10	788	1060.8	3.00	19.27	21.2
11	643	916.3	0.03	20.19	21.0
12	760	1033.2	3.00	23.91	24.6
13	732	1005.2	3.00	28.79	28.4
14	704	977.4	3.00	33.83	32.0
15	677	949.7	3.00	38.97	38.2
16	643	916.3	3.00	45.20	46.8

(*) The ring compression test (Appendix C) was used to measure stresses and Equations 80, 88a to 89d used to calculate stresses. The following values of Equations 88a to 89d were used:

	$643 \leq C < 799$	$799 < C \leq 954$
B(cal/mole)	157265	68840
C(cal/mole-ksi)	30680	8600
A(sec^{-1})	1.662×10^{27}	1.602×10^{8}
n	-11.018	-0.205

TABLE 14

MEASURED AND CALCULATED FLOW STRESS FOR Ti-10V-2Fe-3Al FORGED ISOTHERMALLY TO 0.50 IN/IN, MGD = 8μm*

FORGING CONDITIONS				CALCULATED STRESS	MEASURED STRESS
	TEMPERATURE		SPEED		
	(C)	(K)	(V, ipm)	(σ_c, ksi)	(σ_m, ksi)
3	788	1060.8	0.03	6.46	6.40
5	732	1005.2	0.03	9.32	9.60
9	677	949.7	0.03	13.89	14.30
10	788	1060.8	3.00	18.29	18.20
13	732	1005.2	3.00	26.02	26.10
15	677	949.7	3.00	38.26	38.60

* THE RING COMPRESSION TEST (APPENDIX C) WAS USED TO MEASURE STRESSES AND EQUATIONS 80, 90a TO 90d USED TO CALCULATE STRESSES. THE FOLLOWING VALUES OF EQUATIONS 90a TO 90d WERE USED:

B = 68067 CAL/MOLE
C = 2131 CAL/MOLE-KSI
A = 4.804×10^7 SEC^{-1}
n = 3.512

TABLE 15

ROOM TEMPERATURE MECHANICAL PROPERTIES FOR Ti-10V-2Fe-3Al FORGED ISOTHERMALLY TO 0.50 IN/IN (NOMINAL)

PART A. MGD = 255μm.

	Forging Conditions: Temperature (C)	Forging Conditions: Speed V, ipm	Calculated stress (σ, ksi)	Yield Strength 0.2% offset (YS, ksi)	Ultimate Strength (UTS, ksi)	Ductility (D, % El.)	Modulus of Elasticity (E, ksi x 10^3)	Toughness (W/A, in-lb/in^2)
0	----	----	----	94	121	30.0	12.2	1100
1	954	0.03	2.59	103	115	13.5	14.7	1200
2	871	0.03	4.30	79	122	33.3	13.6	1300
3	788	0.03	5.10	87	124	31.6	14.4	1340
9	677	0.03	15.89	140	144	10.3	14.4	630
15	677	3.00	38.97	153	160	5.7	13.4	280

PART B. MGD = 8μm.

	Forging Conditions: Temperature (C)	Forging Conditions: Speed V, ipm	Calculated stress (σ, ksi)	Yield Strength 0.2% offset (YS, ksi)	Ultimate Strength (UTS, ksi)	Ductility (D, % El.)	Modulus of Elasticity (E, ksi x 10^3)	Toughness (W/A, in-lb/in^2)
0	----	----	----	118	125	19.0	12.5	1100
3	788	0.03	6.46	125	128	14.0	13.9	990
9	677	0.03	13.89	138	141	13.5	14.1	470
13	732	3.00	26.02	137	145	11.5	12.5	190
15	677	3.00	38.26	150	157	10.6	13.6	260

TABLE 16

HARDNESS MEASUREMENTS FOR Ti-10V-2Fe-3Al FORGED ISOTHERMALLY TO 0.50 IN/IN (NOMINAL) AT VARIOUS CONDITIONS, MGD = 255μm

	FORGING CONDITIONS TEMPERATURE (C)	SPEED (V, IPM)	HARDNESS ROCKWELL C	CALCULATED STRESS (σ_c, KSI)	YIELD STRENGTH (YS, KSI)	ULTIMATE STRENGTH (UTS, KSI)
1	954	0.03	32.2	2.6	103	115
2	871	0.03	31.6	4.3	79	122
3	788	0.03	32.1	5.1	87	124
4	760	0.03	33.0	7.2		
5	732	0.03	34.3	9.8		
6	954	3.00	32.1	10.7		
7	704	0.03	33.7	12.7		
8	871	3.00	31.8	16.0		
9	677	0.03	34.1	15.9	140	144
10	788	3.00	34.5	19.3		
11	643	0.03	33.8	20.2		
12	760	3.00	35.6	23.9		
13	732	3.00	35.9	28.8		
14	704	3.00	35.9	33.8		
15	677	3.00	37.0	39.0	153	160
16	643	3.00	40.7	45.2		

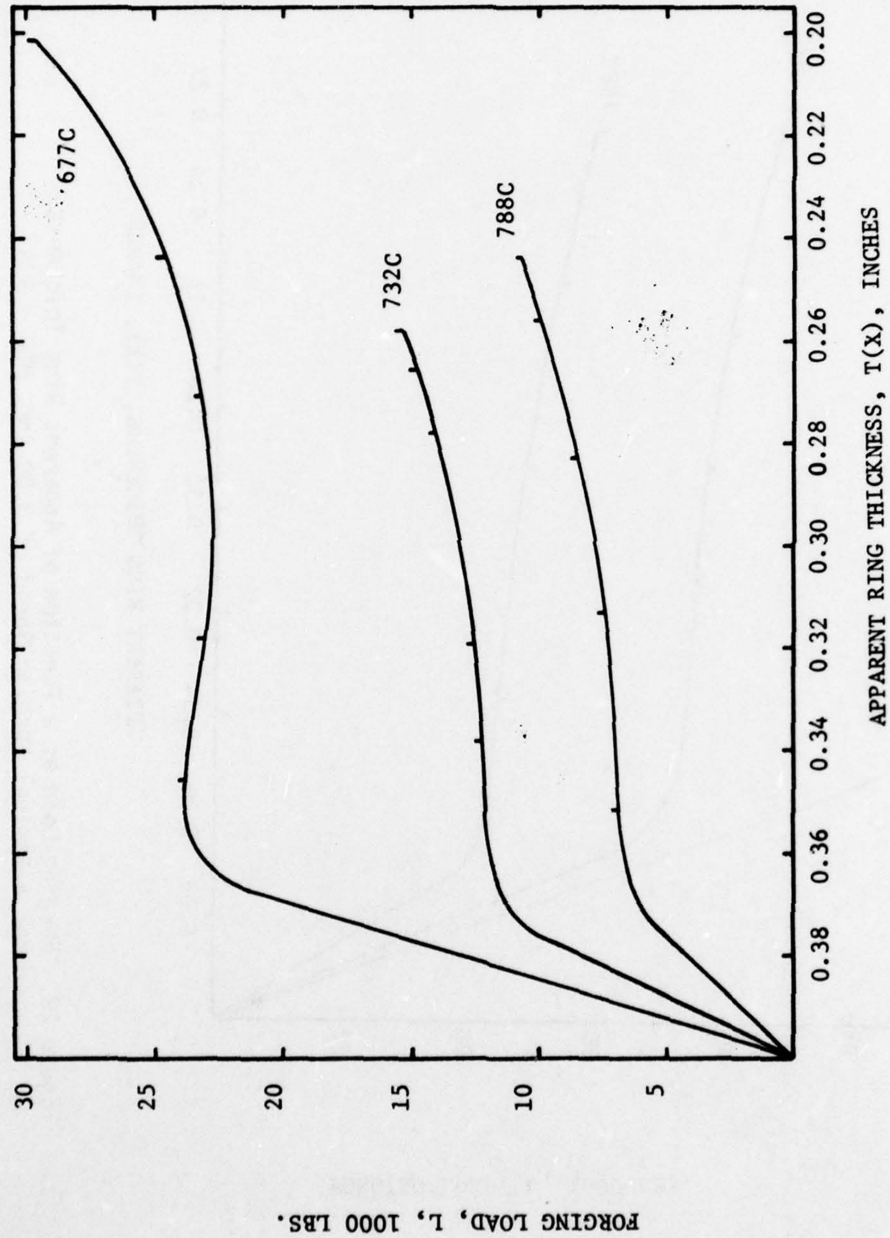

Figure 21. Forging Load as a Function of Apparent Ring Thickness for a Nominal Forging Speed of 0.03 ipm, MGD = 8μm

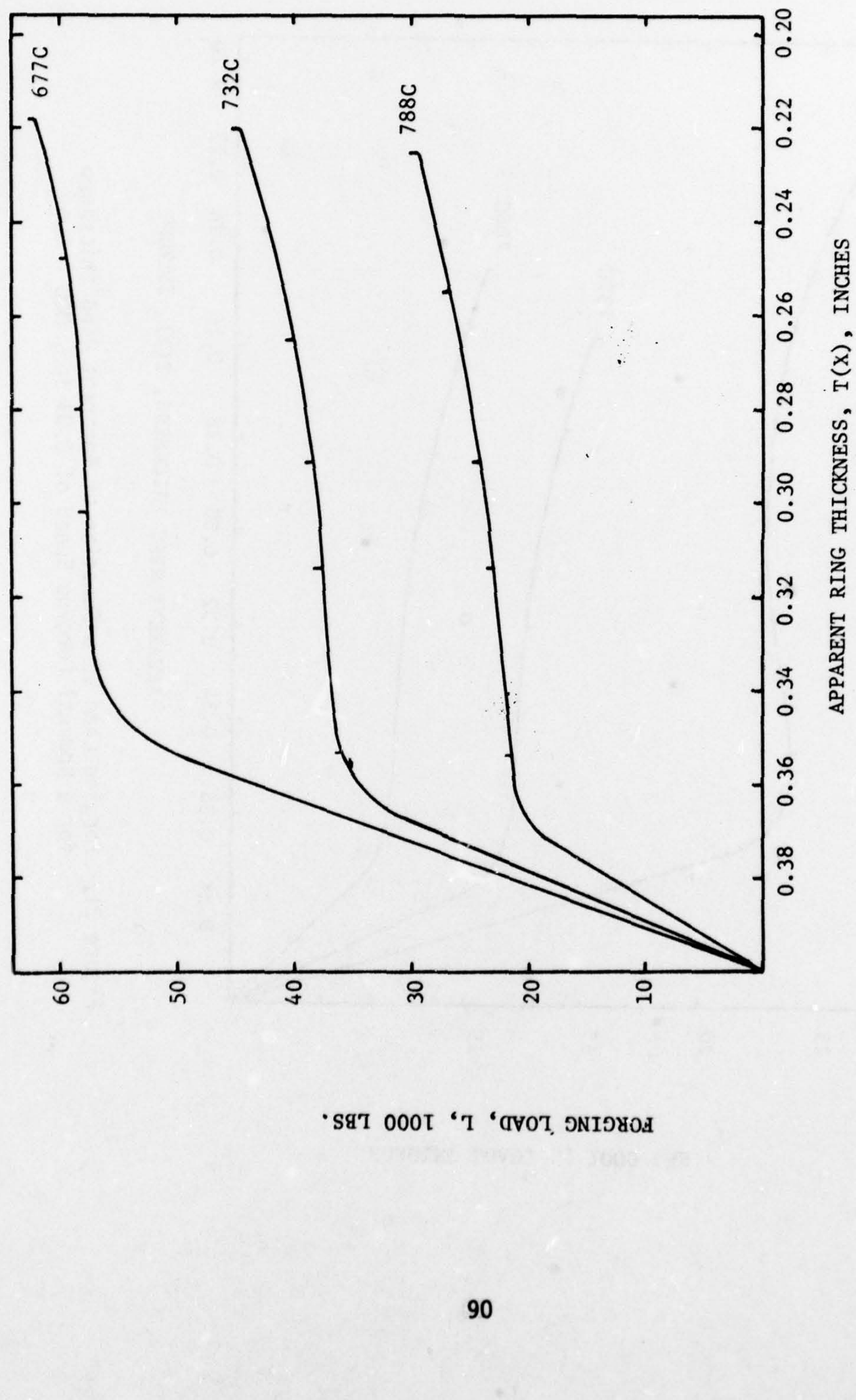

Figure 22. Forging Load as a Function of Apparent Ring Thickness for a Nominal Forging Speed of 3.00 ipm, MGD = 8μm

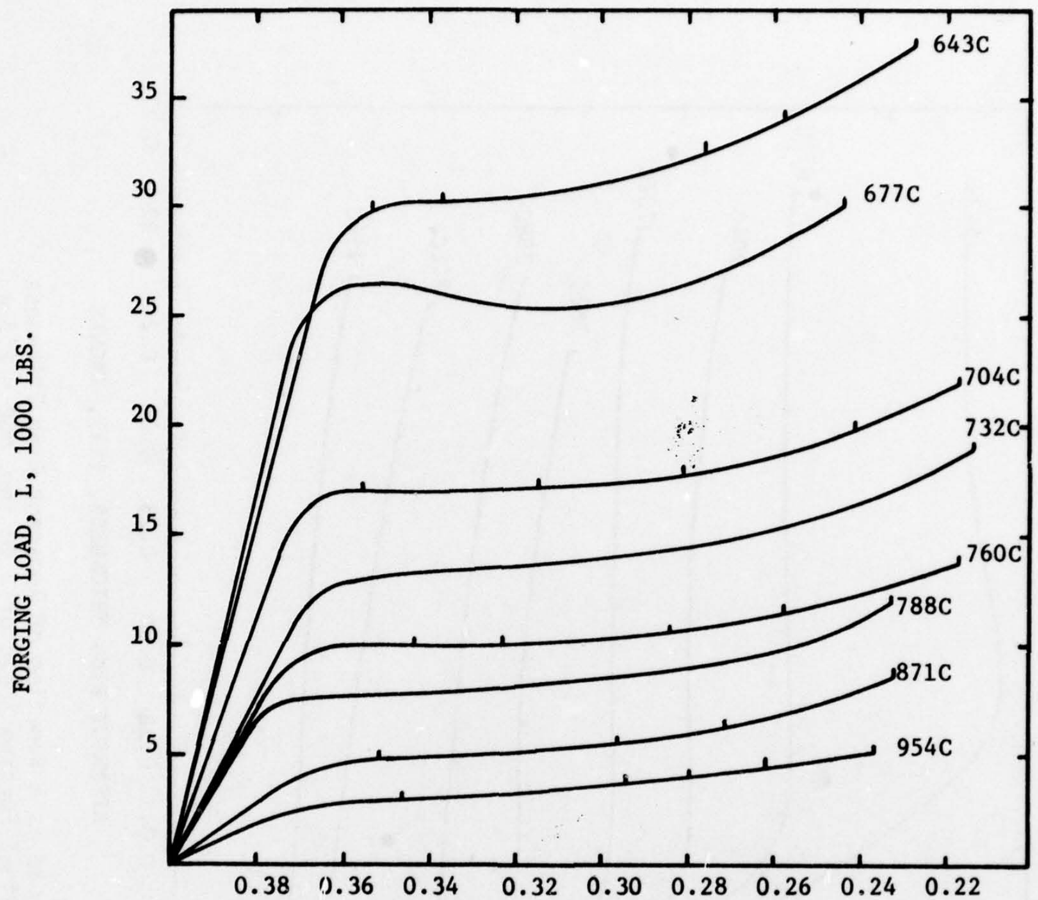

Figure 23. Forging Load as a Function of Apparent Ring Thickness for a Nominal Forging Speed of 0.03 ipm, MGD = 255μm

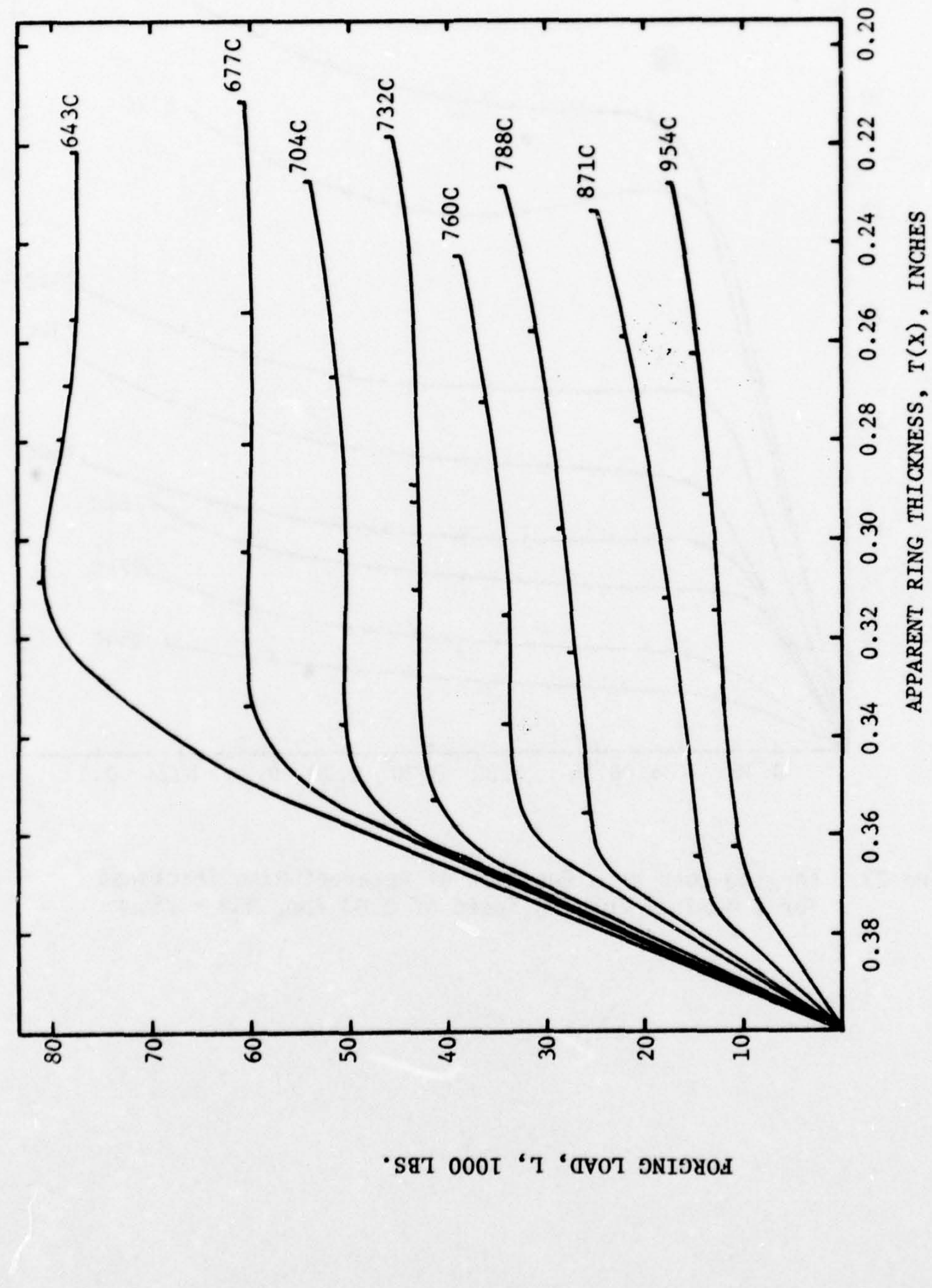

Figure 24. Forging Load as a Function of Apparent Ring Thickness for a Nominal Forging Speed of 3.00 ipm, MGD = 255μm

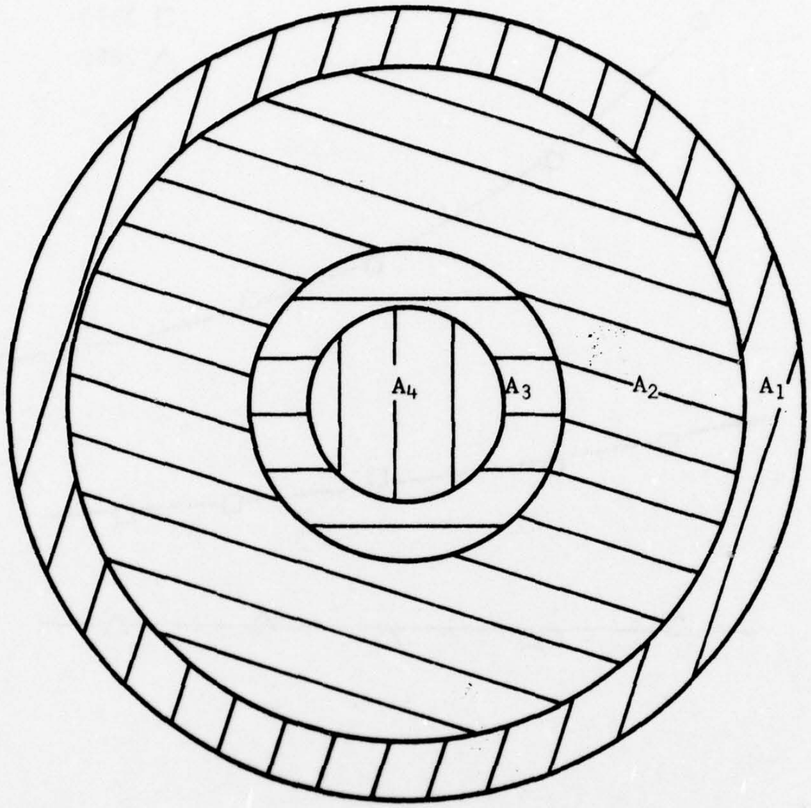

Figure 25. Schematic of Areas Measured with the Quantimet 720 Image Analyzing Computer

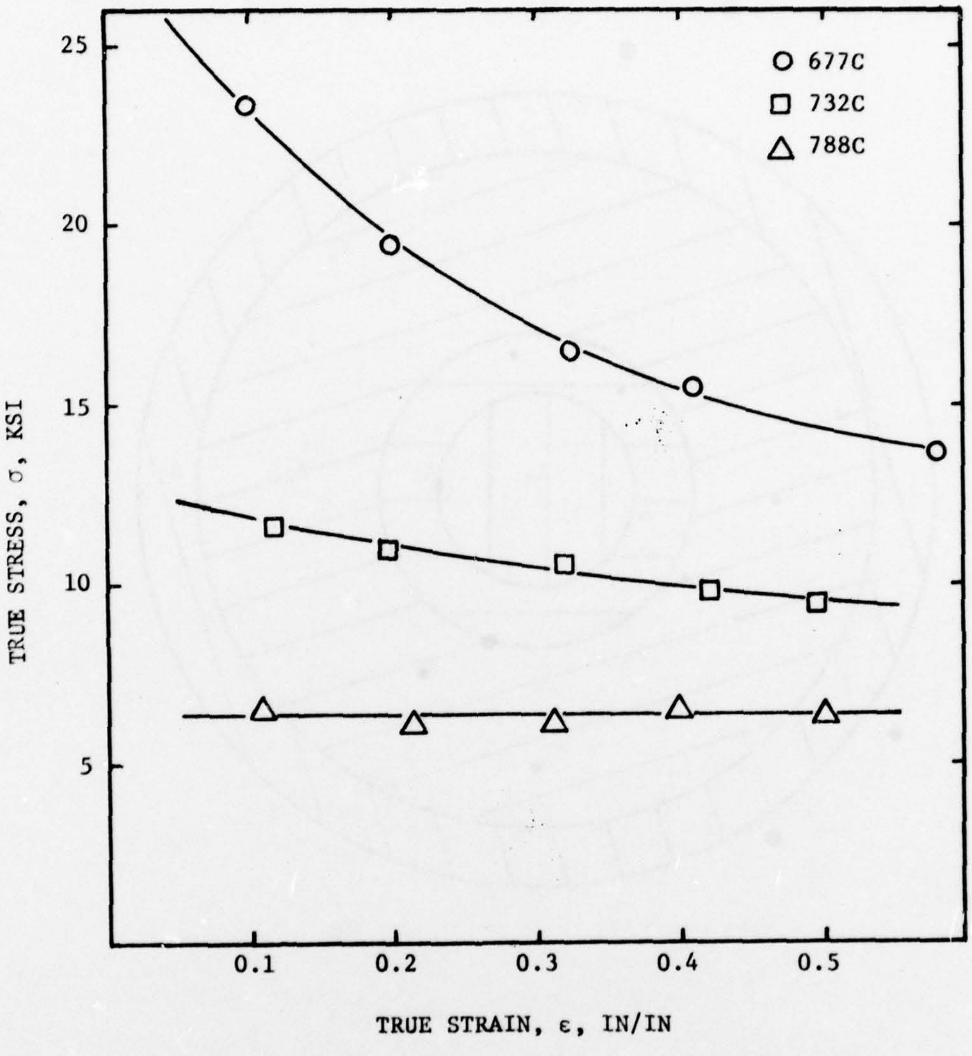

Figure 26. Stress-Strain Curves for Ti-10V-2Fe-3Al Forged Isothermally at 0.03 ipm (Nominal), MGD = 8μm

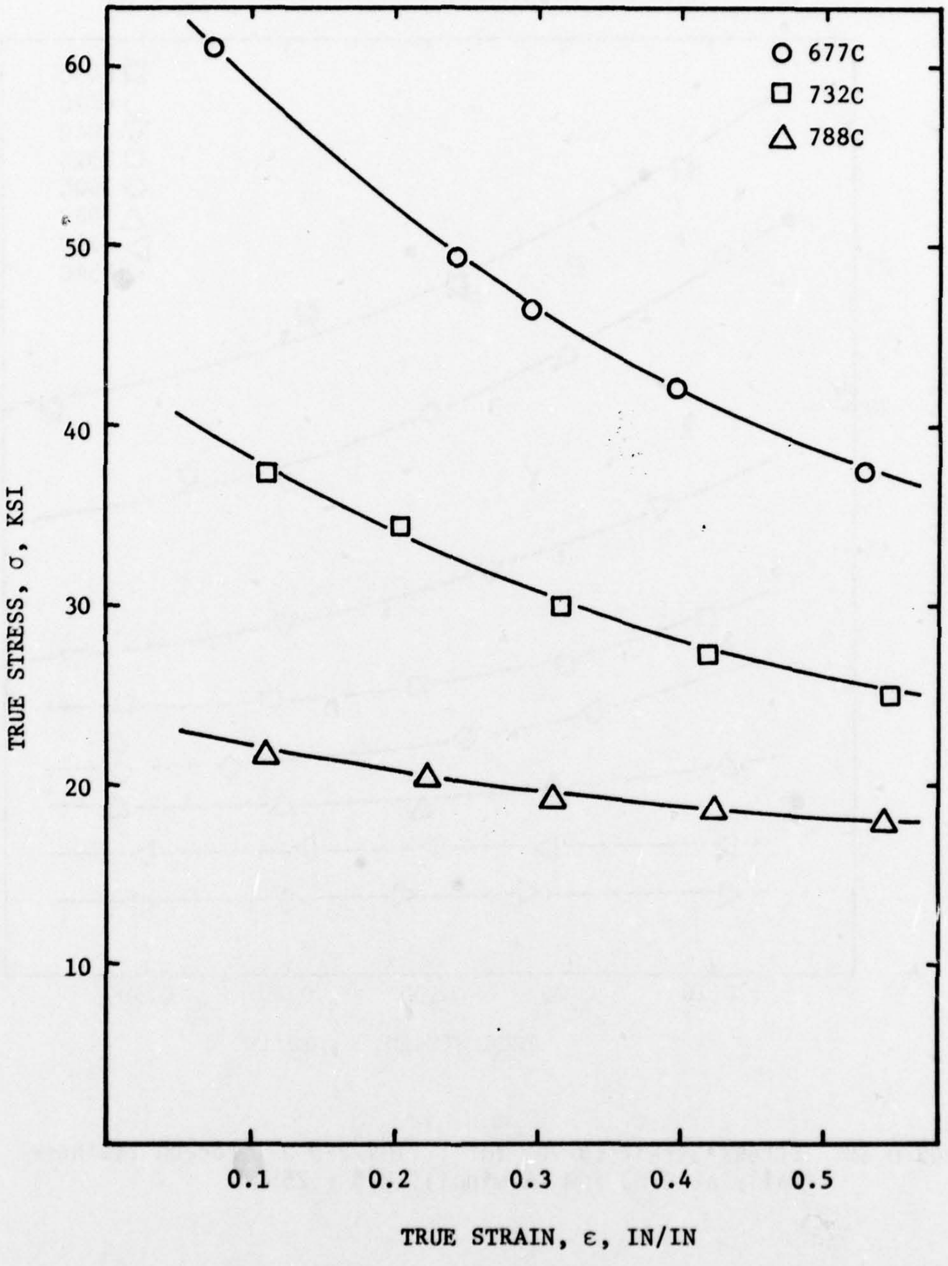

Figure 27. Stress-Strain Curves for Ti-10V-2Fe-3Al Forged Isothermally at 3.00 ipm (Nominal), MGD = 8μm

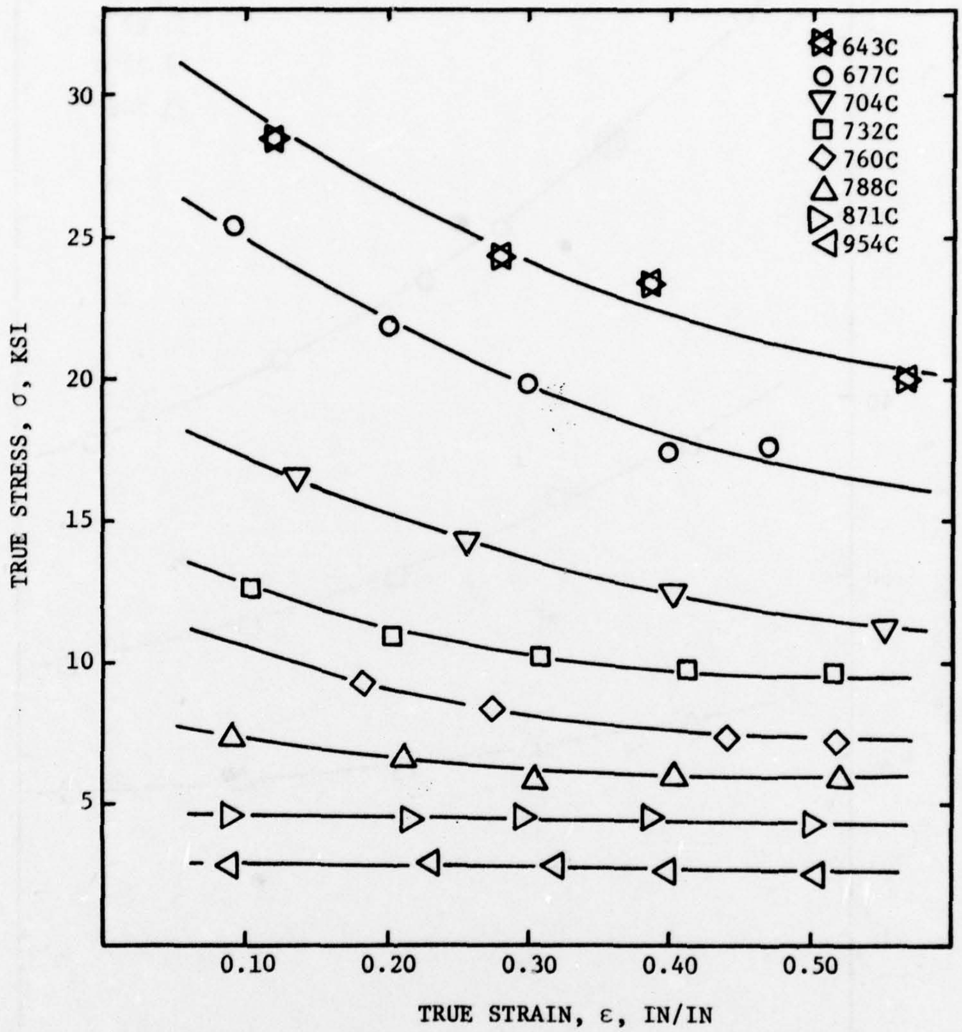

Figure 28. Stress-Strain Curves for Ti-10V-2Fe-3Al Forged Isothermally at 0.03 ipm (Nominal), MGD = 255μm

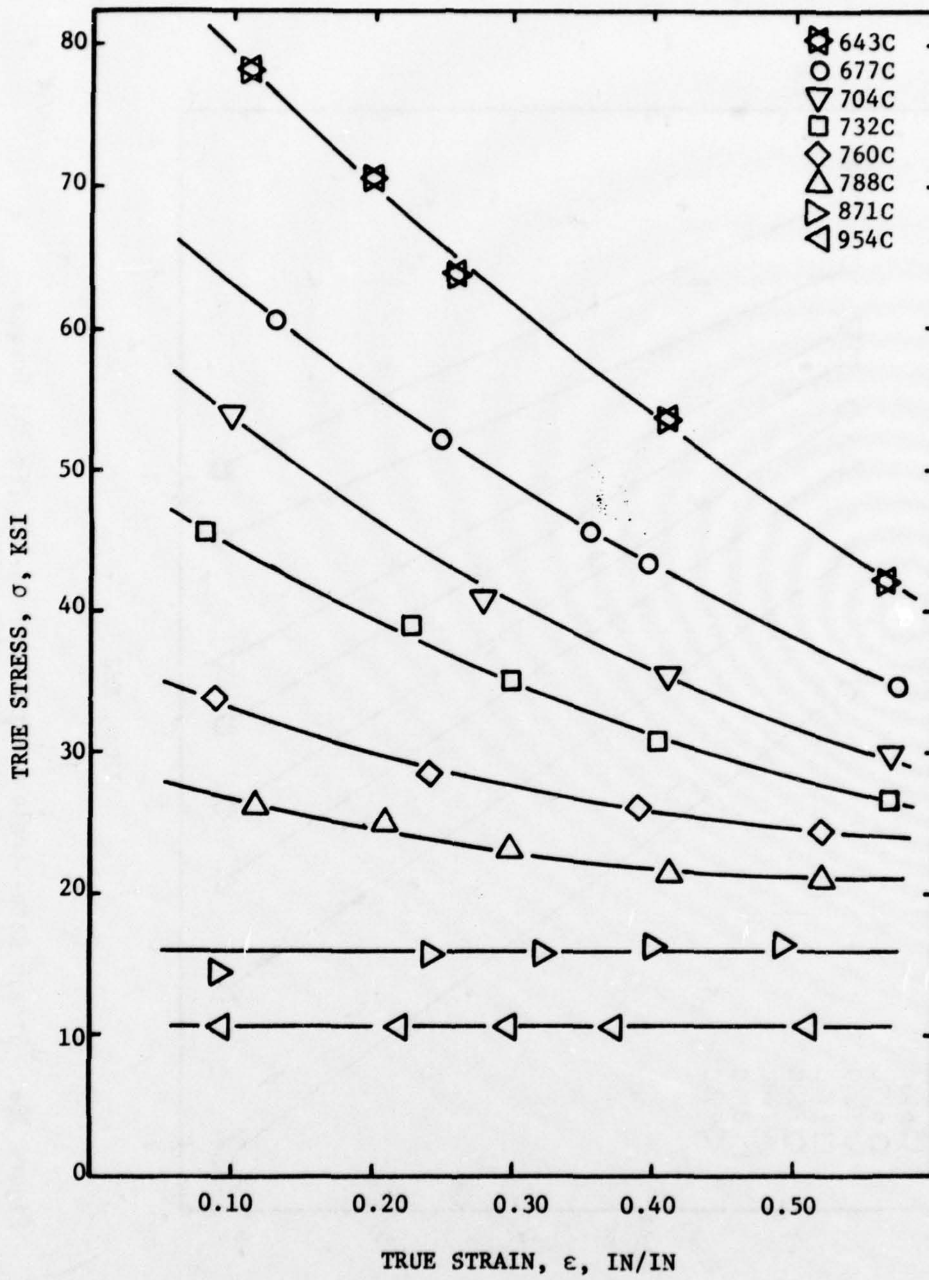

Figure 29. Stress-Strain Curves for Ti-10V-2Fe-3Al Forged Isothermally at 3.00 ipm (Nominal), MGD = 255μm

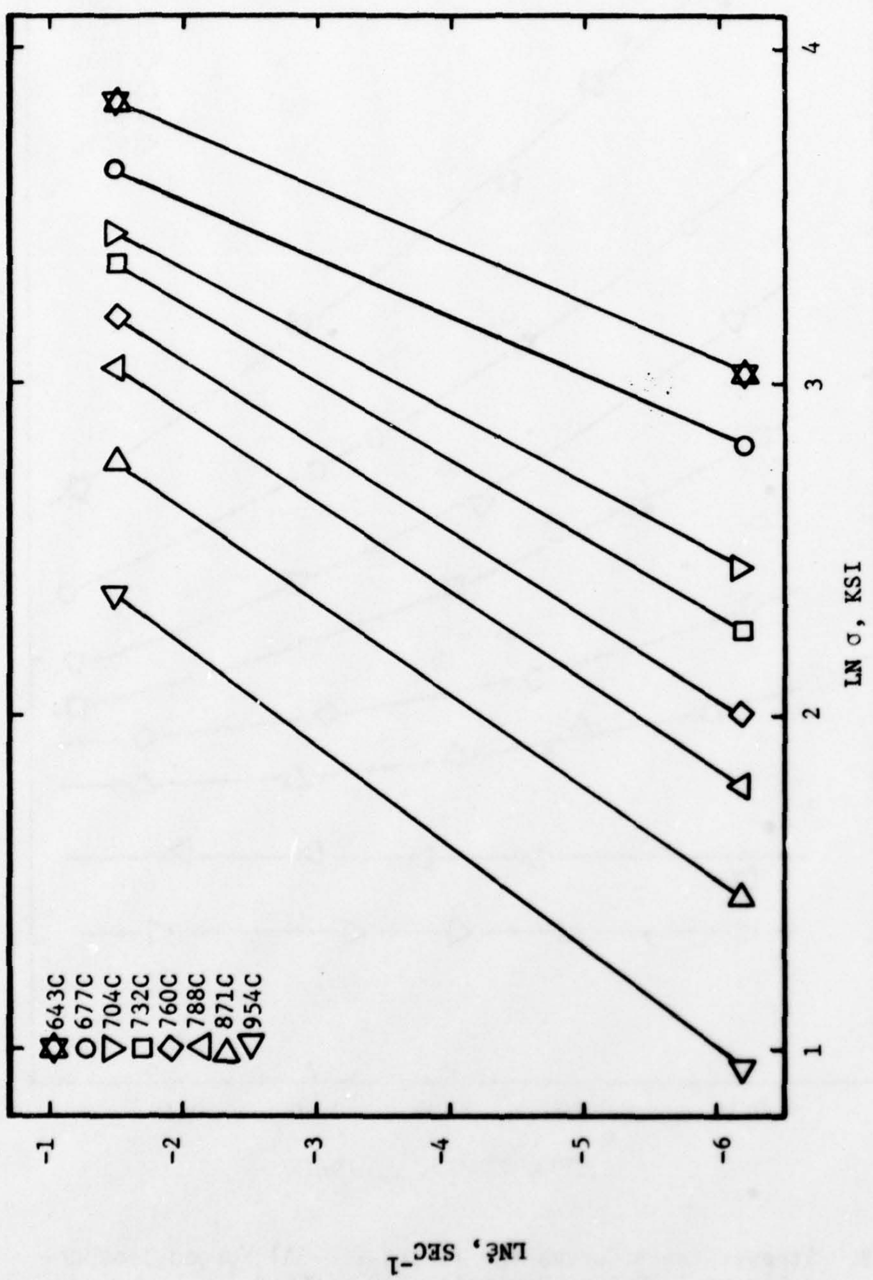

Figure 30a. Strain Rate-Stress Relation for Ti-10V-2Fe-3Al Forged Isothermally to 0.50 in/in, MGD = 255μm

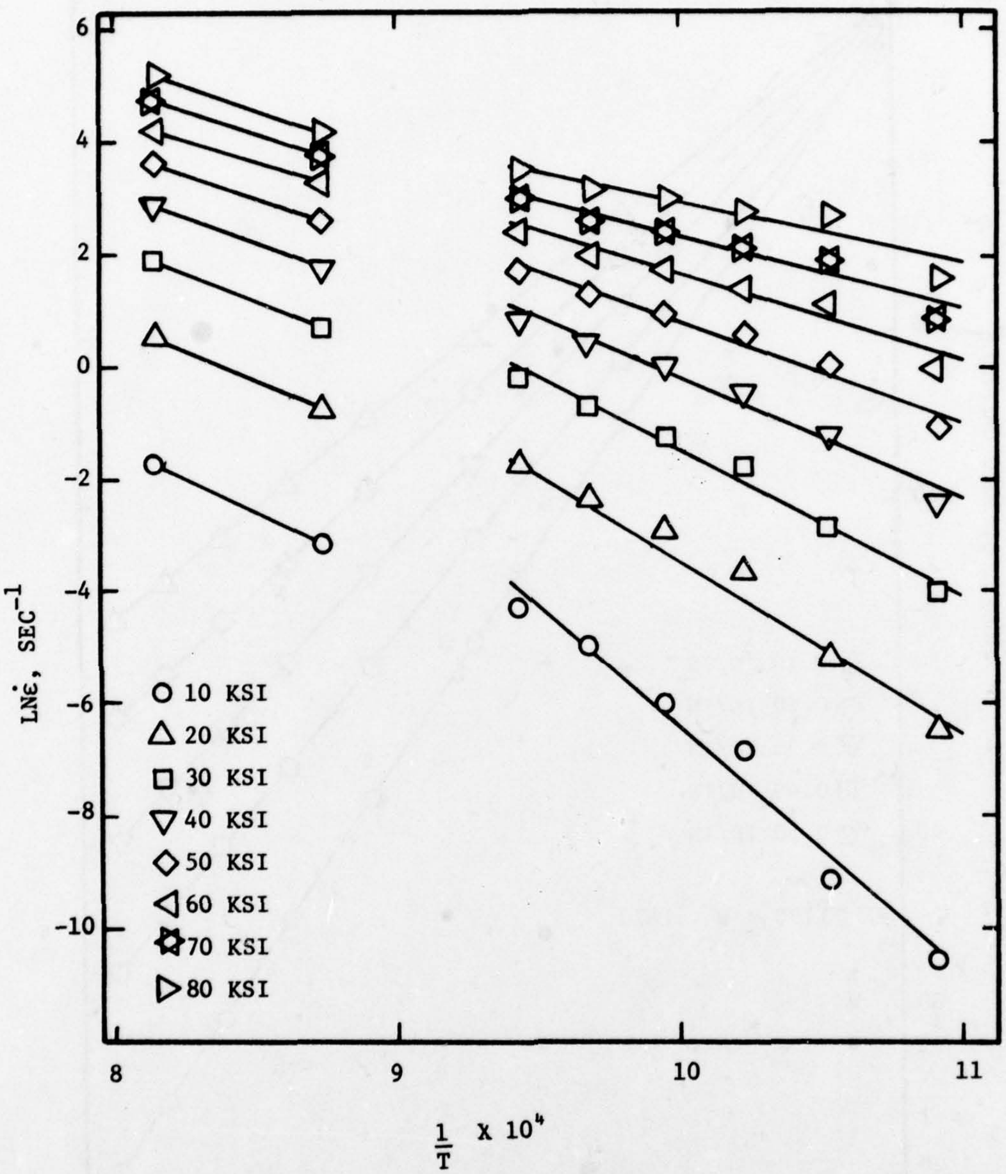

Figure 30b. Strain Rate-Reciprocal Absolute Temperature for Ti-10V-2Fe-3Al Forged Isothermally to 0.50 in/in. Data Used to Calculate Apparent Activation Energy, MGD = 255μm

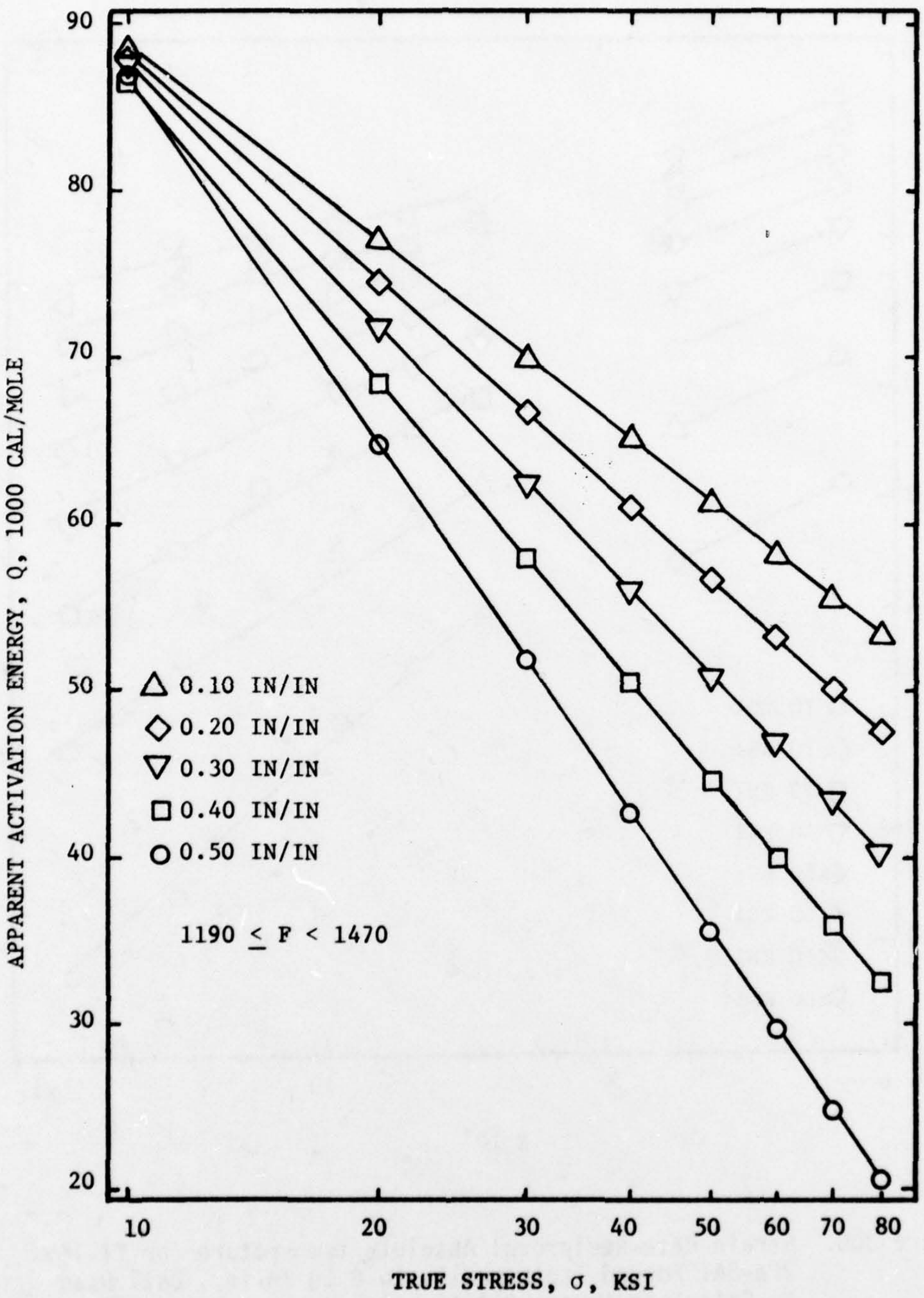

Figure 31. Stress Dependency of the Apparent Activation Energy at Various Strains for Ti-10V-2Fe-3Al Forged Isothermally in the Temperature Region 643 ≤ C < 799, MGD = 255μm

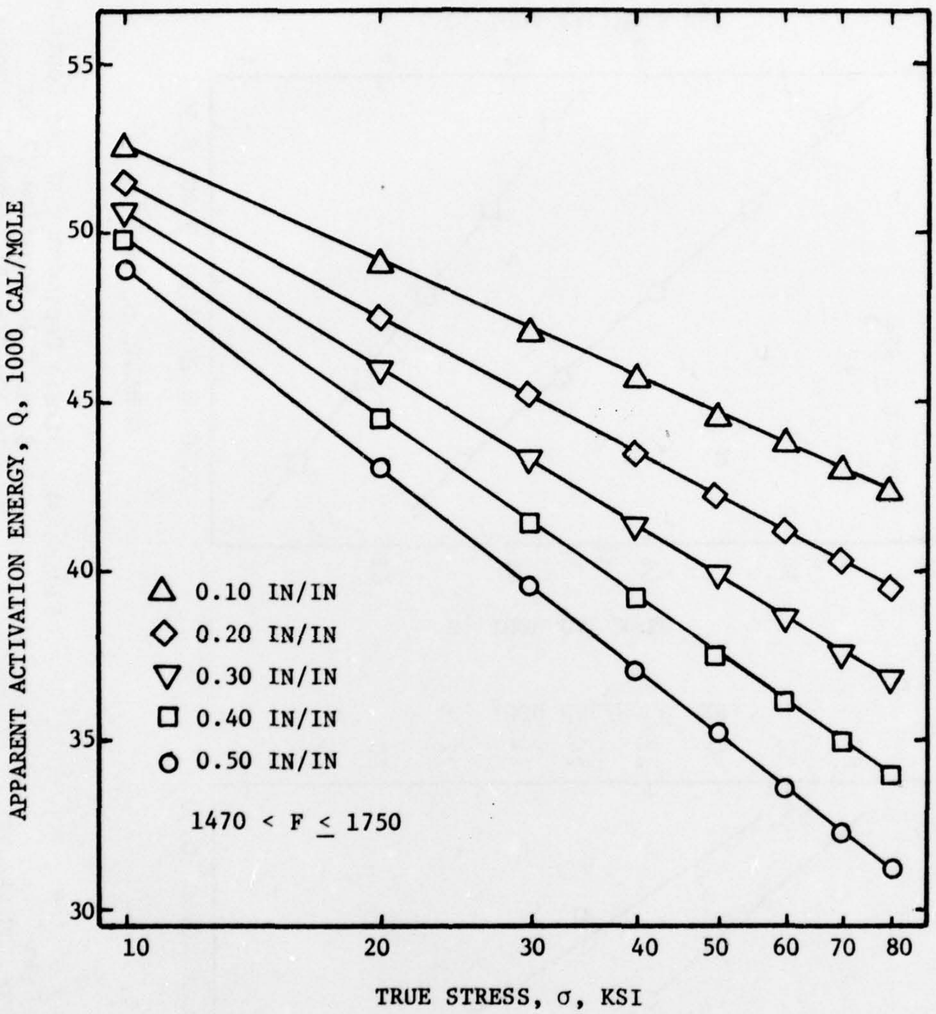

Figure 32. Stress Dependency of the Apparent Activation Energy at Various Strains for Ti-10V-2Fe-3Al Forged Isothermally in the Temperature Region 799 < C ≤ 954, MGD = 255μm

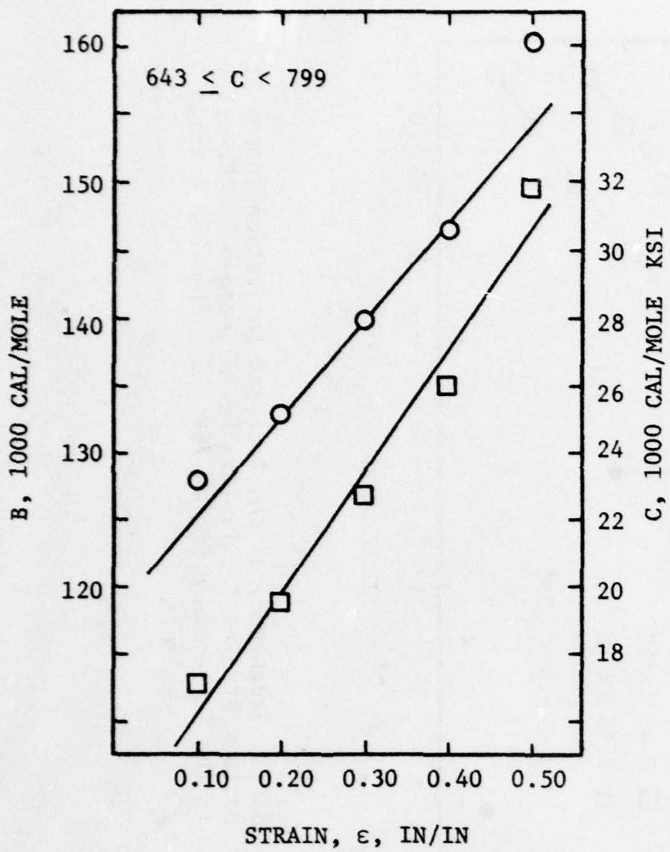

Figure 33. Strain Dependency of the Constants B and C in Equation 77 for Ti-10V-2Fe-3Al Forged Isothermally in the Temperature Region 643 $\leq$ C < 799, MGD = 255μm

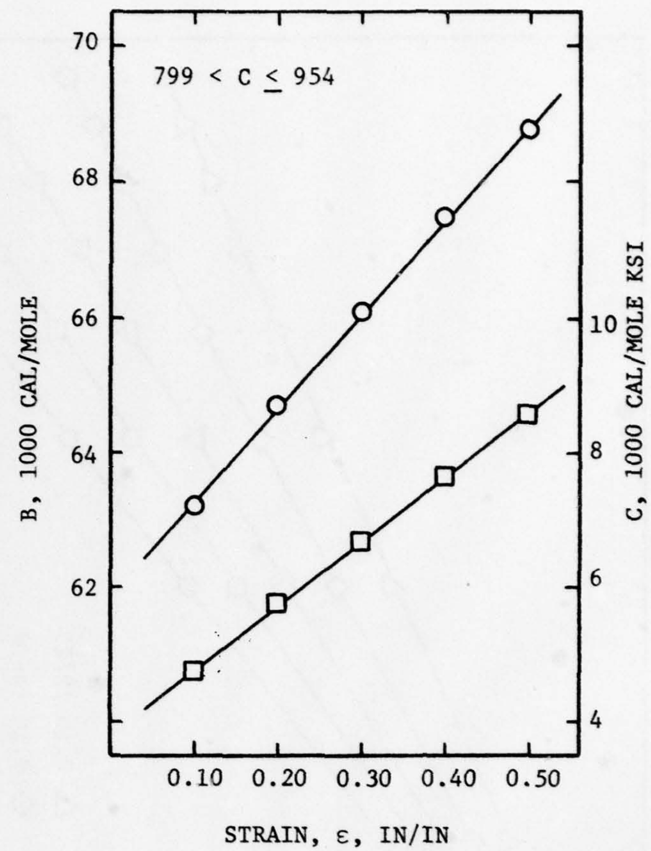

Figure 34. Strain Dependency of the Constants B and C in Equation 77 for Ti-10V-2Fe-3Al Forged Isothermally in the Temperature Region 799 < C $\leq$ 954, MGD = 255μm

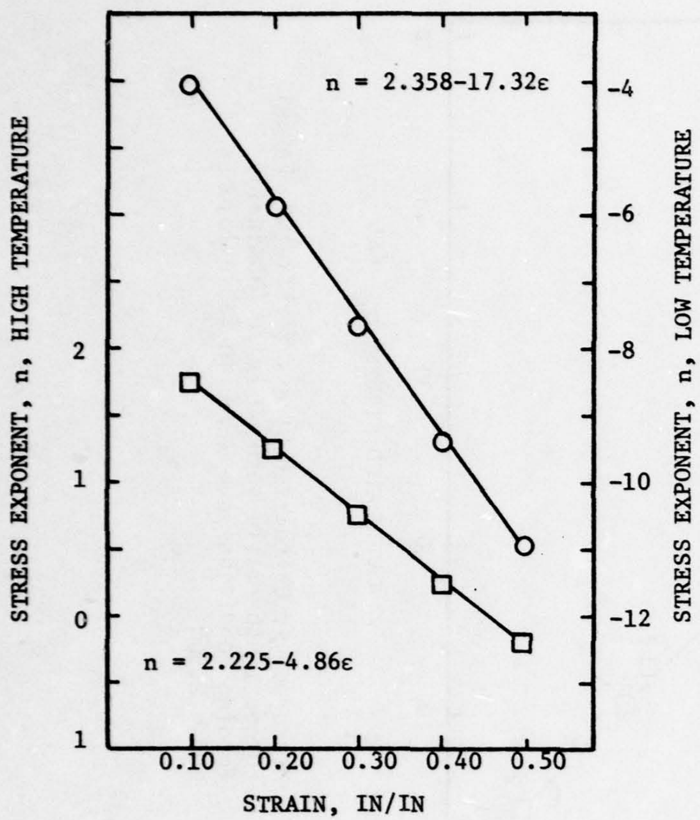

Figure 35. Strain Dependency of the Stress Exponent n for the High Temperature (□) and Low Temperature (○) Regions for Isothermally Forged Ti-10V-2Fe-3Al, MGD = 255μm

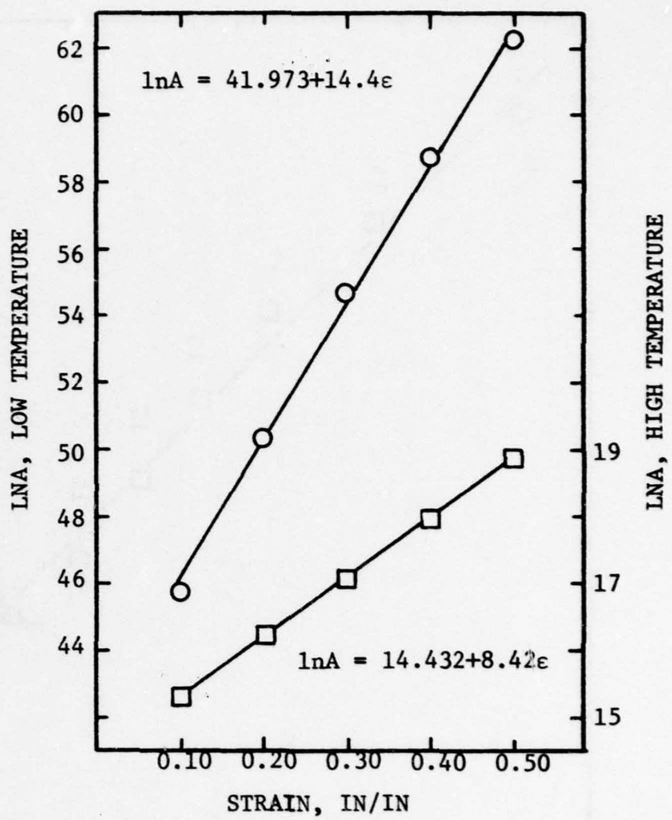

Figure 36. Strain Dependency of the Pre-Exponential A for the High Temperature (□) and Low Temperature (○) Regions for Isothermally Forged Ti-10V-2Fe-3Al, MGD = 255μm

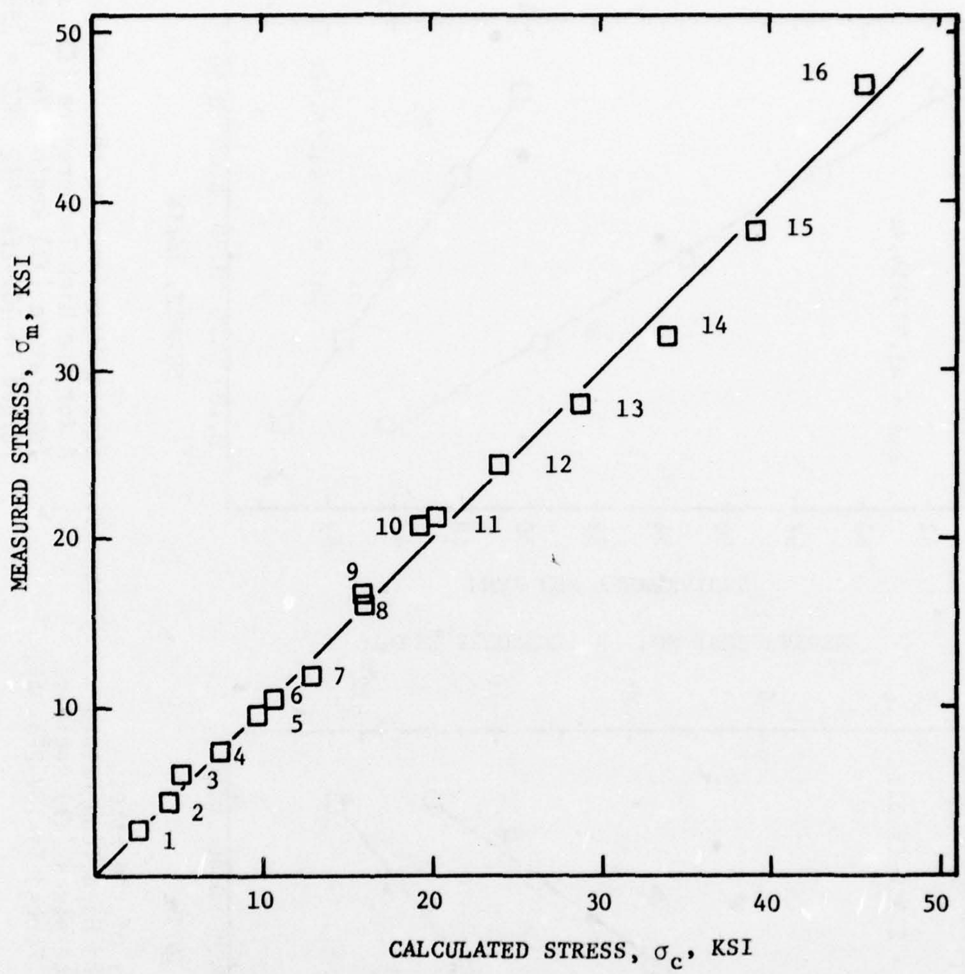

Figure 37. Measured vs. Calculated Stress for Ti-10V-2Fe-3Al Forged Isothermally to 0.50 In/In (Nominal). Forging Conditions are Given in Table 13, MGD = 255μm

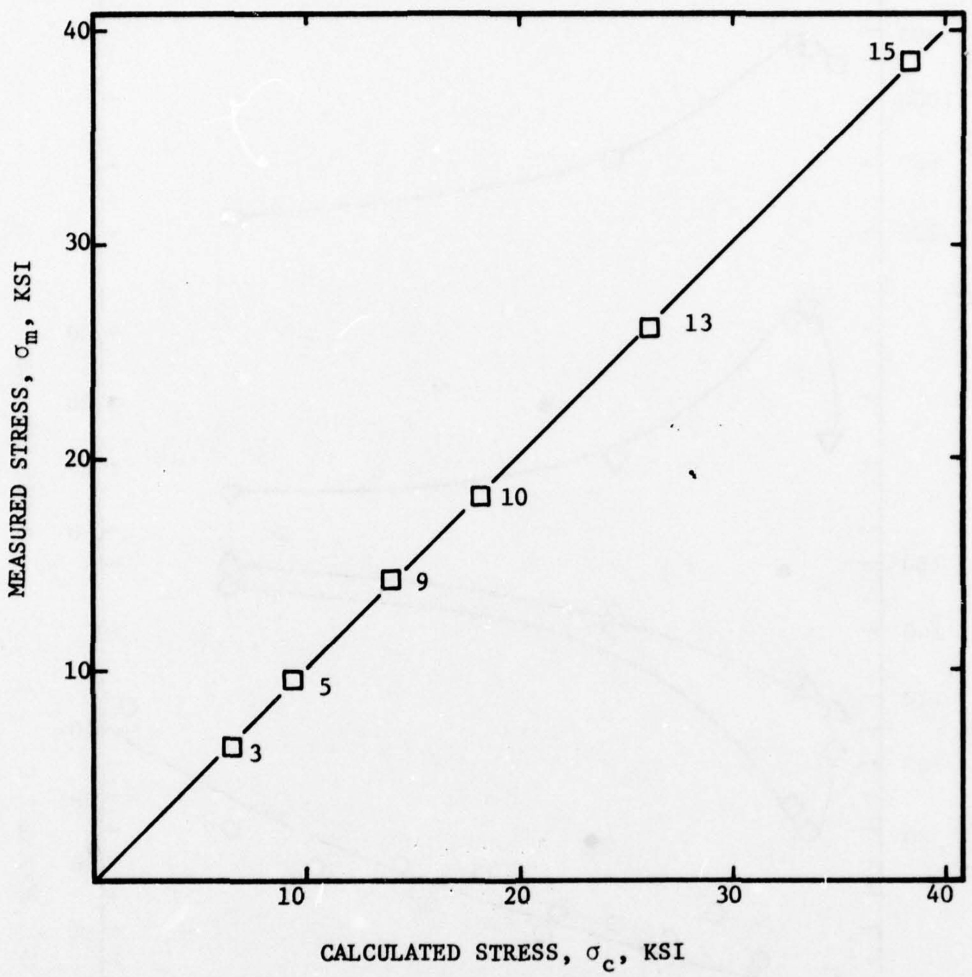

Figure 38. Measured vs. Calculated Stress for Ti-10V-2Fe-3Al Forged Isothermally to 0.50 In/In (Nominal). Forging Conditions are Given in Table 14, MGD = 8μm

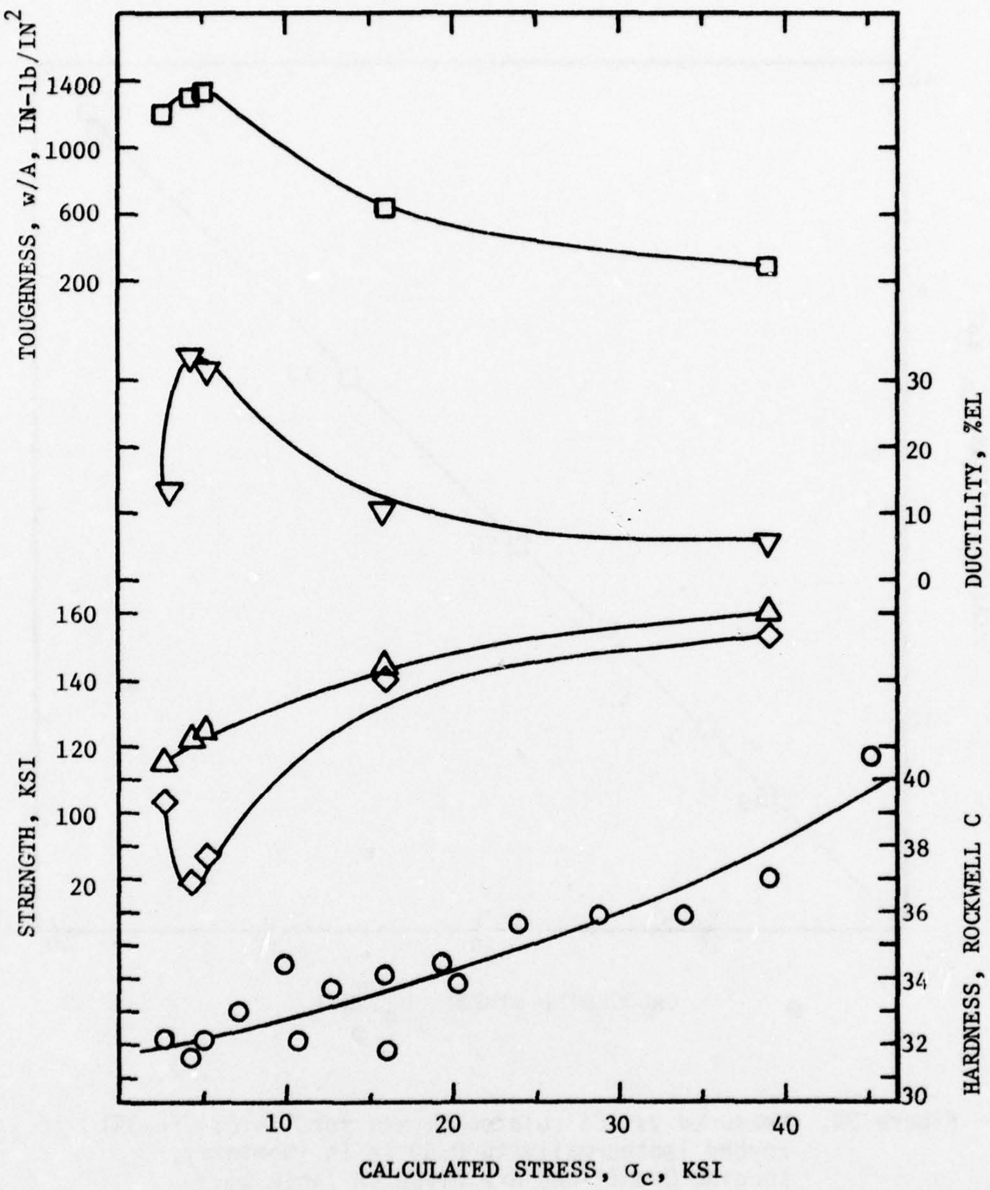

Figure 39. Room Temperature Mechanical Properties for Ti-10V-2Fe-3Al Isothermally Forged to 0.50 In/In (Nominal) Plotted as a Function of Calculated Flow Stress, σ_c, MGD = 255μm. Fracture Toughness, W/A (□); Ductility, % Elongation, (△); Ultimate Strength, UTS (△), Yield Strength, 0.2% Offset, YS (◇); Hardness, Rockwell C (○)

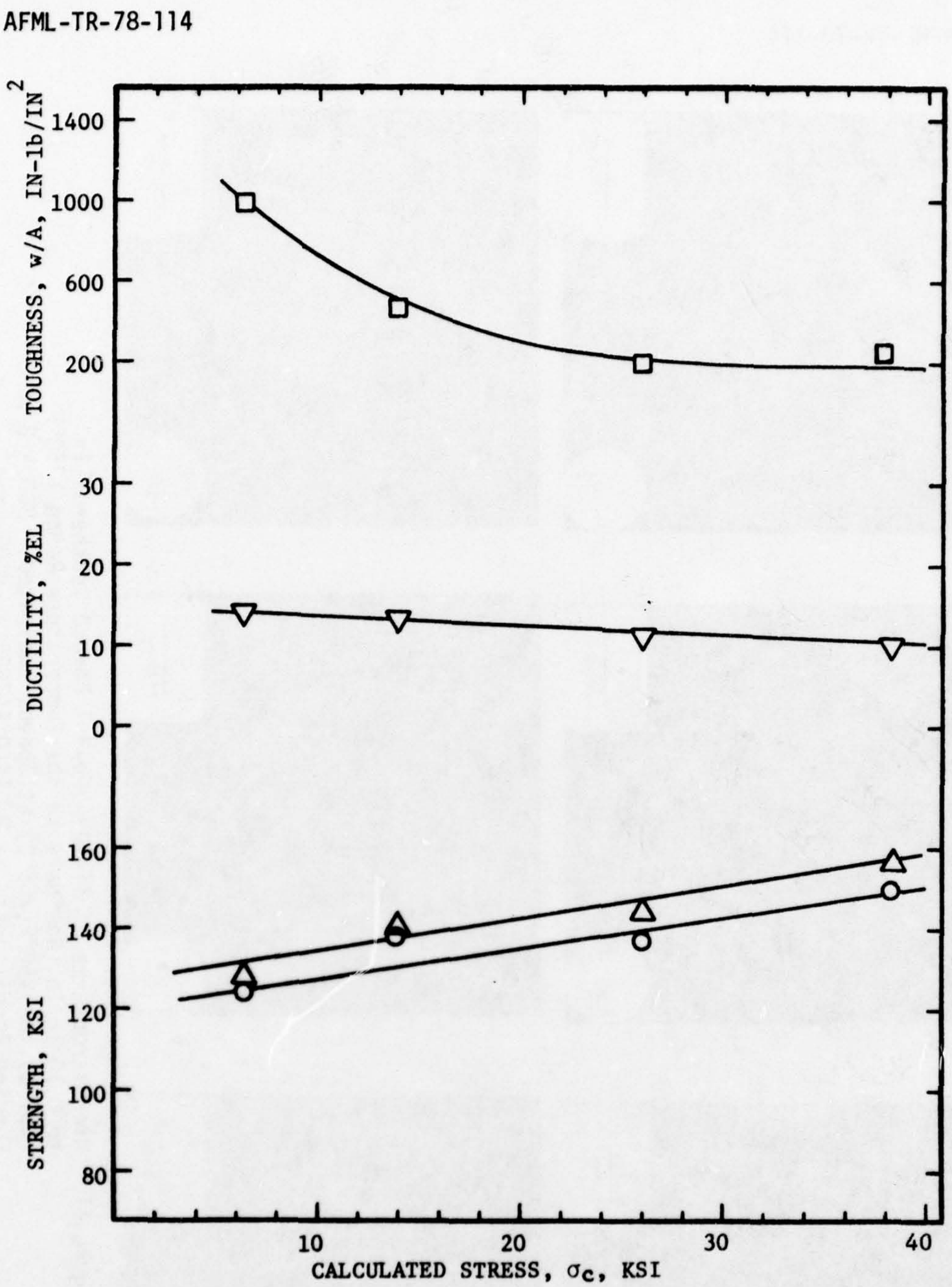

Figure 40. Room Temperature Mechanical Properties for Ti-10V-2Fe-3Al Isothermally Forged to 0.50 In/In (Nominal) Plotted as a Function of Calculated Flow Stress, σ_c, MGD = 8μm. Fracture Toughness, W/A, (□); Ductility, % Elongation (△); Ultimate Strength, UTS (△); Yield Strength, 0.20% Offset, YS (○)

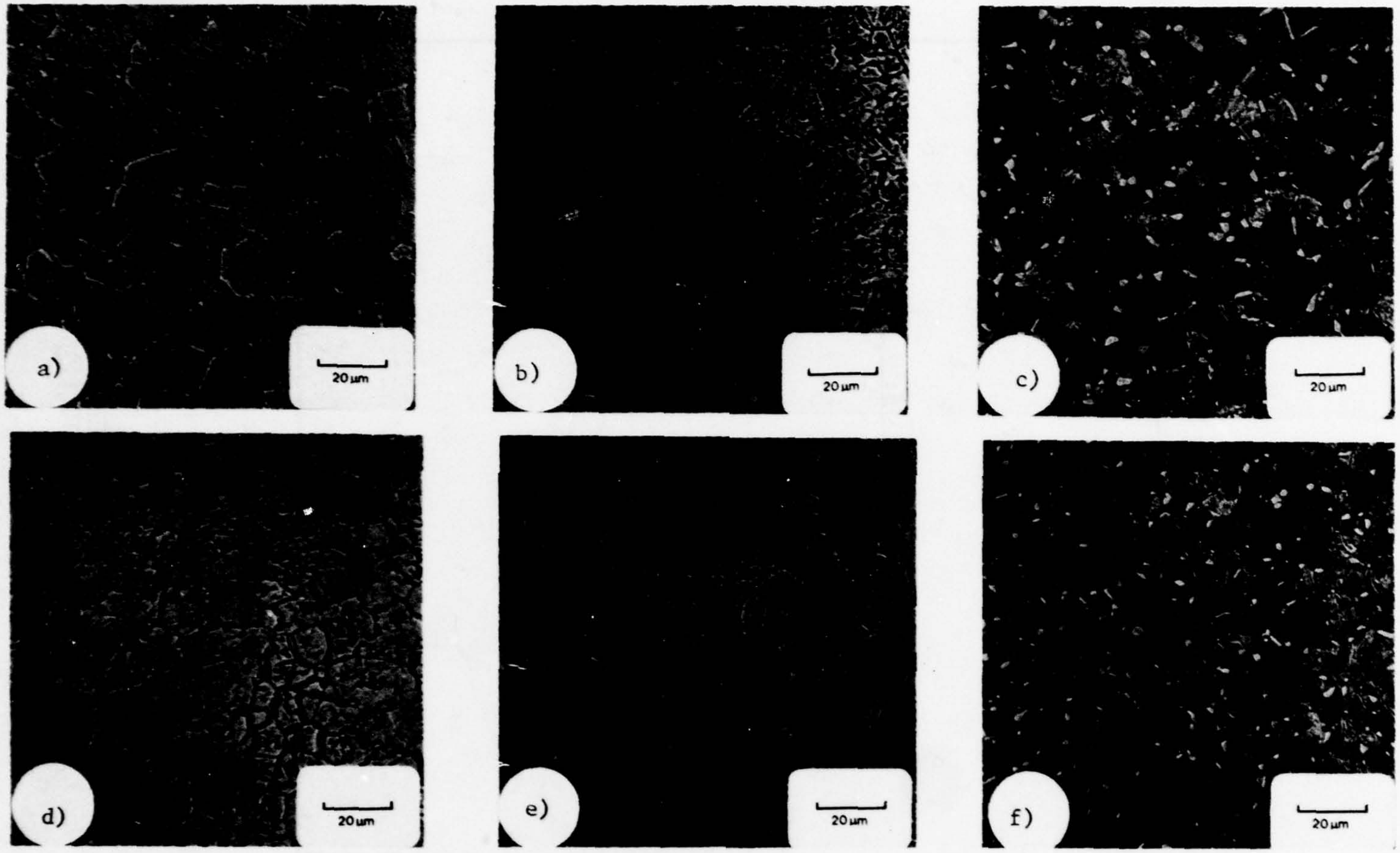

Figure 41. Microstructures of Ti-10V-2Fe-3Al Forged Isothermally to 0.10 In/In (Nominal) in the Temperature Range 1250°F (677°C) to 1450°F(788°C) at Speeds Indicated. MGD = 8 µm. Forging Conditions: a) 3, 1450°F(788°C), 0.03 ipm; b) 5, 1350°F(732°C), 0.03 ipm; c) 9, 1250°F(677°C), 0.03 ipm; d) 10, 1450°F(788°C), 3.0 ipm; e) 13, 1350°F(732°C), 3.0 ipm; f) 15, 1250°F(677°C), 3.0 ipm. Kroll's Reagent.

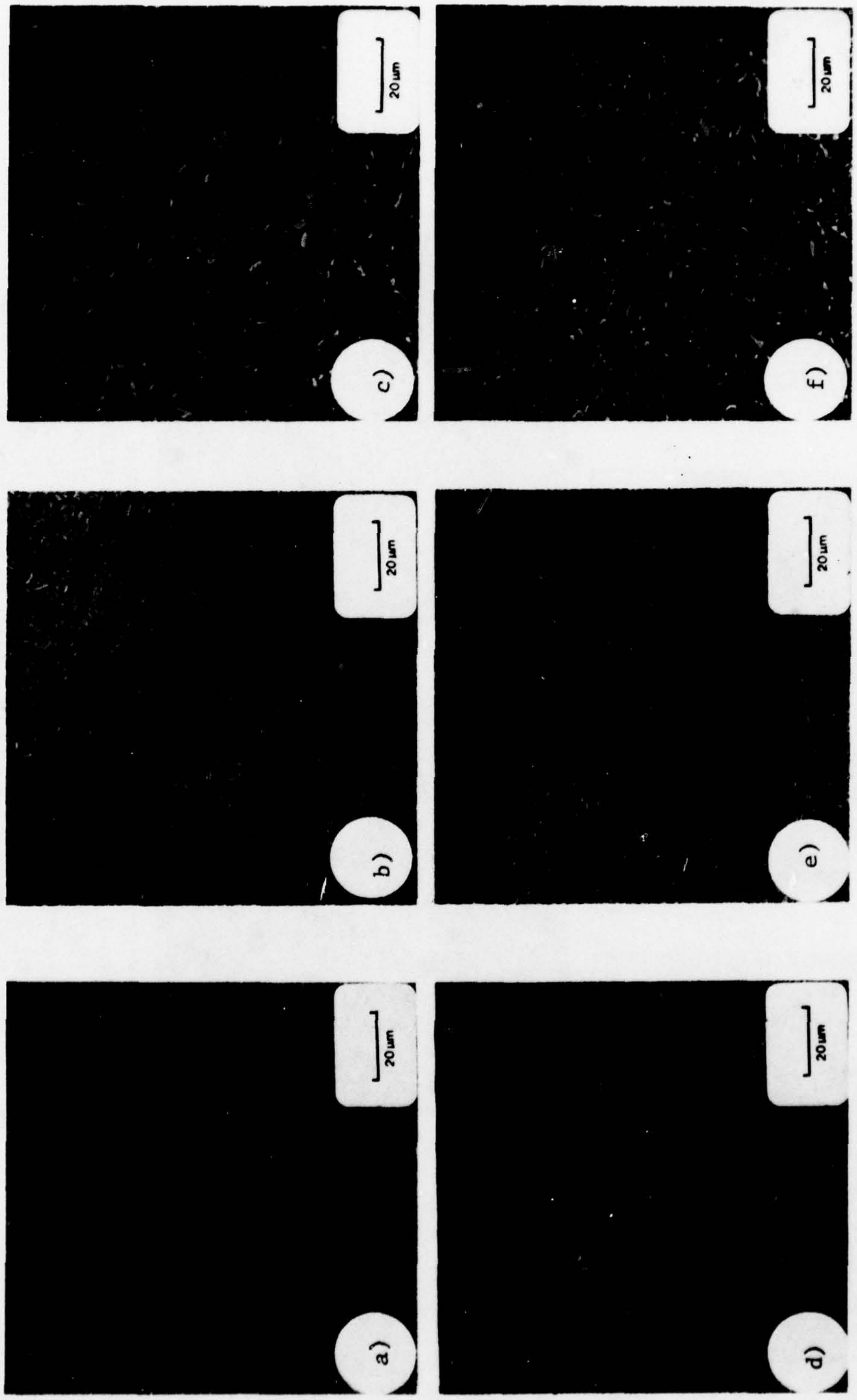

Figure 42. Microstructures of Ti-10V-2Fe-3Al Forged Isothermally to 0.50 In/In (Nominal in the Temperature Range 1250°F (677°C) to 1450°F(788°C) at Speeds Indicated. MGD = 8μm. Forging Conditions: a) 3, 1450°F(788°C), 0.03 ipm; b) 5, 1350°F(732°C), 0.03 ipm; c) 9, 1250°F(677°C), 0.03 ipm; d) 10, 1450°F(788°C), 3.0 ipm; e) 13, 1350°F (732°C), 3.0 ipm; f) 15, 1250°F(677°C), 3.0 ipm. Kroll's Reagent.

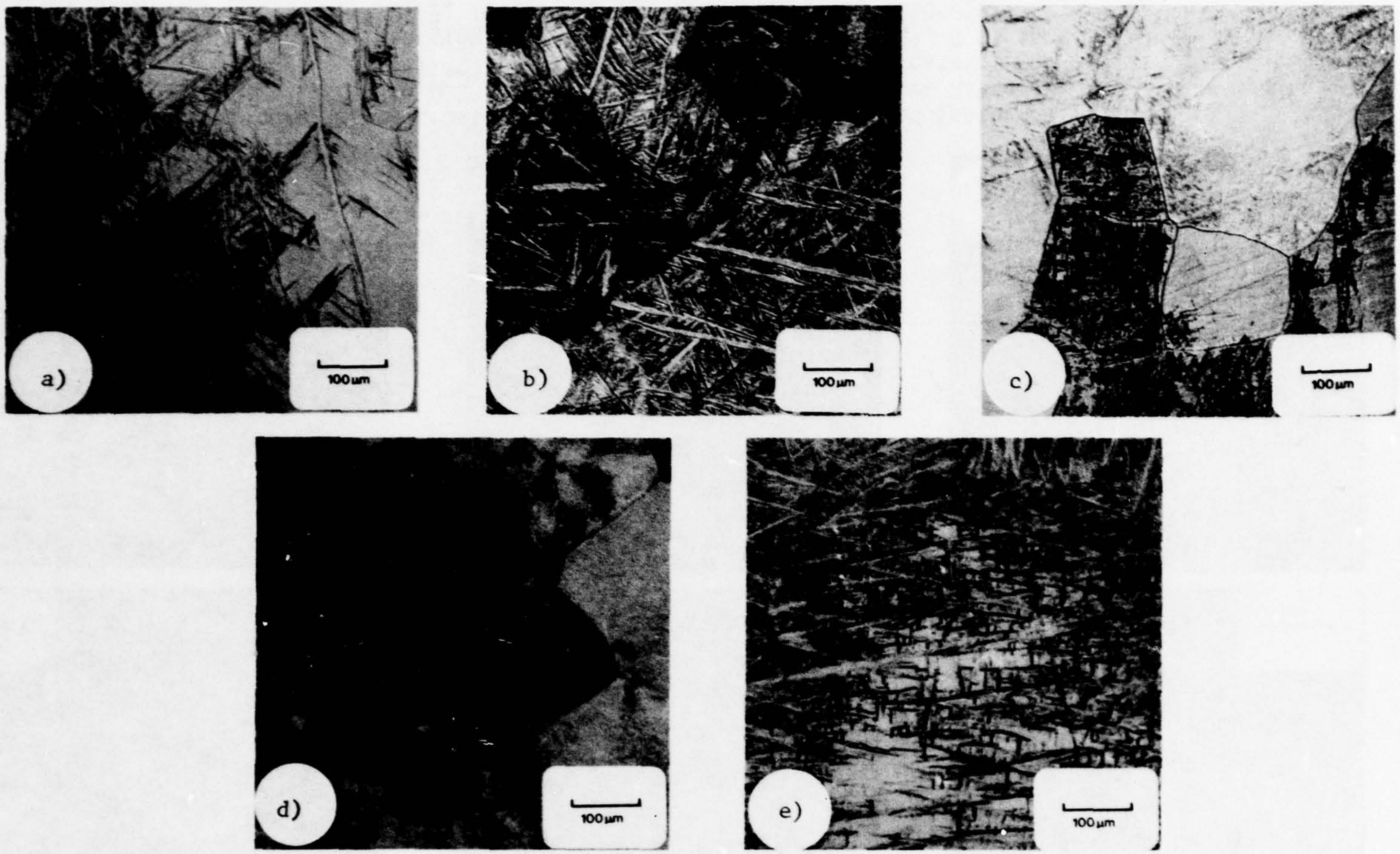

Figure 43. Microstructures of Ti-10V-2Fe-3Al Forged Isothermally to 0.10 In/In (Nominal) in the Temperature Range 1250°F (677°C) to 1750°F(954°C) at Speeds Indicated. MGD = 255μm. Forging Conditions: a) 1, 1750°F(954°C), 0.03 ipm; b) 2, 1600°F(871°C), 0.03 ipm; c) 3, 1450°F(788°C) 0.03 ipm; d) 5, 1350°F(732°C), 0.03 ipm; e) 6, 1750°F (954°C), 3.0 ipm. Kroll's Reagent.

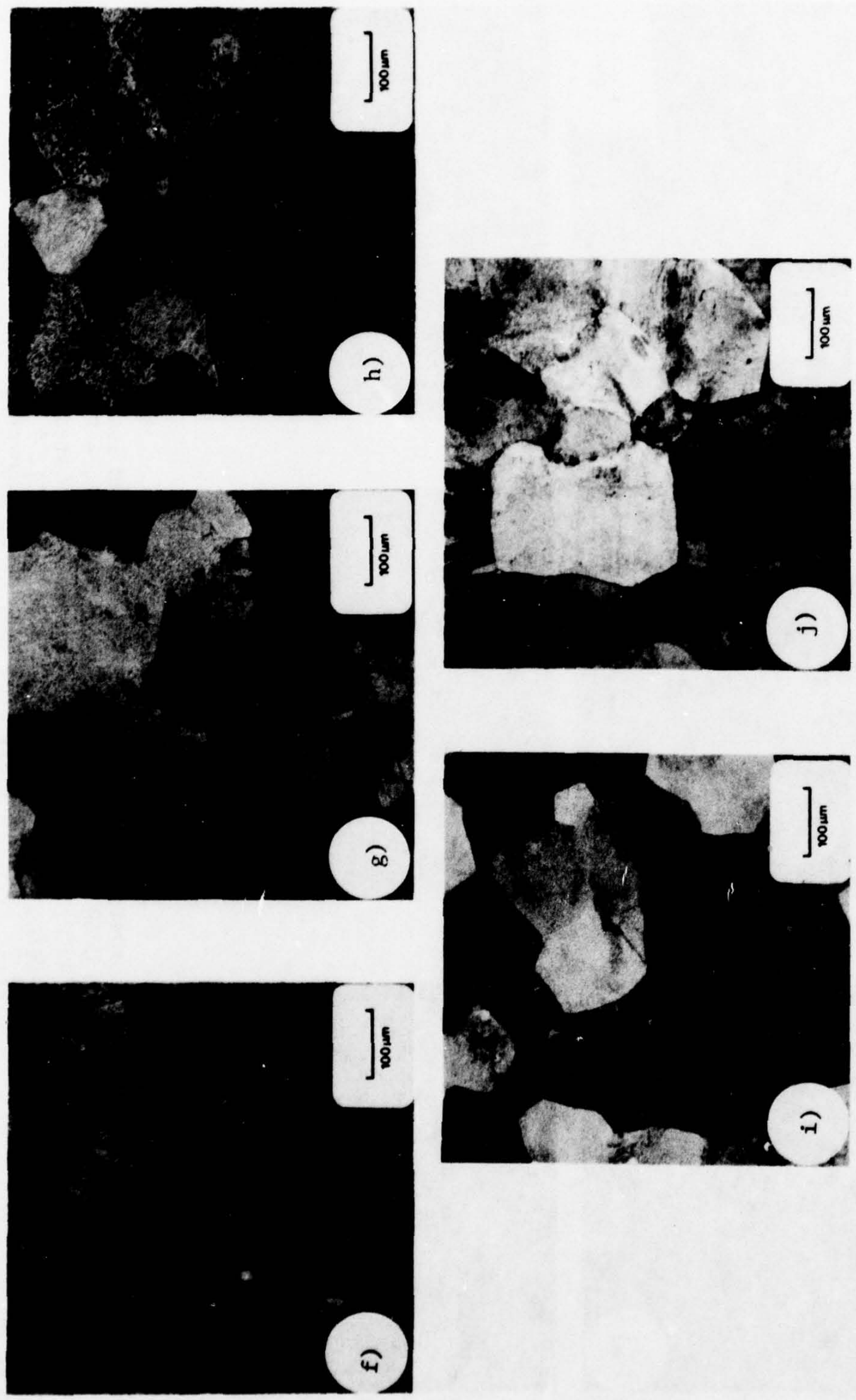

f) 8, 1600°F(871°C) 3.0 ipm; g) 9, 1250°F(677°C), 0.03 ipm; h) 10, 1450°F(788°C), 3.0 ipm; i) 13, 1350°F(732°C), 3.0 ipm; j) 15, 1250°F(677°C), 3.0 ipm. Kroll's Reagent.

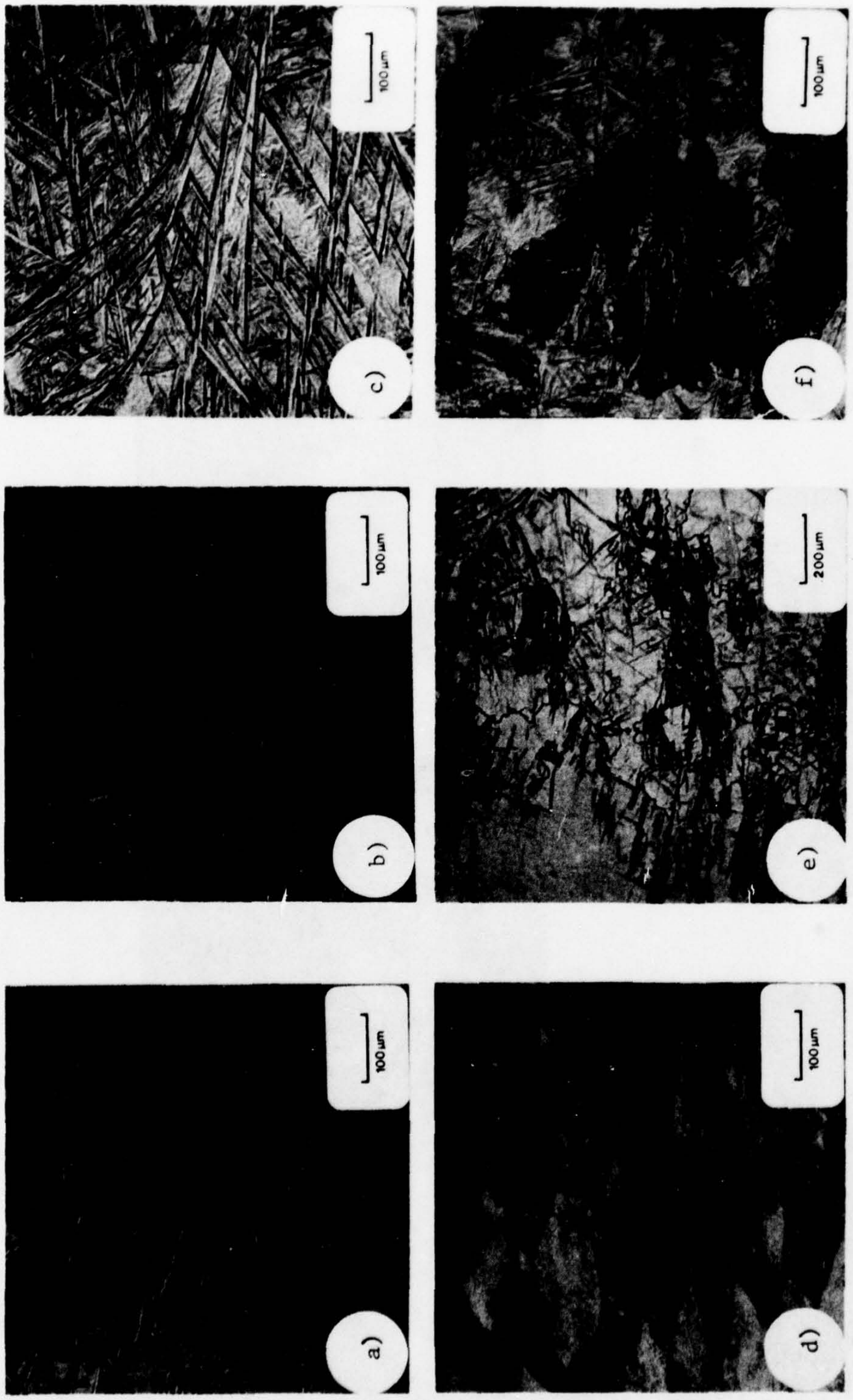

Figure 44. Microstructures of Ti-10V-2Fe-3Al Forged Isothermally to 0.50 In/In (Nominal) in the Temperature Range 1190°F (643°C) to 1750°F(954°C) at Speeds Indicated. MGD = 255μm. Forging Conditions: a) 1, 1750°F(954°C), 0.03 ipm; b) 2, 1600°F(871°C), 0.03 ipm; c) 3, 1450°F(788°C), 0.03 ipm; d) 5, 1350°F(732°C), 0.03 ipm; e) 6, 1750°F (954°C), 3.0 ipm; f) 8, 1600°F(871°C), 3.0 ipm. Kroll's Reagent.

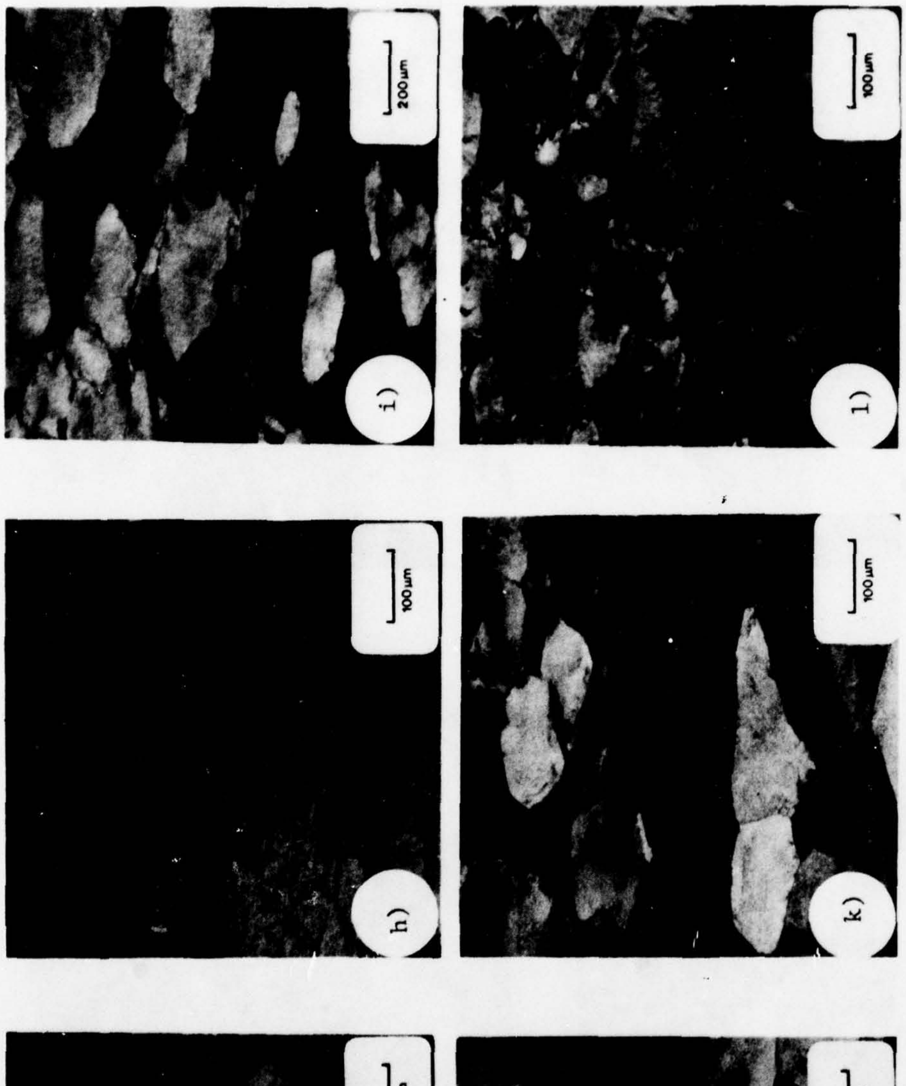

g) 9, 1250°F(677°C), 0.03 ipm; h) 10, 1450°F(788°C), 3.0 ipm;
i) 11, 1190°F(643°C), 0.03 ipm; j) 13, 1350°F(732°C), 3.0 ipm;
k) 15, 1250°F(677°C), 3.0 ipm; l) 16, 1190°F(643°C), 3.0 ipm.
Kroll's Reagent.

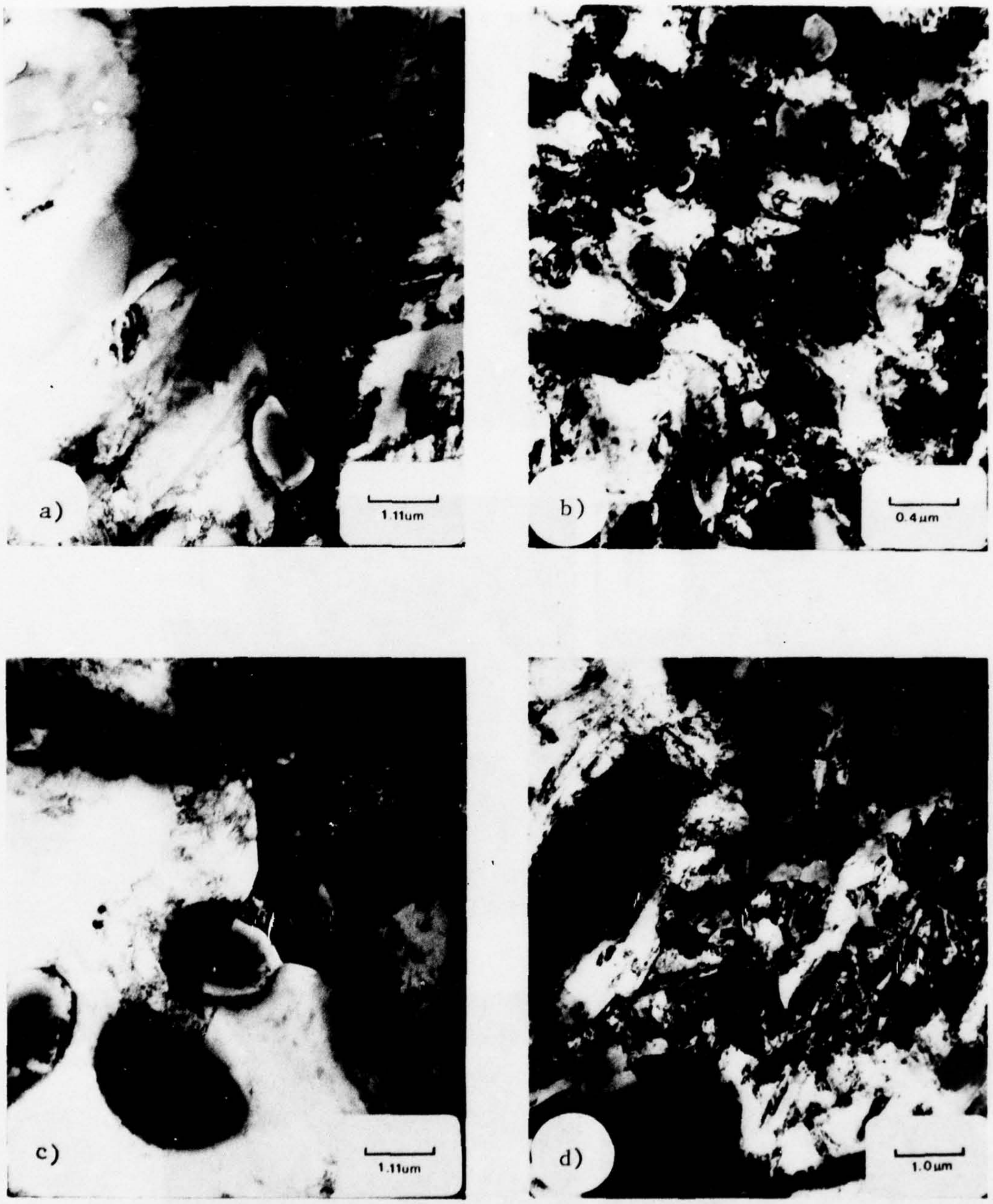

Figure 45. Microstructures (TEM) of Ti-10V-2Fe-3Al Forged Isothermally to 0.50 In/In (Nominal) MGD = 8μm. Forging Conditions: a) 3, 1450°F(788°C), 0.03 ipm; b) 9, 1250°F(677°C), 0.03 ipm; c) 10, 1450°F(788°C), 3.0 ipm; d) 15, 1250°F(677°C), 3.0 ipm

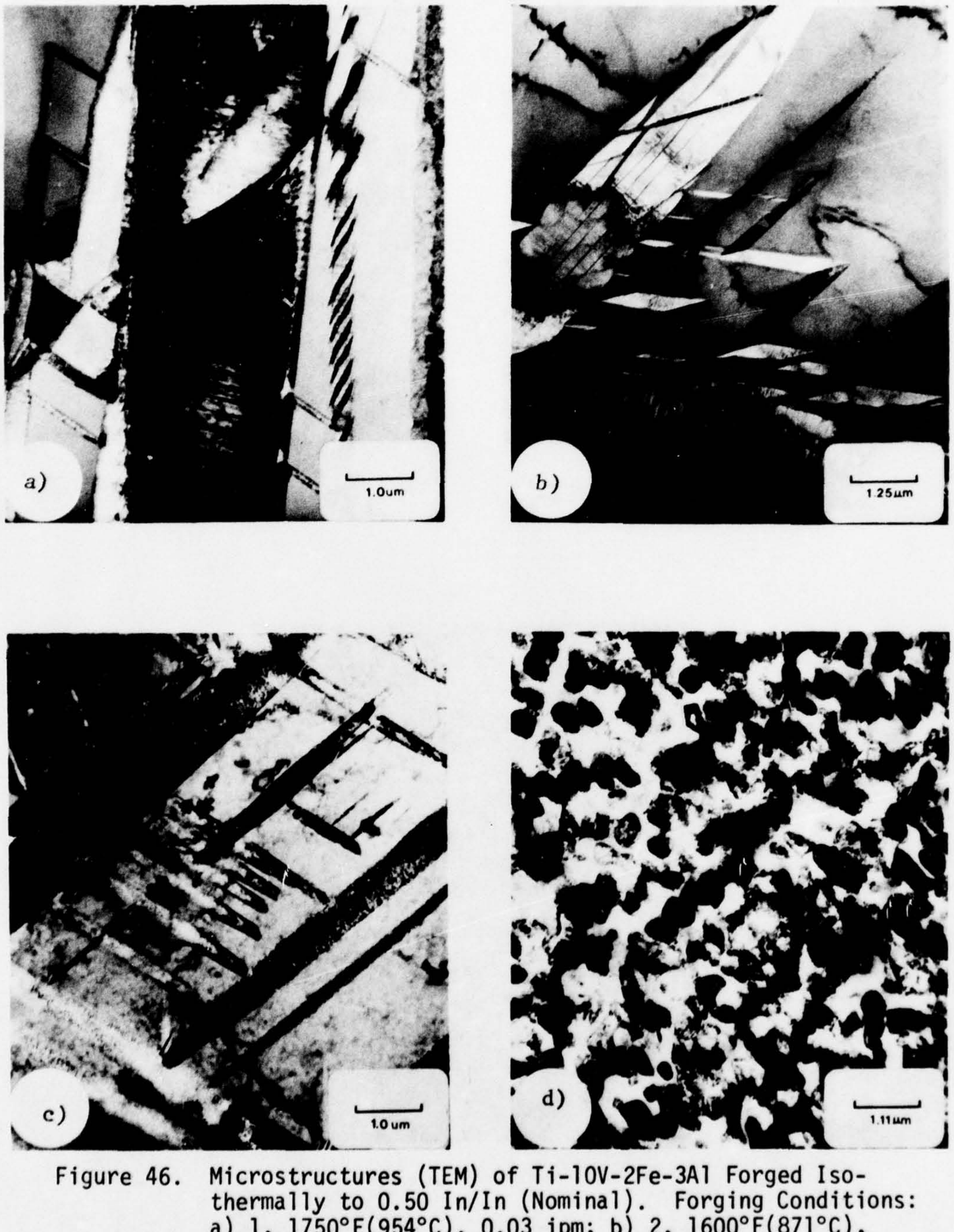

Figure 46. Microstructures (TEM) of Ti-10V-2Fe-3Al Forged Isothermally to 0.50 In/In (Nominal). Forging Conditions: a) 1, 1750°F(954°C), 0.03 ipm; b) 2, 1600°F(871°C), 0.03 ipm; c) 3, 1450°F(788°C), 0.03 ipm; d) 9, 1250°F (677°C), 0.03 ipm;

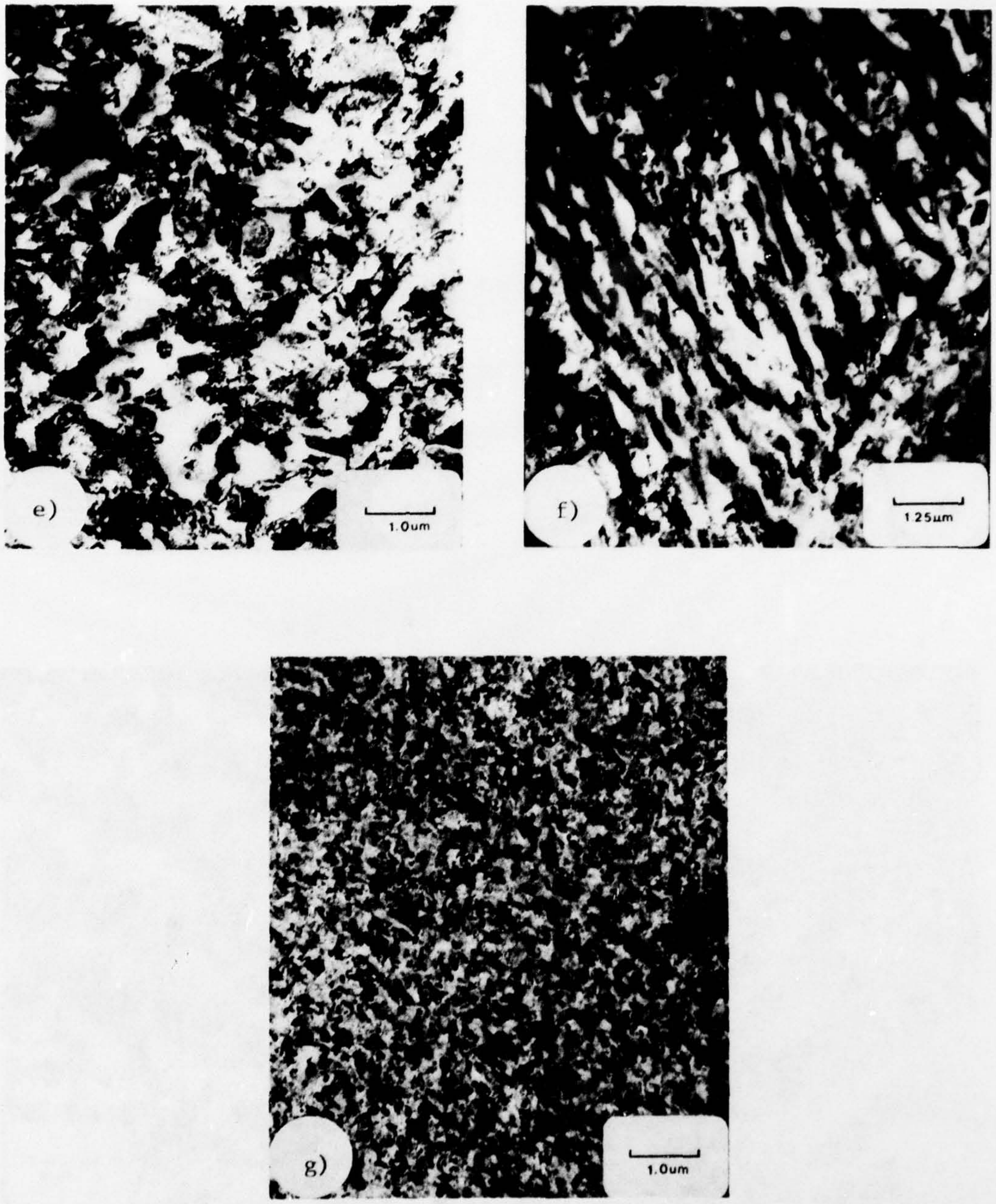

e) 11, 1190°F(643°C), 0.03 ipm; f) 15, 1250°F(677°C), 3.0 ipm; g) 16, 1190°F(643°C), 3.0 ipm.

SECTION V

DISCUSSION

1. THE RING TEST

The ring compression test is a convenient and relatively simple way of determining, not only the flow stress, but also the friction between the workpiece and the die during compression. The accuracy of the values determined depends on the repeatability of the test conditions and on the number of rings forged. A large number of rings forged per condition would result in a better flow stress determination, assuming all other process variables are properly controlled. A continuous measurement of the load and geometry could produce the needed information for calculation of the flow stress and friction while forging only one ring. Although the continuous measurement of the load is possible, the continuous measurement of the diameters presents some experimental difficulty not easily overcome. Nevertheless, as shown in Figure 47, the resulting diameters ($2A_0$, $2A_1$, $2B_0$ and $2B_1$) can be related to the as-forged ring thickness. It might be possible to forge a minimum number of rings, obtain continuous load-thickness curve and diameters-thickness curves, and interpolate to obtain values of $2A_0$, $2A_1$, $2B_0$, $2B_1$, and L for rings not actually forged.

Unfortunately this procedure requires a fairly close correlation between the as-forged ring thickness, T_r, and the apparent ring thickness, $T_r(x)$, obtained from the forging records. This correlation was unsuccessfully attempted, in the present investigation. The discrepancy between $T_r(x)$ and T_r can be as much as 0.030 in. This difference represents over 7% of the ring thickness and over 14% of the reduction in thickness, for the largest deformation.

The discrepancy between $T_r(x)$ and T_r can be attributed to the following:

1) As the ring is being forged, it is initially deformed elastically. As the deformation proceeds, plastic deformation occurs. The elastic deformation is recovered as the ring is unloaded. Since the abscissa of

the forging curves represent deformation time, part of the deformation calculated from the forging records is therefore, elastic deformation. This is in agreement with observed results $T_r(x) < T_r$. The forging records are not proportional to the stress like it is in tension. In compression, a portion of the load delivered to the specimen is utilized to overcome the friction between the die-specimen interfaces. The situation complicates since friction conditions varies with specimen thickness, and the contact area increases with deformation. Accounting for the elastic deformation is not as simple as unloading the specimen with the same slope as the initial loading on a load-time curve. Perhaps a discrepancy between $T_r(x)$ and T_r of a few thousands of an inch (0.001 to 0.006) may be justified by this elastic behavior.

2) The main ram slows down when the secondary ram comes in contact with the side columns. It is possible that some deformation occurs in the specimen at lower speeds. This would result in a thickness calculated from the forging record smaller than that measured from the specimen. As the main ram slows and comes to a virtual stop, the specimen is under load for a short period of time, some relaxation of the specimen may occur.

3) Seldom are the specimens of uniform thickness all the way around. Differences in thickness across the diameter of a thousandth or two is common.

4) The lubricant film used for the forging operation can have a thickness of 0.004 inch to 0.006 inch on each side of the ring. As the dies touch the workpiece and move closer, the film becomes thinner and some of the lubricant is squeezed out. Some load is transmitted to the cell through the workpiece, but little or no actual deformation is seen by the ring. Perhaps up to 0.008 to 0.012 inch discrepancy between $T_r(x)$ and T_r may be explained by the lubricant thickness.

5) Another source of the difference between $T_r(x)$ and T_r is the simple fact that the forging records represent a load-time measurement

and not a load-thickness record. A 1/10 inch uncertainty on the time axis of the forging record represent a deformation of 0.005 inch at a forging speed of 0.050 ips and a chart speed of 1.0 ips.

If it is of interest to obtain diameter-thickness and load-thickness curves to interpolate and obtain more data points than the number of rings forged, it would be necessary to measure the die separation directly to obtain true load-thickness curves.

2. STRESS-STRAIN CURVES

A great majority of the stress-strain curves shown in Figures 26 to 29 exhibit negative slopes. All these except one, were determined at subtransus temperatures. The exception being the stress-strain curve for MGD = 8μm tested at 0.03 ipm and 1450°F(788°C). As the test temperature increases, the stress-strain curves become more shallow, the slope becomes progressively less negative. Above the beta transus the curves are essentially flat.

This decrease in flow stress with increasing strain, work softening, is not believed to be caused entirely by adiabatic heating. Although some adiabatic heating in fact occurs it is not believed to be significant. For example, for the σ-ε curve at 1190°F(643°C), 0.03 ipm and MGD = 255μm the increase in temperature for up to 0.20 in/in was about 9°F. According to Jonas and Luton (Reference 59) adiabatic softening is more likely to occur at higher deformation temperatures. The higher temperatures in Figures 26 to 29 show less decrease of stress with strain, implying (according to Jonas and Luton (Reference 59)) that a re-arrangement of the structure is taking place, instead. Further work in this area may be justified; for example, a study of the change in the structure with strain at constant temperature and speed.

3. ACTIVATION ENERGY

The activation energy represents some energy barrier that must be overcome before the particular deformation process can occur and can produce a deformation increment. An increase in the applied stress could supply some of the energy necessary to overcome the barrier, resulting in an effective lowering of the activation energy. The activation energy then becomes stress dependent.

The dependency of the activation energy on strain could be viewed as a change in the energy barrier brought about by a change in the structure. This argument, although reasonable, and consistent with the negative slope of the stress strain curves, presents some questions that should be considered.

Below the beta transus, the alloy is in a two-phase region and changes in the structure occur with changes in temperature. Nevertheless, the activation energy is temperature independent. Above the transus, the alloy is in a single phase region. It nevertheless, has been known to deform under stress (Bohanek (Reference 14) and this investigation). Changes in structure above the transus could occur under hot-working conditions thereby resulting in changes in activation energy with strain.

4. STRESS-STRAIN RATE-STRAIN-TEMPERATURE RELATION

Equation 81b represents a relation between stress, strain, forging speed, and temperature for Ti-10V-2Fe-3Al. The strain dependency of the pre-exponential and stress exponent and the stress and strain dependency of the activation energy, make this relation a complex one. In spite of the complexity, the equation can be used to determine stress, strain rate, strain, and temperature data for the alloy under hot-working conditions. The accuracy and range of applicability of the variables could be improved and extended, if desired, by additional testing.

It was not possible to include in this equation the effects of grain size because only two grain sizes were investigated and the equation is more complex than anticipated.

The only other strain rate equation (Equation 1) for Ti-10V-2Fe-3Al was reported by Rosenberg (Reference 13) based on work by Chen (Reference 8).

The value of stress obtained from Rosenberg's Equation (Equation 1) at $\dot{\varepsilon} = 1.4 \times 10^{-3}$ sec^{-1} and T = 704C is 17.77 ksi. From Table D.3a the flow stress for isothermally forged Ti-10V-2Fe-3Al at the same strain rate and temperature is 17.3 ksi. Although the results compare favorably, it should be pointed out that the data used by Rosenberg is tensile data with no reference to the grain size or strain, whereas the data presented in this investigation is for isothermal forging, this particular value of 17.3 ksi is for a strain of 0.10 in/in and MGD = 255μm.

5. MECHANICAL PROPERTIES AND STRUCTURES

The mechanical properties shown plotted in Figure 39 and 40, as a function of calculated flow stress, exhibit a dependency on the forging conditions. Forging essentially below the beta transus results in low toughness and ductility and high yield and ultimate strength. These results are in general agreement with results from Bohanek (Reference 14) who also found no deterioration in ductility as a result of beta forging Ti-10V-2Fe-3Al. These results are an exception to the accepted idea that forging in the beta region results in reduced ductility compared to forging in the alpha + beta region. (See Section II.2 and the open literature). It should be remembered that the fracture toughness and tensile data (in Figures 39 and 40) represent an average from two specimens per forging condition and that the properties were determined for only five forging conditions.

The hardness values shown (Figure 39) (although somewhat scattered) exhibit a long trend relation with forging conditions and with the resulting room temperature properties. The relation between hardness and UTS should not be considered as a precise one, but rather as a simple, fast and economical method for screening relative strength properties. Determination of the yield and ultimate strength requires tension tests.

A relation exists between properties and forging conditions, represented here by the calculated flow stress, σ_c. It does appear possible to predict the room temperature mechanical properties resulting from particular forging conditions based on the flow stress. For example, the flow stress σ_c, for forging at 1750°F(954°C) and 3.0 ipm is from (Table 13) 10.7 ksi. For Figure 39 the predicted room temperature mechanical properties are:

YS = 122 ksi

UTS = 136 ksi

%El = 19

W/A = 940 in-lb/in^2

H = 32.7 $\pm$ 1.5 Rockwell C

Increasing the grain size from 8μm to 255μm results in a rather small increase in flow stress. The resulting room temperature properties are not significantly different, except for a consistent improvement of about 250 in-lb/in^2 in the toughness of the larger grain size material for all levels of flow stress (forging conditions) considered. The ductility is in general better, for the smaller grain. The ductility and toughness maximum and the corresponding minimum in yield strength that occurred at above transus temperatures for the larger grain size cannot be explained at present. The absence of these property maxima and minima for the small grain size is not unexpected, since this material was not forged at temperatures above the transus.

The material with the smaller grain size (Figures 41 and 42) shows evidence of grain refinement as the forging temperature decreases. At the higher strain the structure becomes less well defined. As the forging temperature is lowered, alpha coalesces and grows at the boundaries and becomes finer and more evenly distributed within the grains. The effect of forging speed is not very clear. At higher temperatures, the higher speed results in a definite increase of alpha both at grain boundaries and intragranular. This effect is not obvious at lower temperatures. The increase of alpha with decreasing temperature makes it more difficult to detect increase in alpha with speed without a quantitative determination.

The samples with the larger grain size (255μm) show evidence of deformation at the higher strain (Figure 44). The samples forged at 1750°F(954°C) and 1600°F(871°C) for both speeds and for the slow speed at 1450°F(788°C) show titanium martensite or alpha prime covering a large portion of the surface (Figures 43 and 44). The grain boundaries of these samples (Figure 44) are jagged and irregular. The remaining samples (1450°F, 3.0 ipm and both speeds at lower temperatures, Figures 43 and 44) have even grain boundaries with fine sub-grain structure, assumed to be alpha. The sub-grain structure becomes finer for the samples with higher flow stress.

Lower forging temperatures and higher forging speeds result in lower toughness and ductility and higher yield and ultimate strength. These same forging conditions also results in higher content of finer and more evenly distributed alpha. (See Figures 41, 42, 45, and 46).

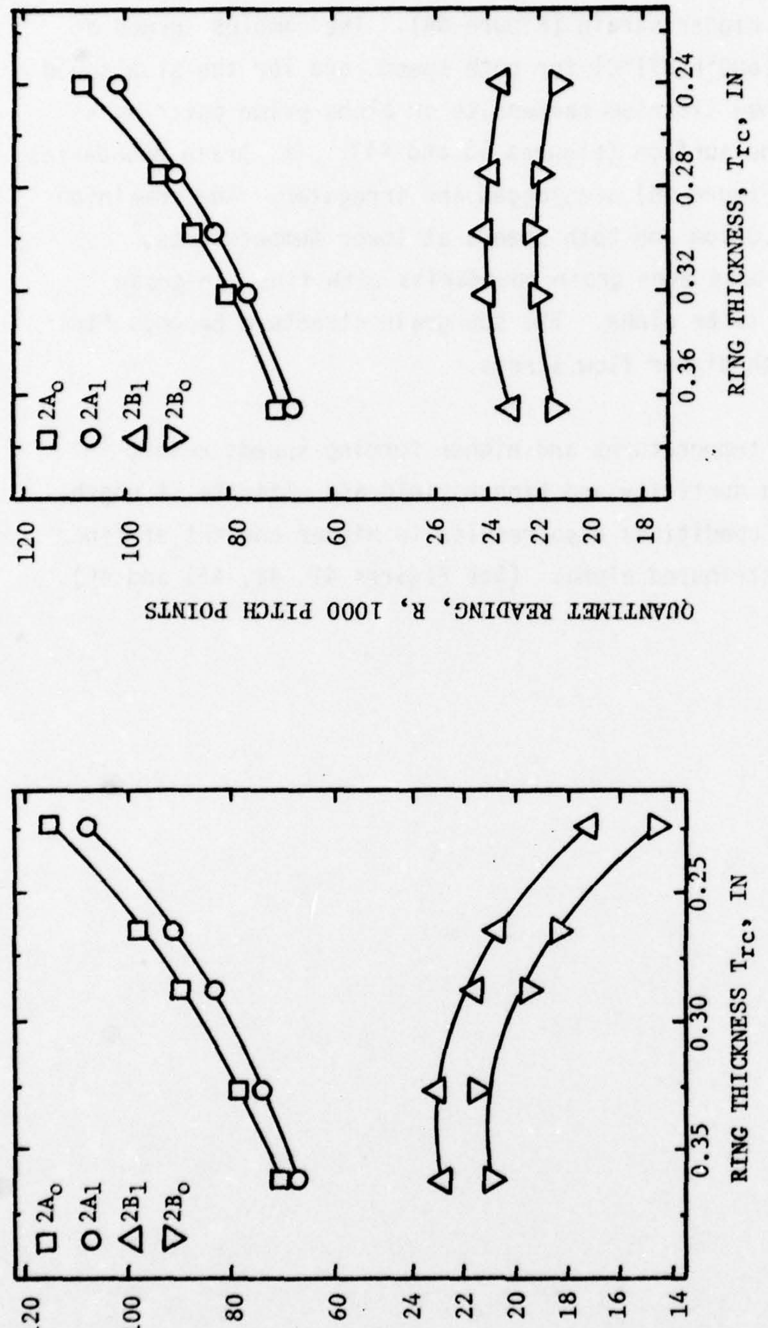

Figure 47. Ring Diameters ($2A_o$, $2A_1$, $2B_o$, $2B_1$) as a Function of Ring Thickness, T_{rc}, for Conditions Indicated. a) Rings Forged at 1250°F(677°C), 0.03 ipm, MGD = 8µm. b) Rings Forged at 1750°F(954°C), 3.0 ipm, MGD = 255µm

SECTION VI

CONCLUSIONS

The evidence presented in this investigation supports the following conclusions:

1) The flow stress of isothermally forged Ti-10V-2Fe-3Al depends on the forging conditions (temperature and speed) and to a lesser extent on the initial grain size. The value of the flow stress can be used to characterize the forging conditions.

2) The room temperature mechanical properties (tensile, hardness and toughness (W/A)) for isothermally forged Ti-10V-2Fe-3Al depend primarily on the forging conditions (flow stress). The properties depend on initial grain size to a lesser extent.

3) The resulting room temperature mechanical properties for isothermally forged Ti-10V-2Fe-3Al may be predicted from knowledge of the flow stress (forging conditions).

4) In general, isothermally forged Ti-10V-2Fe-3Al at temperatures above the beta transus will result in higher toughness (W/A) and ductility as compared to forging below the transus.

5) Lower forging speeds results in higher toughness (W/A) and ductility and lower strength compared to higher speed.

6) The microstructures resulting from isothermally forged Ti-10V-2Fe-3Al also depend on forging conditions. Forging at temperatures above the beta transus results in beta grain with varying amounts of alpha prime. In this temperature region twinning results in both the alpha and beta phase. Forging at sub-transus temperatures results in the formation of sub-grain structure assumed to be mainly alpha precipitate. Some microstructures, specially at higher magnifications (25K and above)

show what appear to be cell structures. Lower forging temperatures results in a finer structure. The dislocations are not easily distinguished in any of the samples inspected.

7) The value of the deformation parameters A, n and Q depends on grain size and strain and are constant with temperature in two regions, above and below the beta transus. The apparent activation energy Q, is also stress dependent.

8) The flow stress for isothermally forged Ti-10V-2Fe-3Al can be expressed in terms of forging temperature, forging speed and strain:

$$\sigma = \left[\frac{0.0455}{A} V^{1.0208} \exp(\varepsilon + B/RT)\right]^{1/(n + c/RT)}$$

The parameters A, B, n and C are grain size and strain dependent and constant with temperature in two regions, above and below the beta transus.

9) The room temperature hardness (Rockwell C) for isothermally forged Ti-10V-2Fe-3Al has a long-term dependency on flow stress (forging condition). The Rockwell C hardness may be used as a screening method for estimating relatively large changes in strength. Determination of yield and ultimate strength requires tension test.

10) The stress strain curves for sub-transus forging temperatures exhibit work softening, resulting mainly from a change in the microstructure as a result of precipitation of the alpha phase. At higher forging temperatures, the slope of the stress strain curves becomes less negative. Above the transus the curves are essentially flat.

11) Finally, a well established, but nevertheless valid conclusion. Higher forging temperatures and slower forging speeds result in lower flow stress.

SECTION VII

RECOMMENDATIONS

During the course of this investigation, a number of areas were identified as areas that require additional information. Supplementary work on these areas is beyond the scope of the present investigation. Nevertheless, better understanding of these topics would add to the general knowledge of the effects of processing conditions on the properties and microstructures of Ti-10V-2Fe-3Al and other alloys. These areas are identified below hoping they will serve as guidelines for future research.

1) Verify that the room temperature mechanical properties (tensile, toughness) of isothermally forged and water quenched Ti-10V-2Fe-3Al may be predicted from knowledge of the forging conditions (flow stress).

2) Investigate if the relation between forging conditions (flow stress) and room temperature properties applies to other properties, other titanium alloys, other materials or other post forging heat treatments such as air-cool.

3) Investigate the grain size dependency of the parameters A, B, C and n in Equation 81.

4) Investigate the possibility that the $\ln\dot{\varepsilon}$ - 1/T curves for the approximate temperature range 1190°F to 1300°F may not have a constant slope.

5) Investigate the change in microstructure with strain for Ti-10V-2Fe-3Al at a fixed temperature and forging speed.

6) Investigate the formation of the omega phase in Ti-10V-2Fe-3Al and its effects on the room temperature properties.

APPENDIX A

MEASUREMENT OF GRAIN SIZE

The grain sizes were determined by using a linear intercept method that is in general agreement with ASTM standard E112-74. In the method used, a line pattern (Figure A.1) was drawn on a transparent plastic and used to count linear intercept from microphotographs of the structure under study. The magnification of the photograph, the intercept count, and the length of the line pattern were used to calculate the mean grain diameter, MGD.

The criteria for counting intercepts was incorporated directly from paragraph 10.3 of ASTM E112-74:

Condition	Intercept Count
1) Test line cuts grain boundary	1
2) Test line ends inside a grain	1/2
3) Test line tangent to grain boundary	1
4) Test line cuts tripoint	1-1/2

When the grain sizes were measured for equiaxed grains, the intercepts were counted on three different fields and the average intercept distance computed using Equation A.1 and identified as mean grain diameter

$$MGD = \bar{L} = \frac{L}{nM} \qquad \text{A.1}$$

where

n is the total number of intercepts

L is the total length of test lines

M is the magnification of the microphotograph

When the grain sizes were measured for deformed grains, the intercepts were measured in at least two different fields, each in a different plane perpendicular to each other. In each field, the intercepts were measured in two mutually perpendicular directions using the parallel lines of the line pattern. The average intercept distance was computed using Equation A.3 and identified as mean grain diameter

$$\bar{L} = \frac{3}{M[(n/L)_r + (n/L)_t + (n/L)_n]} \qquad \text{A.2}$$

$$\text{MGD} = \bar{L}_{(L/n)_r/(L/n)_t,\ (L/n)_r/(L/n)_n} \qquad \text{A.3}$$

The factors $(n/L)_r$, $(n/L)_t$, and $(n/L)_n$ are the intercepts per unit length of line pattern in each of the three orthogonal directions r,t and n. The system of coordinates used to identify directions and planes is shown in Figure A.2.

The ratios $(L/n)_r,/L/n)_t$ and $(L/n)_r/(L/n)_n$* are shape factors. These ratios are an indication of how deformed the grains are. The combination photograph magnification and length of line pattern used was selected such that at least 50 intercepts would result from each field.

*The normal direction "n", will be the direction of extrusion or forging which will be identified by "e" or "f" where appropriate.

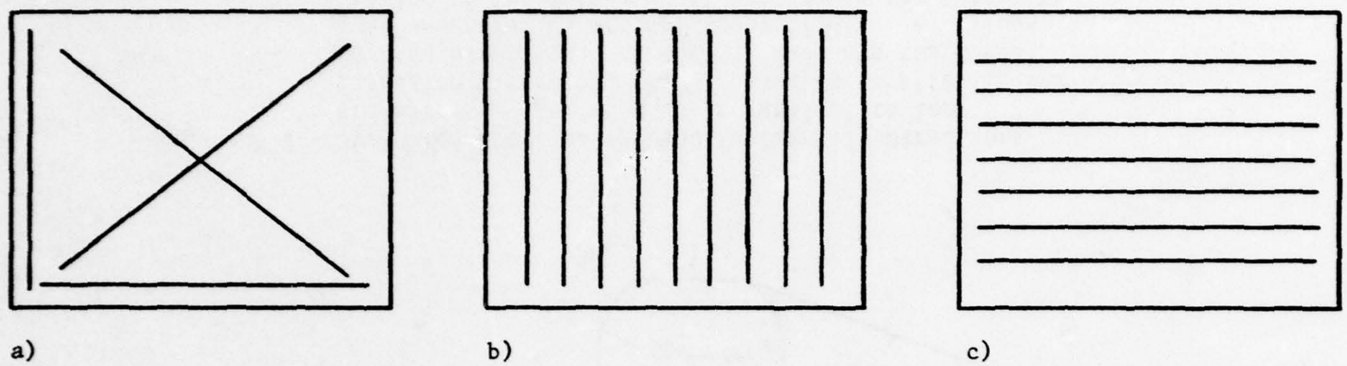

Figure A.1. Line Pattern Used to Count Intercepts for Grain Size Determination. The Line Patterns Are Shown Half Size. Pattern (a) Is Used for Measuring Sizes of Equiaxed Grains, Patterns (b) and (c) Are Used to Measure Sizes of Deformed Grains.

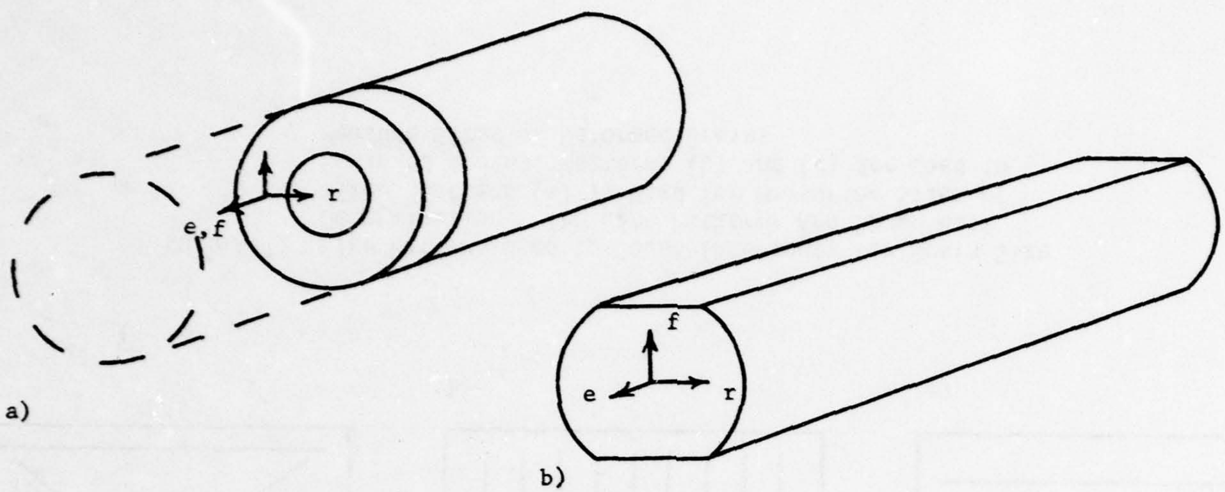

Figure A.2 System of Coordinates Used to Identify Directions and Planes. The "e" Axis Is Parallel to the Extrusion Direction, the "f" Axis Is Parallel to the Forging Direction, "r" and "t" Axis Are the Radial and Tangential Directions Respectively. a) Illustration of the System as it Applies to the Extrusion and Forging of the Rings, b) Illustration of the System as it Applies to the Extrusion and Forging of the Tensile and Charpy Blanks

APPENDIX B

CALIBRATION OF THE FORGING PRESS RAM SPEED

The analysis of the ring test data, Section IV, requires an accurate knowledge of the forging press ram speed. For this reason the ram speed was measured in the velocity range of interest for this investigation. The speed was measured using a ruler, a pointer, and an electronic digital clock. The ruler was attached to the frame of the forging press and the pointer to the ram. The time was measured for a known movement of the ram at each of the five nominal speeds, (Table B.1). The travel of the ram was then plotted against time for all the measurements at the same speed (Figure B.1). The true ram speed was then calculated as the slope of the travel-time curve, using a least square linear regression technique. The nominal speed was then plotted versus true speed in log-log coordinate system (Figure B.2). The equation relating the true forging speed (TS) to the nominal speed (V) is

$$TS = 1.0912\ (V)^{1.0208},\ \text{ipm*}$$

* $TS = 1.16638\ (V)^{1.0208}$, cm/sec

TABLE B.1

TIME-DISPLACEMENT DATA FOR THE RAM OF THE 500-TON LOMBARD HYDRAULIC FORGING PRESS

RAM TRAVEL	RAM DISPLACEMENT TIME (SECS) FOR NOMINAL SPEEDS (V, IPM) INDICATED				
(RT, 1/16 INCH)	0.031	0.101	0.502	1.001	3.012
1	---	37	8	---	---
2	---	69	15	---	---
3	---	106	21	---	---
4	---	139	28	14	5
5	---	178	36	---	---
6	---	208	43	21	---
7	818	248	---	---	---
8	938	288	---	28	10
9	1061	324	64	---	---
10	1175	360	---	35	---
11	1296	395	78	---	---
12	1414	432	---	42	14
13	1529	468	92	---	---
14	1651	503	---	49	---
15	1766	539	106	---	---
16	1880	576	---	56	18
17	2003	613	120	---	---
18	2127	648	---	63	---
20	---	---	---	70	23
24	---	---	---	84	27
28	---	---	---	98	31
32	---	---	---	---	36
36	---	---	---	---	40

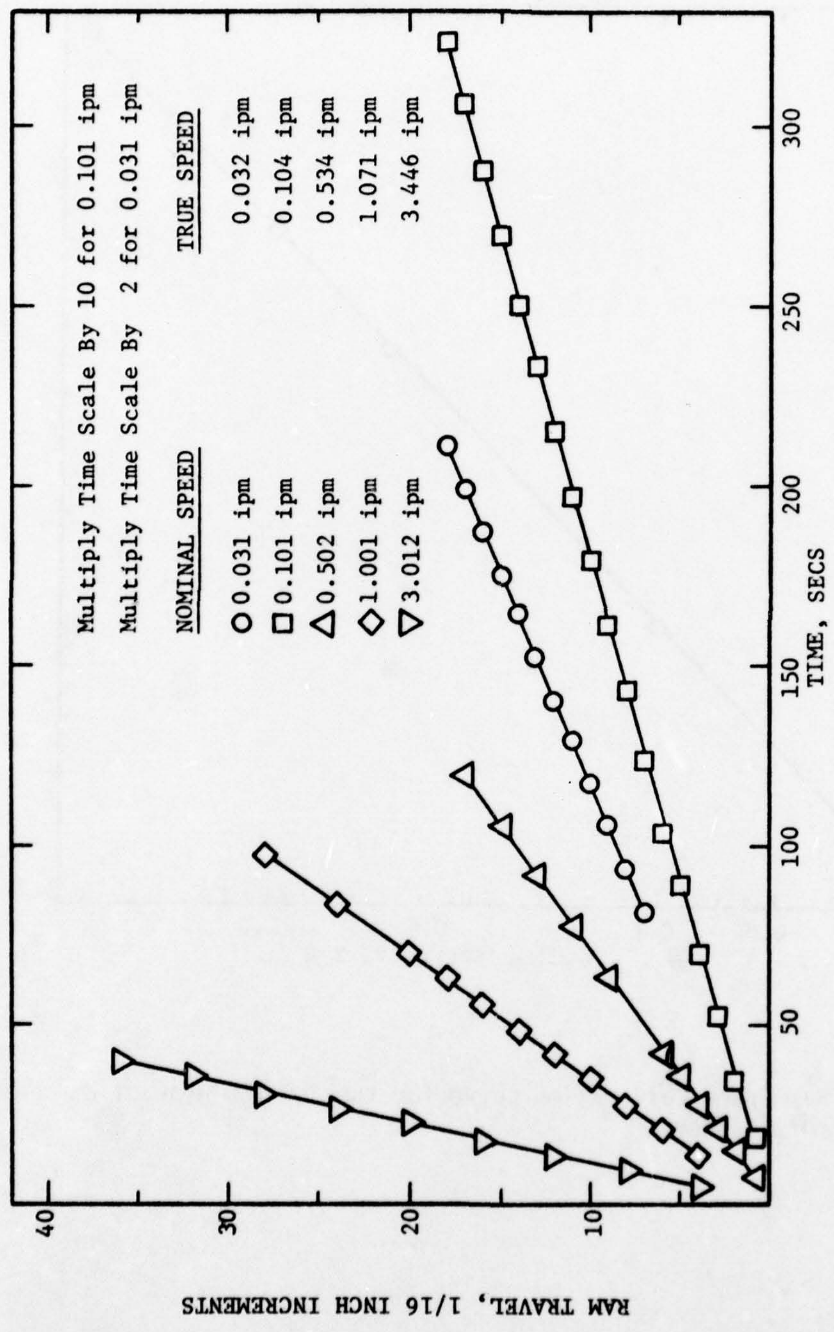

Figure B.1. Ram Travel vs. Time for Five Nominal Speeds for the 500-Ton Hydraulic Forging Press

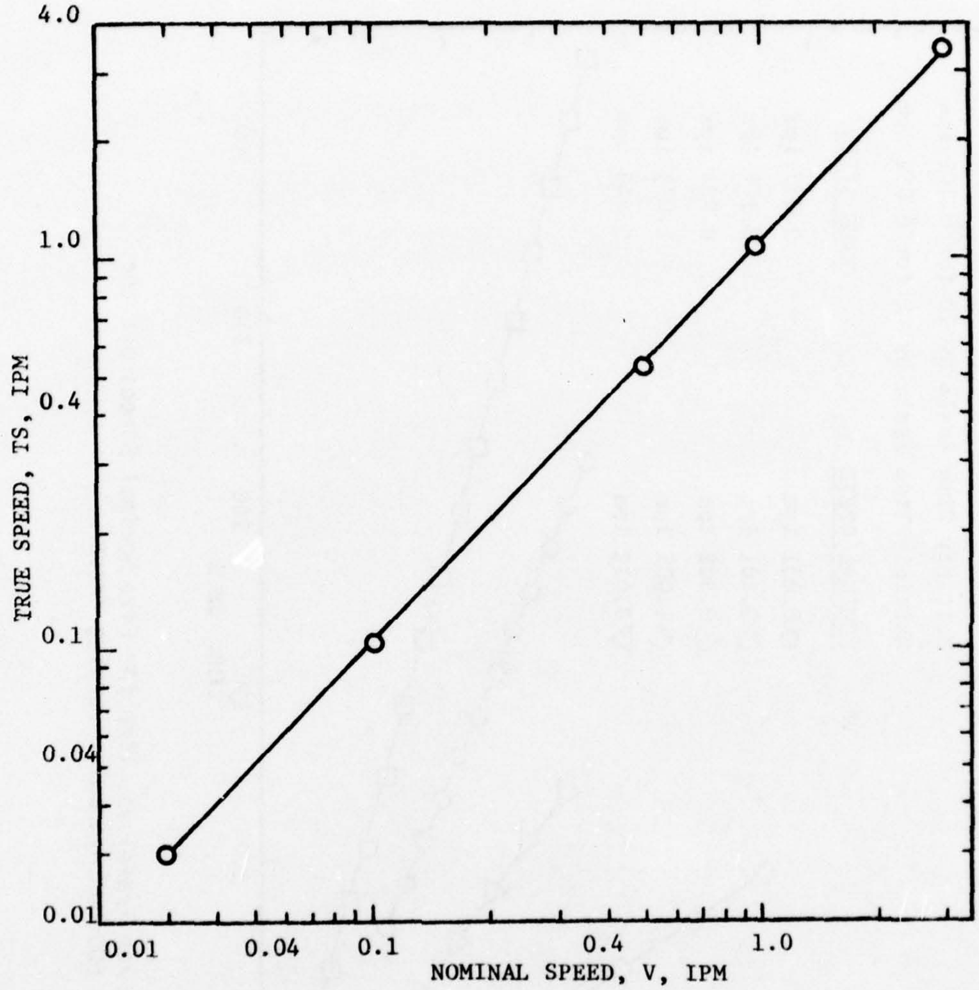

Figure B.2. Ram Speed Calibration Curve for the 500-Ton Hydraulic Forging Press

APPENDIX C

MATHEMATICAL ANALYSIS FOR A RING IN COMPRESSION

The determination of the flow stress of a material using the ring compression test is based on the mathematical analysis of the hollow disk made by Avitzur (References 56, 57) and on the method of solution to Avitzur's equations by DePierre and Gurney (Reference 58). Avitzur developed an equation for the ratio of the average forging pressure to the flow stress of the material (P/σ_0) in terms of the neutral radius (R_n), the ring geometry (Figure 19), the interface friction (m) between the die and the ring, and a bulge parameter (b). Avitzur obtained this equation for P/σ_0 as an upper bound solution to the balance of power on the ring specimen. Minimization of the power with respect to b results in an equation of the bulging parameter in terms of R_n, m, and the ring geometry. Since there are only three equations and four unknowns (σ_0, m, b and R_n), the value of R_n and m are chosen by successive approximations to minimize the factor P/σ_0.

Avitzur considered the bulge formation through the selection of a radial velocity field, $\dot{U}_R$, which is a function of y (Figure 19). His analysis assumes that the ring being deformed has, initially, no bulge. Successive approximations of the variables R_n and b to minimize P/σ_0 does not take into consideration a ring that already has a bulge.

Before presenting a summary of Avitzur's analysis it is appropriate to list the applicable assumptions:

1) The ring does not rotate during forging, therefore, $\dot{U}_\theta = o$
2) The material is incompressible
3) The material is a Von-Mises material, therefore,
    a) it obeys Von-Mises' stress-strain law
    b) it obeys Von-Mises' yield criteria
    c) hydrostatic stresses have no effect on yielding or flow of the material

d) it is perfectly plastic

Summary of Avitzur's Analysis (References 56, 57)

Consider a ring deformed in compression by two flat dies each moving at a speed of $\dot{U}/2$, as shown in Figure 19. The power delivered by the forging press, will be used to deform the ring and to overcome the friction between the ring-die interface. Through a balance of power, an upper bound solution is obtained for the ratio P_{av}/σ_o in terms of the ring geometry (R_o, R_i, T), the interface friction (m), the neutral radius (R_n), and the bulge parameter (b).

$$\frac{P_{av}}{\sigma_o} = f\left[\frac{R_o}{R_i}, \frac{R_o}{T}, m, \frac{R_n}{R_o}, b\right] \quad * \text{(C.1)}$$

The values of P_{av}, R_o, R_i and T can be obtained from experimental measurements but m, b, σ_o and R_n remain unknowns.

Since the equation for P_{av}/σ_o was obtained from consideration of upper bound theorem (References 56, 57), the values for R_n and b should be those that minimize the total power and hence, the ratio P_{av}/σ_o. An equation is obtained for b by minimizing P_{av}/σ_o with respect to b. The value of R_n is chosen by successive approximations to minimize the ration P/σ_o. The resulting equations for the ratio P/σ_o for a ring deformed in compression between two dies are given by Equations C.2 to C.9.

DePierre and Gurney's Solution to Avitzur's Equations

DePierre and Gurney modified Avitzur's analysis of the hollow disc and developed a computer program to calculate σ_o and m (Reference 58). They developed an equation for the neutral radius, R_n, in terms of the ring geometry and corrected for the bulged specimen by calculating an

*This equation corresponds to Equations 6 and 7 in Reference 57, Equation 6 applies for $R_n < R_i$ and Equation 7 for $R_i \leq R_n \leq R_o$. The thickness T corresponds to T_r in the main body.

equivalent ring geometry for equal ring volume without a bulge. They also derived an expression for the friction, m, that minimizes P/σ_0. This approach refined the calculation of σ_0 and m and offered a correction for bulge formation.

The calculations of σ_0 and m using the ring test can be further improved by minimizing the bulge. This can be accomplished by choosing a thin ring, and by utilizing a lubricant for the forging operation that results in the lowest friction possible.

$$\text{For } R_n \leq R_i \text{ and } \frac{mR_o}{T} \leq \frac{1}{2(1-R_i/R_o)} \ln\left(\frac{3(R_o/R_i)^2}{1+\sqrt{1+3(R_o/R_i)^4}}\right) \qquad \text{C.2}$$

$$\frac{P_{ave}}{\sigma_o} = \frac{\frac{1}{\sqrt{3}}\left(\frac{R_n}{R_o}\right)^2}{1-\left(\frac{R_i}{R_o}\right)^2}\left\{+\sqrt{1+3(R_o/R_n)^4} - \sqrt{1+3(R_i/R_o)^4\,(R_o/R_n)^4}\right.$$

$$-\ln\left[\left(\frac{R_i}{R_o}\right)^2 \frac{1+\sqrt{1+3(R_o/R_n)^4}}{1+\sqrt{1+3(R_i/R_o)^4(R_o/R_n)^4}}\right]$$

$$+\frac{b^2}{4}\left(\frac{R_o}{T}\right)^2 \frac{1}{\sqrt{1+3(R_o/R_n)^4}}\left\langle\frac{1}{4}\left(\frac{R_o}{R_n}\right)^4\left[1-\left(\frac{R_i}{R_o}\right)^4\right]-\left(\frac{R_o}{R_n}\right)^2\left[1-\left(\frac{R_i}{R_o}\right)^2\right]+\ln\left(\frac{R_o}{R_i}\right)\right\rangle$$

$$\left.+\,2m\,\frac{R_n}{R_o}\,\frac{R_o}{T}\left\langle\frac{1}{3}\left(\frac{R_o}{R_n}\right)^3\left[1-\left(\frac{R_i}{R_o}\right)^3\right]-\left(\frac{R_o}{R_n}\right)\left(1-\frac{R_i}{R_o}\right)\right\rangle\left(1-\frac{b}{4}+\frac{b^2}{48}\right)\right\} \qquad \text{C.3}$$

$$b = \frac{m\left\langle\frac{1}{3}\left(\frac{R_o}{R_n}\right)^2\left[1-\left(\frac{R_i}{R_o}\right)^3\right]-\left(1-\frac{R_i}{R_o}\right)\right\rangle}{\frac{m}{6}\left\langle\frac{1}{3}\left(\frac{R_o}{R_n}\right)^2\left[1-\left(\frac{R_i}{R_o}\right)^3\right]-\left(1-\frac{R_i}{R_o}\right)\right\rangle+\frac{R_o/T}{\sqrt{1+3(R_o/R_n)^4}}\left\langle\frac{1}{4}\left(\frac{R_o}{R_n}\right)^4\left[1-\left(\frac{R_i}{R_o}\right)^4\right]-\left(\frac{R_o}{R_n}\right)^2\left[1-\left(\frac{R_i}{R_o}\right)^2\right]+\ln\frac{R_o}{R_i}\right\rangle} \qquad \text{C.4}$$

Minimize the value of Pav/σ_o by successive approximations of R_n. As a first approximation use the value of R_n from (Equation 7.15a of Reference 56).

$$\left(\frac{R_n}{R_o}\right)^2 = \frac{\sqrt{3}}{2} \; \frac{1 - (R_i/R_o)^4 x^2}{\sqrt{x(x-1)}\,\left[1 - (R_i/R_o)^4 x\right]} \qquad \text{C.5}$$

$$x = \left\{\frac{R_o}{R_i} \exp\left[-m \; \frac{R_o}{T}\left(1 - \frac{R_i}{R_o}\right)\right]\right\}^2 \qquad \text{C.6}$$

For $R_i \le R_n \le R_o$ and $m \; \frac{R_o}{T} \le \frac{1}{2(1 - Ri/R_o)} \ln \frac{3(R_o/R_i)^2}{1 + \sqrt{1 + 3(R_o/R_i)^4}}$ C.7

$$\frac{Pave}{\sigma_o} = \frac{\frac{1}{\sqrt{3}}\left(\frac{R_n}{R_o}\right)^2}{1 - (R_i/R_o)^2} \left\{+ \sqrt{1 + 3\left(\frac{R_o}{R_n}\right)^4} - \sqrt{1 + 3\left(\frac{R_i}{R_o}\right)^4\left(\frac{R_o}{R_n}\right)^4} - \ln\left[\left(\frac{R_i}{R_o}\right)^2 \frac{1 + \sqrt{1 + \left(\frac{R_o}{R_n}\right)^4}}{1 + \sqrt{1 + 3\left(\frac{R_i}{R_o}\right)^4\left(\frac{R_o}{R_n}\right)^4}}\right]\right.$$

$$+ \frac{b^2}{4}\left(\frac{R_o}{T}\right)^2 \frac{1}{\sqrt{1+3\left(\frac{R_o}{R_n}\right)^4}} \left\langle \frac{1}{4}\left(\frac{R_o}{R_n}\right)^4\left[1 - \left(\frac{R_i}{R_o}\right)^4\right] - \left(\frac{R_o}{R_n}\right)^2\left[1 - \left(\frac{R_i}{R_o}\right)^2\right] + \ln \frac{R_o}{R_i}\right\rangle$$

$$\left. + 2m \; \frac{R_n}{R_o} \; \frac{R_o}{T} \left\langle \frac{4}{3} + \frac{1}{3}\left(\frac{R_o}{R_n}\right)^3\left[1 + \left(\frac{R_i}{R_o}\right)^3\right] - \left(\frac{R_o}{R_n}\right)\left(1 + \frac{R_i}{R_o}\right)\right\rangle \left(1 - \frac{b}{4} + \frac{b^2}{48}\right)\right\} \qquad \text{C.8}$$

$$b = \frac{m\,\frac{R_n}{R_o}\left\langle \frac{4}{3} + \frac{1}{3}\left(\frac{R_o}{R_n}\right)^3\left[1 + \left(\frac{R_i}{R_o}\right)^3\right] - \frac{R_o}{R_n}\left[1 + \frac{R_i}{R_o}\right]\right\rangle}{\frac{m}{6}\,\frac{R_n}{R_o}\left\langle \frac{4}{3} + \frac{1}{3}\left(\frac{R_o}{R_n}\right)^3\left[1+\left(\frac{R_i}{R_o}\right)^3\right] - \frac{R_o}{R_n}\left(1+\frac{R_i}{R_o}\right)\right\rangle + \frac{R_o/T}{\sqrt{1+3\left(\frac{R_o}{R_n}\right)^4}}\left\langle \frac{1}{4}\left(\frac{R_o}{R_n}\right)^4\left[1-\left(\frac{R_i}{R_o}\right)^4\right] - \left(\frac{R_o}{R_n}\right)^2\left[1-\left(\frac{R_i}{R_o}\right)^2\right] + \ln\frac{R_o}{R_i}\right\rangle} \qquad \text{C.9}$$

Minimize the value of Pav/σ_o by successive approximations of R_n. As a first approximation use a value of $R_n = R_i$

APPENDIX D

DATA USED FOR DETERMINATION OF FLOW STRESS ACTIVATION ENERGY, PRE-EXPONENTIAL AND STRESS EXPONENT

TABLE D.1

SUMMARY OF THE RING TEST DATA FOR ISOTHERMALLY FORGED Ti-10V-2Fe-3Al. MGD = 8 μm.

Temperature (C)	Forging Speed (V, ipm)	Thickness (Tc, in)	Forging Load (L, 1000 lbs)	Pressure/Stress (P/σ)	Stress (σ, ksi)	Strain (ε, in/in)
677	0.03	0.400	---	---	---	----
		0.3626	23.8	1.123	23.4	0.098
		0.3274	23.0	1.179	19.5	0.200
		0.2883	23.2	1.250	16.6	0.328
		0.2656	24.6	1.310	15.6	0.410
		0.2245	29.5	1.495	13.7	0.578
677	3.00	0.4005	---	---	---	---
		0.3713	56.5	1.038	61.3	0.076
		0.3134	57.5	1.110	49.5	0.245
		0.2973	58.0	1.120	46.7	0.298
		0.2685	59.0	1.412	42.3	0.400
		0.2357	62.0	1.197	37.6	0.530
732	0.03	0.400	---	---	---	---
		0.3560	12.2	1.119	11.8	0.117
		0.3281	12.6	1.142	11.0	0.198
		0.2905	14.0	1.178	11.6	0.320
		0.2629	14.6	1.196	9.9	0.420
		0.2438	15.2	1.216	9.5	0.495
732	3.00	0.400	---	---	---	---
		0.3570	36.0	1.036	37.5	0.114
		0.3258	37.5	1.0[illegible]9	34.6	0.205
		0.2909	38.5	1.120	30.1	0.319
		0.2628	40.0	1.164	27.5	0.420
		0.2313	44.5	1.254	25.1	0.548

TABLE D.1 (CONTINUED)

SUMMARY OF THE RING TEST DATA FOR ISOTHERMALLY FORGED Ti-10V-2Fe-3Al. MGD = 8 μm.

Temperature (C)	Forging Speed (V,ipm)	Thickness (Tc, in)	Forging Load (L,1000 lbs)	Pressure/Stress (P/σ)	Stress (σ, ksi)	Strain (ε, in/in)
788	0.03	0.400	---	---	---	---
		0.3579	6.9	1.144	6.6	0.111
		0.3229	7.5	1.206	6.2	0.214
		0.2923	8.5	1.233	6.2	0.314
		0.2681	9.9	1.229	6.8	0.400
		0.2419	10.5	1.229	6.4	0.503
788	3.00	0.4005	---	---	---	---
		0.3585	21.5	1.066	21.9	0.111
		0.3204	23.0	1.078	20.7	0.223
		0.2930	24.0	1.098	19.4	0.313
		0.2621	26.5	1.125	18.8	0.424
		0.2327	29.3	1.149	18.0	0.543

TABLE D.2

SUMMARY OF RING TEST DATA FOR ISOTHERMALLY FORGED Ti-10V-2Fe-3Al. MGD = 255 μm.

Temperature (C)	Forging Speed (V, ipm)	Thickness (Tc, in)	Forging Load (L, 1000 lbs)	Pressure / Stress (P/σ)	Stress (σ, ksi)	Strain (ε, in/in)
643	0.03	0.3990	----	----	----	----
		0.3525	29.8	1.093	28.47	0.120
		0.3015	30.1	1.105	24.33	0.280
		0.2710	32.5	1.114	23.41	0.387
		0.2263	34.0	1.130	20.18	0.567
643	3.00	0.400	----	----	----	----
		0.3567	80.75	1.118	78.43	0.115
		0.3278	78.80	1.116	70.61	0.199
		0.3072	77.80	1.141	63.98	0.264
		0.2655	77.57	1.213	53.85	0.410
		0.2272	77.57	1.318	42.36	0.566
677	0.03	0.400	----	----	----	----
		0.3642	26.0	1.133	25.4	0.094
		0.3270	25.4	1.175	21.8	0.202
		0.2971	26.6	1.233	19.9	0.298
		0.2676	27.6	1.313	17.4	0.402
		0.2498	29.9	1.349	17.7	0.471
677	3.00	0.400	----	----	----	----
		0.3510	60.2	1.062	60.6	0.131
		0.3122	60.3	1.097	52.1	0.248
		0.2795	59.8	1.128	45.7	0.358
		0.2690	59.8	1.136	43.6	0.397
		0.2252	60.8	1.210	34.8	0.575

TABLE D.2 (CONTINUED)

SUMMARY OF RING TEST DATA FOR ISOTHERMALLY FORGED Ti-10V-2Fe-3Al. MGD = 255 μm.

Temperature (C)	Forging Speed (V, ipm)	Thickness (Tc, in)	Forging Load (L,1000 lbs)	Pressure / Stress (P/σ)	Stress (σ,ksi)	Strain (ε, in/in)
704	0.03	0.3995	----	----	----	----
		0.3490	17.1	1.064	16.6	0.135
		0.3093	17.1	1.094	14.3	0.256
		0.2671	17.8	1.122	12.5	0.403
		0.2297	20.0	1.149	11.3	0.553
704	3.00	0.3995	----	----	----	----
		0.3620	50.5	1.000	53.9	0.099
		0.3007	50.5	1.097	40.9	0.284
		0.2657	51.5	1.136	35.5	0.408
		0.2256	54.0	1.203	29.9	0.571
732	0.03	0.400	----	----	----	----
		0.3600	13.2	1.139	12.8	0.105
		0.3262	13.5	1.222	11.0	0.204
		0.2939	14.2	1.268	10.3	0.308
		0.2649	15.8	1.349	9.7	0.412
		0.2387	18.8	1.457	9.7	0.516
732	3.00	0.3995	----	----	----	----
		0.3681	41.3	1.008	45.6	0.082
		0.3181	43.0	1.068	39.0	0.228
		0.2960	43.0	1.102	35.3	0.300
		0.2669	43.0	1.131	30.8	0.403
		0.2264	45.5	1.190	26.7	0.568

TABLE D.2 (CONTINUED)

SUMMARY OF RING TEST DATA FOR ISOTHERMALLY FORGED Ti-10V-2Fe-3Al. MGD = 255 μm.

Temperature (C)	Forging Speed (V, ipm)	Thickness (Tc, in)	Forging Load (L,1000 lbs)	Pressure / Stress (P/σ)	Stress (σ,ksi)	Strain (ε, in/in)
760	0.03	0.400	----	----	----	----
		0.3330	10.7	1.125	9.3	0.183
		0.3033	11.0	1.153	8.6	0.277
		0.2572	12.2	1.248	7.4	0.442
		0.2383	13.5	1.307	7.3	0.518
760	3 00	0.400	----	----	----	----
		0.3667	34.0	1.088	33.8	0.087
		0.3136	34.0	1.093	28.8	0.243
		0.2709	36.0	1.093	26.3	0.390
		0.2389	38.5	1.103	24.6	0.515
788	0.03	0.400	----	----	----	----
		0.3659	7.8	1.163	7.45	0.089
		0.3232	8.2	1.215	6.68	0.213
		0.2947	8.2	1.270	5.94	0.306
		0.2666	10.0	1.364	6.11	0.406
		0.2378	12.0	1.501	5.93	0.520
788	3.00	0.400	----	----	----	----
		0.3560	25.5	1.043	26.5	0.117
		0.3246	26.8	1.047	25.1	0.209
		0.2962	28.0	1.078	23.4	0.301
		0.2645	30.8	1.124	21.4	0.414
		0.2373	34.0	1.156	21.4	0.522

TABLE D.2 (CONTINUED)

SUMMARY OF RING TEST DATA FOR ISOTHERMALLY FORGED Ti-10V-2Fe-3Al. MGD = 255 μm.

Temperature (C)	Forging Speed (V, ipm)	Thickness (Tc, in)	Forging Load (L,1000 lbs)	Pressure / Stress (P/σ)	Stress (σ,ksi)	Strain (ε, in/in)
871	0.03	0.400	----	----	----	----
		0.3657	4.8	1.149	4.65	0.090
		0.3226	5.6	1.245	4.48	0.215
		0.2974	6.3	1.270	4.64	0.296
		0.2715	7.2	1.323	4.64	0.387
		0.2420	8.0	1.418	4.31	0.503
871	3.00	0.3995	----	----	----	----
		0.3647	14.1	1.056	14.8	0.091
		0.3133	17.5	1.053	15.9	0.243
		0.2894	19.5	1.079	16.1	0.322
		0.2673	22.0	1.094	16.5	0.402
		0.2438	24.5	1.102	16.7	0.494
954	0.03	0.400	----	----	----	----
		0.3654	3.0	1.175	2.85	0.090
		0.3172	3.8	1.230	3.02	0.232
		0.2905	4.1	1.301	2.86	0.320
		0.2688	4.5	1.384	2.75	0.398
		0.2412	5.2	1.526	2.57	0.506
954	3.00	0.400	----	----	----	----
		0.3651	10.5	1.095	10.6	0.091
		0.3215	12.5	1.125	10.9	0.219
		0.2975	13.5	1.136	10.7	0.296
		0.2751	15.0	1.151	10.8	0.374
		0.2397	17.2	1.193	10.6	0.512

TABLE D.3a

STRESS-STRAIN RATE-TEMPERATURE DATA FOR Ti-10V-2Fe-3Al FORGED ISOTHERMALLY TO 0.10 IN/IN. DATA FROM FIGURES 28 AND 29. MGD = 255 μm.

Temperature (C)	Forging Speed (V, imp)	Strain Rate ($\dot{\epsilon}$, sec^{-1})	Stress (σ, ksi)	($\ln\sigma$, $\ln\dot{\epsilon}$)	Intercept (b)	Slope (m)
643	0.03 3.00	1.401×10^{-3} 1.542×10^{-1}	29.6 79.6	(3.388,-6.57) (4.377,-1.87)	-22.666	4.751
677	0.03 3.00	1.401×10^{-3} 1.542×10^{-1}	25.0 63.2	(3.219,-6.57) (4.146,-1.87)	022.883	5.068
704	0.03 3.00	1.401×10^{-3} 1.542×10^{-1}	17.3 53.8	(2.851,-6.57) (3.985,-1.87)	-18.379	4.143
732	0.03 3.00	1.401×10^{-3} 1.542×10^{-1}	12.8 44.8	(2.549,-6.57) (3.802,-1.87)	-16.135	3.752
760	0.03 3.00	1.401×10^{-3} 1.542×10^{-1}	10.5 33.2	(2.351,-6.57) (3.503,-1.87)	-16.170	4.083
788	0.03 3.00	1.401×10^{-3} 1.542×10^{-1}	7.4 26.4	(2.001,-6.57) (3.288,-1.87)	-13.880	3.652
871	0.03 3.00	1.401×10^{-3} 1.542×10^{-1}	4.70 16.0	(1.548,-6.57) (2.773,-1.87)	-12.507	3.837
954	0.03 3.00	1.401×10^{-3} 1.542×10^{-1}	3.0 10.7	(1.099,-6.57) (2.370,-1.87)	-10.631	3.696

TABLE D.3b

STRAIN RATES FOR VARIOUS STRESS LEVELS AND TEMPERATURES FOR Ti-10V-2Fe-3Al FORGED ISOTHERMALLY TO 0.10 IN/IN. DATA FROM TABLE D.3A. MGD = 255 μm.

Temperature (C)	Reciprocal Absolute Temperature (°/K x 10^{-4})	$\ln\dot{\epsilon}$ (sec^{-1}) for stress (ksi) indicated							
		10	20	30	40	50	60	70	80
643	10.91	-11.726	-8.433	-6.506	-5.139	-4.079	-3.213	-2.481	-1.846
677	10.53	-11.214	-7.701	-5.646	-4.188	-3.057	-2.133	-1.352	-0.675
704	10.23	-8.841	-5.969	-4.290	-3.098	-2.173	-1.418	-0.780	-0.226
732	9.95	-7.496	-4.896	-3.374	-2.295	-1.458	-0.774	-0.196	0.305
760	9.68	-6.769	-3.939	-2.284	-1.109	-0.198	0.546	1.176	1.721
788	9.43	-5.470	-2.939	-1.458	-0.407	0.408	1.073	1.636	2.124
	Intercept	36.674	33.591	31.787	30.507	29.515	28.704	28.018	27.424
	Slope	-44716	-38765	-35284	-32814	-30899	-29333	-28010	-26863
	Activation Energy	88851	77026	70110	65202	61395	58285	55656	53378
871	8.74	-3.673	-1.014	0.542	1.645	2.502	3.201	3.793	4.305
954	8.15	-2.120	0.442	1.940	3.004	3.828	4.502	5.072	5.566
	Intercept	19.335	20.550	21.261	21.766	22.157	22.477	22.747	22.981
	Slope	-26325	-24673	-23707	-23021	-22489	-22055	-21687	-21369
	Activation Energy	52308	49025	47105	45743	44686	43823	43093	42460

TABLE D.4a

STRESS-STRAIN RATE-TEMPERATURE DATA FOR Ti-10V-2Fe-3Al FORGED ISOTHERMALLY TO 0.20 IN/IN. DATA FROM FIGURES 28 AND 29. MGD = 255 μm.

Temperature (C)	Forging Speed (V, imp)	Strain Rate ($\dot{\varepsilon}$, sec^{-1})	Stress (σ, ksi)	($\ln\sigma$, $\ln\dot{\varepsilon}$)	Intercept (b)	Slope (m)
643	0.03 3.00	1.549×10^{-3} 1.705×10^{-1}	26.6 70.2	(3.281,-6.47) (4.251,-1.77)	-22.360	4.843
677	0.03 3.00	1.549×10^{-3} 1.705×10^{-1}	22.1 55.6	(3.096,-6.47) (4.018,-1.77)	-22.240	5.094
704	0.03 3.00	1.549×10^{-3} 1.705×10^{-1}	15.3 46.6	(2.728,-6.47) (3.842,-1.77)	-17.982	4.220
732	0.03 3.00	1.549×10^{-3} 1.705×10^{-1}	11.3 39.4	(2.425,-6.47) (3.674,-1.77)	-15.595	3.763
760	0.03 3.00	1.549×10^{-3} 1.705×10^{-1}	9.1 30.1	(2.208,-6.47) (3.405,-1.77)	-15.146	3.929
788	0.03 3.00	1.549×10^{-3} 1.705×10^{-1}	6.7 24.6	(1.902,-6.47) (3.203,-1.77)	-13.343	3.614
871	0.03 3.00	1.549×10^{-3} 1.705×10^{-1}	4.6 16.0	(1.526,-6.47) (2.773,-1.77)	-12.224	3.770
954	0.03 3.00	1.549×10^{-3} 1.705×10^{-1}	2.9 10.7	(1.065,-6.47) (2.37,-1.77)	-10.303	3.600

TABLE D.4b

STRAIN RATES FOR VARIOUS STRESS LEVELS AND TEMPERATURES FOR Ti-10V-2Fe-3Al FORGED ISOTHERMALLY TO 0.20 IN/IN. DATA FROM TABLE D.4A. MGD = 255 μm.

Temperature (C)	Reciprocal Absolute Temperature ($1/K \times 10^{-4}$)	$\ln\dot{\varepsilon}$ (sec^{-1}) for stress (ksi) indicated							
		10	20	30	40	50	60	70	80
643	10.91	-11.208	-7851	-5.887	-4.494	-3.413	-2.530	-1.780	-1.137
671	10.53	-10.510	-6.979	-4.913	-3.448	-2.311	-1.382	-0.597	0.084
704	10.23	-8.265	-5.340	-3.628	-2.414	-1.473	-0.703	-0.053	0.511
732	9.95	-6.93	-4.322	-2.796	-1.713	-0.873	-0.187	0.393	0.895
760	9.68	-6.099	-3.376	-1.783	-0.653	0.224	0.940	1.546	2.071
788	9.43	-5.023	-2.518	-1.053	-0.013	0.793	1.452	2.009	2.491
	Intercept	36.881	32.939	30.633	28.996	27.727	26.690	25.813	25.054
	Slope	-44348	-37546	-33568	-30745	-28555	-26766	-25254	-23944
	Activation Energy	88119	74604	66700	61090	56739	53185	50179	47576
871	8.74	-3.542	-0.929	0.600	1.685	2.526	3.214	3.795	4.298
954	8.15	-2.014	0.482	1.941	2.977	3.781	4.437	4.992	5.473
	Intercept	19.101	19.965	20.47	20.829	21.107	21.334	21.526	21.693
	Slope	-25908	-23906	-22735	-21904	-21259	-20733	-20288	-19902
	Activation Energy	51479	47501	45174	43523	42243	41196	40312	39545

TABLE D.5a

STRESS-STRAIN RATE-TEMPERATURE DATA FOR Ti-10V-2Fe-3Al FORGED ISOTHERMALLY TO 0.30 IN/IN. DATA FROM FIGURES 28 AND 29. MGD = 255 μm.

Temperature (C)	Forging Speed (V, imp)	Strain Rate ($\dot{\varepsilon}$, sec^{-1})	Stress (σ, ksi)	($\ln\sigma$, $\ln\dot{\varepsilon}$)	Intercept (b)	Slope (m)
643	0.03 3.00	$1.712x10^{-3}$ $1.88x10^{-1}$	24.2 61.6	(3.186,-6.37) (4.121,-1.67)	-22.399	5.030
677	0.03 3.00	$1.712x10^{-3}$ $1.88x10^{-1}$	19.8 49.0	(2.986,-6.37) (3.892,-1.67)	-21.856	5.187
704	0.03 3.00	$1.712x10^{-3}$ $1.88x10^{-1}$	13.7 40.6	(2.617,-6.37) (3.704,-1.67)	-17.694	4.326
732	0.03 3.00	$1.712x10^{-3}$ $1.88x10^{-1}$	10.3 35.0	(2.332,-6.37) (3.55,-1.67)	-15.331	3.842
760	0.03 3.00	$1.712x10^{-3}$ $1.88x10^{-1}$	8.1 27.6	(2.092,-6.37) (3.135,-1.67)	-14.390	3.834
788	0.03 3.00	$1.712x10^{-3}$ $1.88x10^{-1}$	6.2 23.0	(1.825,-6.37) (3.135,-1.67)	-12.911	3.585
871	0.03 3.00	$1.712x10^{-3}$ $1.88x10^{-1}$	4.5 16.00	(1.504,-6.37) (2.773,-1.67)	-11.943	3.705
954	0.03 3.00	$1.712x10^{-3}$ $1.88x10^{-1}$	2.8 10.7	(1.030,-6.37) (2.370,-1.67)	-9.980	3.506

TABLE D.5b

STRAIN RATES FOR VARIOUS STRESS LEVELS AND TEMPERATURES FOR Ti-10V-2Fe-3Al FORGED ISOTHERMALLY TO 0.30 IN/IN. DATA FROM TABLE D.5A. MGD = 255 μm.

Temperature (C)	Reciprocal Absolute Temperature ($1/K \times 10^{-4}$)	$\ln\dot{\varepsilon}(sec^{-1})$ for stress (ksi) indicated							
		10	20	30	40	50	60	70	80
643	10.91	-10.816	-7.329	-5.289	-3.842	-2.720	-1.802	-1.027	-0.355
677	10.53	-9.913	-6.318	-4.215	-2.723	-1.565	-0.620	0.180	0.873
704	10.23	-7.732	-4.733	-2.979	-1.734	-.769	0.020	0.687	1.264
732	9.95	-6.484	-3.820	-2.262	-1.157	-.300	0.401	0.993	1.506
760	9.68	-5.562	-2.905	-1.350	-0.247	0.608	1.307	1.898	2.410
788	9.43	-4.656	-2.171	-0.717	0.314	1.114	1.768	2.320	2.799
	Intercept	37.069	32.023	29.070	26.976	25.351	24.021	22.901	21.929
	Slope	-44060	-36129	-31489	-28197	-25644	-23556	-21794	-20266
	Activation Energy	87548	71788	62569	56028	50955	46805	43305	40268
871	8.74	-3.411	-0.843	0.659	1.725	2.552	3.227	3.798	4.293
954	8.15	-1.907	0.523	1.944	2.953	3.735	4.374	4.915	5.383
	Intercept	18.872	19.393	19.699	19.915	20.083	20.220	20.336	20.437
	Slope	-25495	-23154	-21784	-20812	-20059	-19443	-18922	-18471
	Activation Energy	50659	46007	43285	41354	39857	38633	37598	36702

TABLE D.6a

STRESS-STRAIN RATE-TEMPERATURE DATA FOR Ti-10V-2Fe-3Al FORGED ISOTHERMALLY TO 0.40 IN/IN. DATA FROM FIGURES 28 AND 29. MGD = 255 μm.

Temperature (C)	Forging Speed (V, imp)	Strain Rate ($\dot{\varepsilon}$, sec^{-1})	Stress (σ, ksi)	($\ln\sigma$, $\ln\dot{\varepsilon}$)	Intercept (b)	Slope (m)
643	0.03 3.00	$1.892X10^{-3}$ $2.080X10^{-1}$	22.4 54.0	(3.109,-6.27) (3.989,-1.57)	-22.877	5.341
677	0.03 3.00	$1.892X10^{-3}$ $2.080X10^{-1}$	18.0 43.4	(2.890,-6.27) (3.77,-1.57)	-21.706	5.340
704	0.03 3.00	$1.892X10^{-3}$ $2.080X10^{-1}$	12.4 35.8	(2.518,-6.27) (3.578,-1.57)	-17.431	4.433
732	0.03 3.00	$1.892X10^{-3}$ $2.080X10^{-1}$	9.7 31.4	(2.272,-6.27) (3.447,-1.57)	-15.361	4.001
760	0.03 3.00	$1.892X10^{-3}$ $2.080X10^{-1}$	7.6 25.8	(2.028,-6.27) (3.250,-1.57)	-14.069	3.845
788	0.03 3.00	$1.892X10^{-3}$ $2.080X10^{-1}$	6.0 21.8	(1.792,-6.27) (3.082,-1.57)	-12.797	3.643
871	0.03 3.00	$1.892X10^{-3}$ $2.080X10^{-1}$	4.4 16.0	(1.482,-6.27) (2.773,-1.57)	-11.664	3.641
954	0.03 3.00	$1.892X10^{-3}$ $2.080X10^{-1}$	2.7 10.7	(0.993,-6.27) (2.37,-1.57)	-9.660	3.413

TABLE D.6b

STRAIN RATES FOR VARIOUS STRESS LEVELS AND TEMPERATURES FOR Ti-10V-2Fe-3Al FORGED ISOTHERMALLY TO 0.40 IN/IN. DATA FROM TABLE D.6A. MGD = 255 μm.

Temperature (C)	Reciprocal Absolute Temperature (1/K X 10^{-4})	$\ln\dot{\epsilon}(sec^{-1})$ for stress (ksi) indicated							
		10	20	30	40	50	60	70	80
643	10.91	-10.578	-6.875	-4.710	-3.173	-1.981	-1.007	-0.184	0.529
677	10.53	-9.409	-5.707	-3.542	-2.006	-0.814	0.160	0.983	1.696
704	10.23	-7.224	-4.151	-2.354	1.078	-0.089	0.719	1.402	1.994
732	9.95	-6.148	-3.375	-1.752	-0.601	0.291	1.021	1.638	2.172
760	9.68	-5.215	-2.549	-0.990	0.116	0.974	1.675	2.268	3.782
788	9.43	-4.409	-1.884	-0.407	0.641	1.454	2.118	2.680	3.166
	Intercept	36.984	30.877	27.304	24.769	22.803	21.196	19.838	18.662
	Slope	-43617	-34546	-29241	-25476	-22556	-20170	-18153	-16405
	Activation Energy	86667	68644	58101	50621	44818	40078	36069	32597
871	8.74	-3.281	-0.758	0.719	1.766	2.578	3.242	3.803	4.289
954	8.15	-1.801	0.565	1.949	2.931	3.692	4.315	4.841	5.297
	Intercept	18.646	18.834	18.944	19.023	19.083	19.133	19.175	19.211
	Slope	-25088	-22416	-20853	-19745	-18885	-18182	-17588	-17073
	Activation Energy	49849	44541	41436	39233	37524	36128	34947	33924

TABLE D.7

DATA USED FOR DETERMINATION OF PRE-EXPONENTIAL AND STRESS EXPONENT, FOR ISOTHERMALLY FORGED Ti-10V-2Fe-3Al. MGD = 255 μm.

Temperature (C)	Temperature (K)	B (cal/mole)	C (cal/mole-ksi)	Intercept (b)	Slope (m)	lnA (sec^{-1})	n
TRUE STRAIN OF 0.10 in/in							
643	916.3	125962	16204	-22.666	4.751	46.52	-4.15
677	949.7			-22.883	5.068	43.87	-3.52
704	977.4			-18.379	4.143	46.48	-4.20
732	1005.2			-16.135	3.752	46.92	-4.36
760	1033.0			-16.170	4.083	45.20	-3.81
788	1060.8			-13.880	3.652	45.88	-4.04
				AVERAGE VALUE		45.81	-4.01
871	1144.1	63268	4768	-12.507	3.837	15.32	1.74
954	1227.4			-10.631	3.696	15.31	1.74
				AVERAGE VALUE		15.32	1.74
TRUE STRAIN OF 0.20 in/in							
643	916.3	133789	19822	-22.360	4.843	51.12	-6.04
677	949.7			-22.240	5.094	48.66	-5.41
704	977.4			-17.982	4.220	50.91	-5.99
732	1005.2			-15.595	3.763	51.39	-6.16
760	1033.0			-15.146	3.929	50.04	-5.73
788	1060.8			-13.343	3.614	50.13	-5.79
				AVERAGE VALUE		60.38	-5.85
871	1144.1	64661	5726	-12.224	3.770	16.22	1.25
954	1227.4			-10.303	3.600	16.21	1.25
				AVERAGE VALUE		16.22	1.25
TRUE STRAIN OF 0.30 in/in							
643	916.3	141616	23440	-22.399	5.030	55.38	-7.84
677	949.7			-21.856	5.187	53.19	-7.23
704	977.4			-17.694	4.326	55.23	-7.74
732	1005.2			-15.331	3.842	55.57	-7.89
760	1033.0			-14.390	3.834	54.60	-7.59
788	1060.8			-12.911	3.585	54.28	-7.54
				AVERAGE VALUE		54.71	-7.64
871	1144.1	66054	6684	-11.943	3.705	17.11	0.76
954	1227.4			-9.980	3.506	17.10	0.77
				AVERAGE VALUES		17.11	0.77

TABLE D.7 (CONTINUED)

DATA USED FOR DETERMINATION OF PRE-EXPONENTIAL AND STRESS EXPONENT, FOR ISOTHERMALLY FORGED Ti-10V-2Fe-3Al. MGD = 255 μm.

Temperature (C)	Temperature (K)	B (cal/mole)	C (cal/mole-ksi)	Intercept (b)	Slope (m)	lnA (sec^{-1})	n
TRUE STRAIN OF 0.40 in/in							
643	916.3	149443	27058	-22.877	5.341	59.20	-9.52
677	949.7			-21.705	5.340	57.49	-9.00
704	977.4			-17.431	4.433	59.52	-9.50
732	1005.2			-15.361	4.001	59.46	-9.55
760	1033.0			-14.069	3.845	58.74	-9.34
788	1060.8			-12.797	3.643	58.10	-9.19
				AVERAGE VALUE		58.75	-9.35
871	1155.1	67447	7642	-11.664	3.641	18.00	+0.28
954	122 .4			-9.66	3.413	18.00	+0.28
				AVERAGE VALUE		18.00	0.28
TRUE STRAIN OF 0.50 in/in							
643	916.3	157270	30676	-24.026	5.865	62.35	-10.98
677	949.7			-22.313	5.722	61.03	-10.53
704	977.4			-17.558	4.646	63.42	-11.15
732	1005.2			-15.973	4.334	62.77	-11.02
760	1033.0			-14.002	3.913	62.62	-11.03
788	1060.8			-12.843	3.724	61.77	-10.83
				AVERAGE VALUE		62.33	-10.92
871	1144.1	68840	8600	-11.387	3.577	18.89	-0.206
954	1227.4			-9.344	3.322	18.89	-0.204
				AVERAGE VALUE		18.89	-0.205

TABLE D.8a

STRESS-STRAIN RATE-TEMPERATURE DATA FOR Ti-10V-2Fe-3Al FORGED ISOTHERMALLY TO VARIOUS STRAINS. DATA FROM FIGURES 26 AND 27. MGD = 8 μm.

Temperature (C)	Forging Speed (V,ipm)	Strain Rate ($\dot{\varepsilon}$, sec^{-1})	Stress (σ,ksi)	($\ln\sigma$, $\ln\dot{\varepsilon}$)	Intercept (b)	Slope (m)
TRUE STRAIN OF 0.10 in/in						
677	0.03	1.401×10^{-3}	23.3	(3.148,-6.57)	-22.439	5.040
	3.00	1.542×10^{-1}	59.2	(4.081,-1.87)		
732	0.03	1.401×10^{-3}	11.9	(2.477,-6.57)	-18.210	4.700
	3.00	1.542×10^{-1}	38.4	(4.648,-1.87)		
788	0.03	1.401×10^{-3}	6.4	(1.856,-6.57)	-13.585	3.779
	3.00	1.542×10^{-1}	22.2	(3.100,-1.87)		
TRUE STRAIN OF 0.20 in/in						
677	0.03	1.549×10^{-3}	19.7	(2.981,-6.47)	-20.846	4.823
	3.00	1.705×10^{-1}	52.2	(3.955,-1.77)		
732	0.03	1.549×10^{-3}	11.2	(2.416,-6.47)	-16.642	4.210
	3.00	1.705×10^{-1}	34.2	(3.532,-1.77)		
788	0.03	1.549×10^{-3}	6.4	(1.856,-6.47)	-13.872	3.988
	3.00	1.705×10^{-1}	20.8	(3.035,-1.77)		
TRUE STRAIN OF 0.30 in/in						
677	0.03	1.712×10^{-3}	17.2	(2.845,-6.37)	-19.785	4.716
	3.00	1.884×10^{-1}	46.6	(3.842,-1.67)		
732	0.03	1.712×10^{-3}	10.5	(2.351,-6.37)	-16.640	4.367
	3.00	1.884×10^{-1}	30.8	(3.428,-1.67)		
788	0.03	1.712×10^{-3}	6.4	(1.856,-6.37)	-14.165	4.199
	3.00	1.884×10^{-1}	19.6	(2.976,-1.67)		

TABLE D.8a (CONTINUED)

STRESS-STRAIN RATE-TEMPERATURE DATA FOR Ti-10V-2Fe-3Al FORGED ISOTHERMALLY TO VARIOUS STRAINS. DATA FROM FIGURES 26 AND 27. MGD = 8 μm.

Temperature (C)	Forging Speed (V,ipm)	Strain Rate ($\dot{\varepsilon}$,sec^{-1})	Stress (σ,ksi)	($\ln\sigma$, $\ln\dot{\varepsilon}$)	Intercept (b)	Slope (m)
TRUE STRAIN OF 0.40 in/in						
677	0.03	$1.892X10^{-3}$	15.4	(2.7 4,-6.27)	-19.079	4.685
	3.00	$2.082X10^{-1}$	42.0	(3.748,-1.57)		
732	0.03	$1.892X10^{-3}$	10.0	(2.303,-6.27)	-16.709	4.533
	3.00	$2.082X10^{-1}$	28.2	(3.339,-1.57)		
788	0.03	$1.892X10^{-3}$	6.4	(1.856,-6.27)	-14.367	4.362
	3.00	$2.082X10^{-1}$	18.8	(2.934,-1.57)		
TRUE STRAIN OF 0.50 in/in						
677	0.03	$2.091X10^{-3}$	14.3	(2.660,-6.17)	-18.761	4.733
	3.00	$2.301X10^{-1}$	38.6	(3.653,-1.47)		
732	0.03	$2.091X10^{-3}$	9.6	(2.262,-6.17)	-16.798	4.699
	3.00	$2.301X10^{-1}$	26.1	(3.262,-1.47)		
788	0.03	$2.091X10^{-3}$	6.4	(1.856,-6.17)	-14.518	4.497
	3.00	$3.301X10^{-1}$	18.2	(2.901,-1.47)		

TABLE D.8b

STRAIN RATES FOR VARIOUS STRESS LEVELS AND TEMPERATURES FOR Ti-10V-2Fe-3Al FORGED ISOTHERMALLY TO VARIOUS STRAINS. DATA FROM TABLE D.8A. MGD = 8 μm.

Temperature (C)	Reciprocal Absolute Temperature ($1/K \times 10^{-4}$)	$\ln\dot{\varepsilon}(sec^{-1})$ for stress (ksi) indicated							
		10	20	30	40	50	60	70	80
TRUE STRAIN OF 0.10 in/in									
677	10.53	-10.834	-7.340	-5.296	-3.846	-2.721	-1.802	-1.020	-0.352
732	9.95	-7.388	-4.130	-2.224	-0.872	0.177	1.034	1.758	2.386
788	9.43	-4.884	-2.264	-0.732	0.355	1.198	1.887	2.470	2.974
	INTERCEPT	46.328	41.605	38.835	[illegible].872	35.346	34.102	33.055	32.139
	SLOPE	-54193	-46322	-41711	-38442	-35902	-33831	-32083	-30561
	ACTIVATION ENERGY	107681	92041	82879	76383	71337	67221	63749	60726
TRUE STRAIN OF 0.20 in/in									
677	10.53	-9.740	-6.397	-4.441	-3.054	-1.978	-1.098	-0.355	0.289
732	9.95	-6.947	-4.029	-2.322	-1.110	-0.171	0.597	1.246	1.808
788	9.43	-4.690	-1.926	-0.310	0.838	1.727	2.454	3.069	3.602
	INTERCEPT	38.689	36.410	35.065	34.131	33.392	32.786	32.287	31.852
	SLOPE	-45952	-40649	-37535	-35346	-33633	-32232	-31060	-30043
	ACTIVATION ENERGY	91307	80769	74582	70233	66830	64045	61716	59695
TRUE STRAIN OF 0.30 in/in									
677	10.53	-8.927	-5.659	-3.747	-2.390	-1.338	-0.478	0.249	-0.878
732	9.95	-6.583	-3.556	-1.785	-0.528	0.446	1.242	1.916	2.499
788	9.43	-4.496	-1.585	0.118	1.326	2.263	3.028	3.676	4.236
	INTERCEPT	33.495	33.310	33.201	33.118	33.057	32.999	32.962	32.924
	SLOPE	-40284	-37021	-35111	-33750	-32698	-31830	-31108	-30478
	ACTIVATION ENERGY	80045	73562	69766	67061	64972	63247	61812	60560

TABLE D.8b (CONTINUED)

STRAIN RATES FOR VARIOUS STRESS LEVELS AND TEMPERATURES FOR Ti-10V-2Fe-3Al FORGED ISOTHERMALLY TO VARIOUS STRAINS. DATA FROM TABLE D.8A. MGD = 8 μm.

Temperature (C)	Reciprocal Absolute Temperature ($1/K \times 10^{-4}$)	$\ln\dot{\varepsilon}(sec^{-1})$ for stress (ksi) indicated: 10	20	30	40	50	60	70	80
TRUE STRAIN OF 0.040 in/in									
677	10.53	-8.293	-5.046	-3.146	-1.799	-0.753	0.101	0.823	1.449
732	9.95	-6.270	-3.128	-1.289	0.015	1.026	1.853	2.552	3.157
788	9.43	-4.323	-1.300	0.468	1.723	2.696	3.492	4.164	4.746
	INTERCEPT	29.664	30.776	31.418	31.888	32.237	32.237	32.784	32.990
	SLOPE	-36068	-34036	-32839	-32004	-31341	-30815	-30362	-29963
	ACTIVATION ENERGY	71667	67629	65250	63592	62276	61230	60329	59536
TRUE STRAIN OF 0.50 in/in									
677	10.53	-7.863	-4.582	-2.663	-1.301	-0.245	0.618	1.347	1.979
732	9.95	-5.978	-2.721	-0.816	0.536	1.585	2.442	3.166	3.794
788	9.43	-4.163	-1.046	0.778	2.071	3.075	3.895	4.588	5.188
	INTERCEPT	27.512	29.265	30.298	31.017	31.589	32.053	32.445	32.779
	SLOPE	-33615	-32144	-31293	-30674	-30208	-29823	-29500	-29213
	ACTIVATION ENERGY	66792	63871	62178	60949	60023	59558	58617	58047

TABLE D.9

DATA FOR DETERMINATION OF PRE-EXPONENTIAL AND STRESS EXPONENT FOR ISOTHERMALLY FORGED Ti-10V-2Fe-3Al. MGD = 8 μm.

Temperature (C)	Temperature (K)	B (cal/mole)	C (cal/mole-ksi)	Intercept (b)	Slope (m)	lnA (sec^{-1})	n
TRUE STRAIN OF 0.10 in/in							
677	949.7	149701	20115	-22.439	5.040	56.892	-5.619
732	1005.2			-18.210	4.700	56.740	-5.371
788	1060.8			-13.585	3.779	57.437	-5.764
				AVERAGE VALUES		57.023	-5.585
TRUE STRAIN OF 0.20 in/in							
677	949.7	129292	15619	-20.846	4.823	47.669	-3.454
732	1005.2			-16.642	4.210	48.090	-3.610
788	1060.8			-13.872	3.988	47.468	-3.422
				AVERAGE VALUES		47.742	-3.495
TRUE STRAIN OF 0.30 in/in							
677	949.7	108884	11123	-19.785	4.716	37.916	-1.178
732	1005.2			-16.640	4.367	37.875	-1.202
788	1060.8			-14.165	4.199	47.492	-1.078
				AVERAGE VALUES		37.761	-1.153
TRUE STRAIN OF 0.40 in/in							
677	949.7	88475	6627	-19.079	4.685	27.806	1.173
732	1005.2			-16.709	4.533	27.588	1.215
788	1060.8			-14.367	4.362	27.608	1.218
				AVERAGE VALUES		27.667	1.202
TRUE STRAIN OF 0.50 in/in							
677	949.7	68067	2131	-18.761	4.733	17.310	3.604
732	1005.2			-16.798	4.699	17.281	3.632
788	1060.8			-14.518	4.497	17.775	3.486
				AVERAGE VALUES		17.455	3.574

TABLE D.10

STRESS AND STRAIN DEPENDENCY OF THE APPARENT ACTIVATION ENERGY, STRESS EXPONENT AND PRE-EXPONENTIAL FOR ISOTHERMALLY FORGED Ti-10V-2Fe-3Al, MGD = 8 μm.

STRAIN (ε, IN/IN)	APPARENT ACTIVATION ENERGY (Q, CAL/MOLE)	STRESS EXPONENT n	PRE-EXPONENTIAL lnA
0.10	$Q = 159683 - 22582 \ln\sigma$	-5.585	57.023
0.20	$Q = 126317 - 15206 \ln\sigma$	-3.495	47.742
0.30	$Q = 101638 - 9374 \ln\sigma$	-1.153	37.761
0.40	$Q = 85089 - 5830 \ln\sigma$	1.202	27.667
0.50	$Q = 76358 - 4163 \ln\sigma$	3.574	17.455

$B = 170109 - 204084\varepsilon$

$C = 24611 - 44961\varepsilon$

$\ln A = 67.293 - 99.21\varepsilon$

$n = 7.99+23.015\varepsilon$

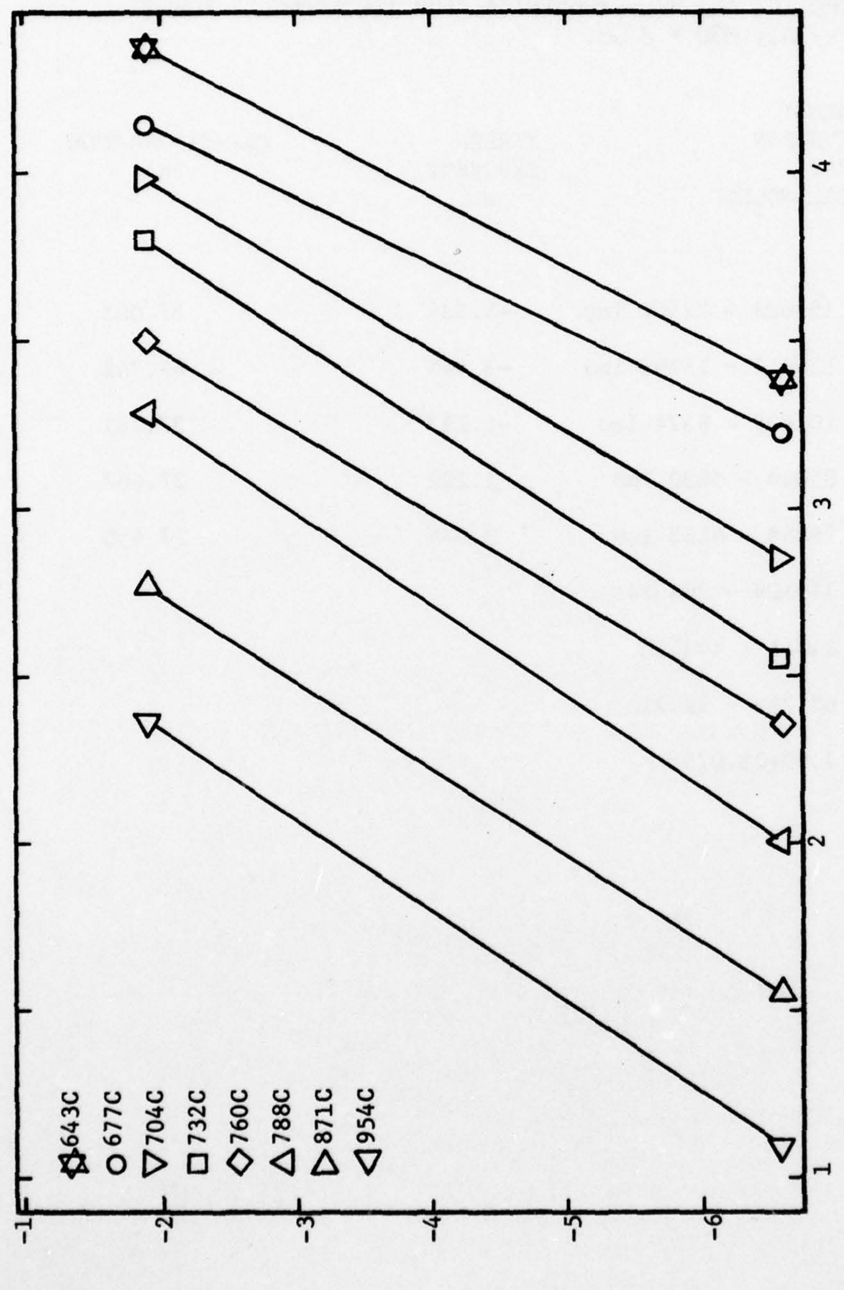

Figure D.1a. Strain Rate-Stress Relation for Ti-10V-2Fe-3Al Forged Isothermally to 0.10 In/In, MGD = 255μm

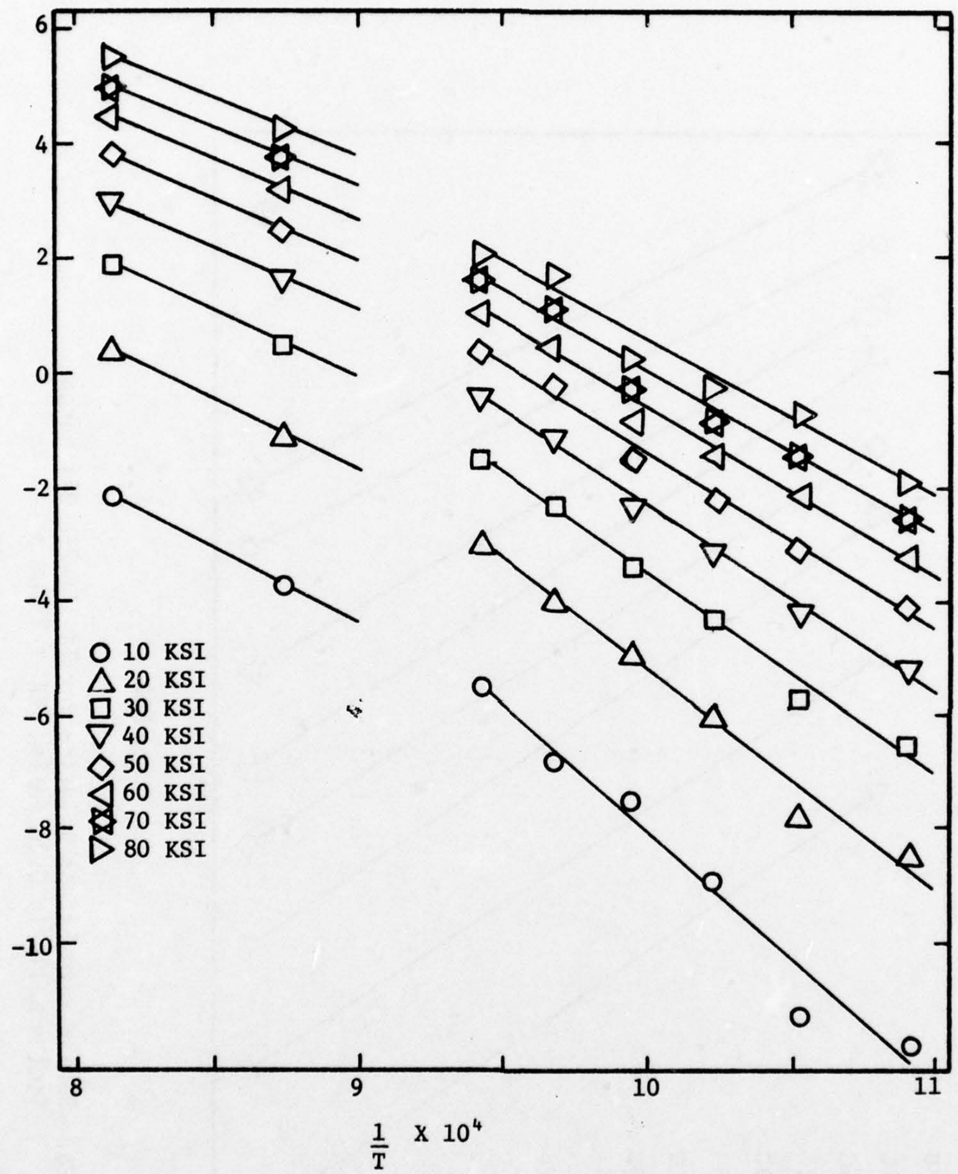

Figure D.1b. Strain Rate-Reciprocal Absolute Temperature for Ti-10V-2Fe-3Al Forged Isothermally to 0.10 In/In. Data Used to Calculate Apparent Activation Energy, MGD = 255μm

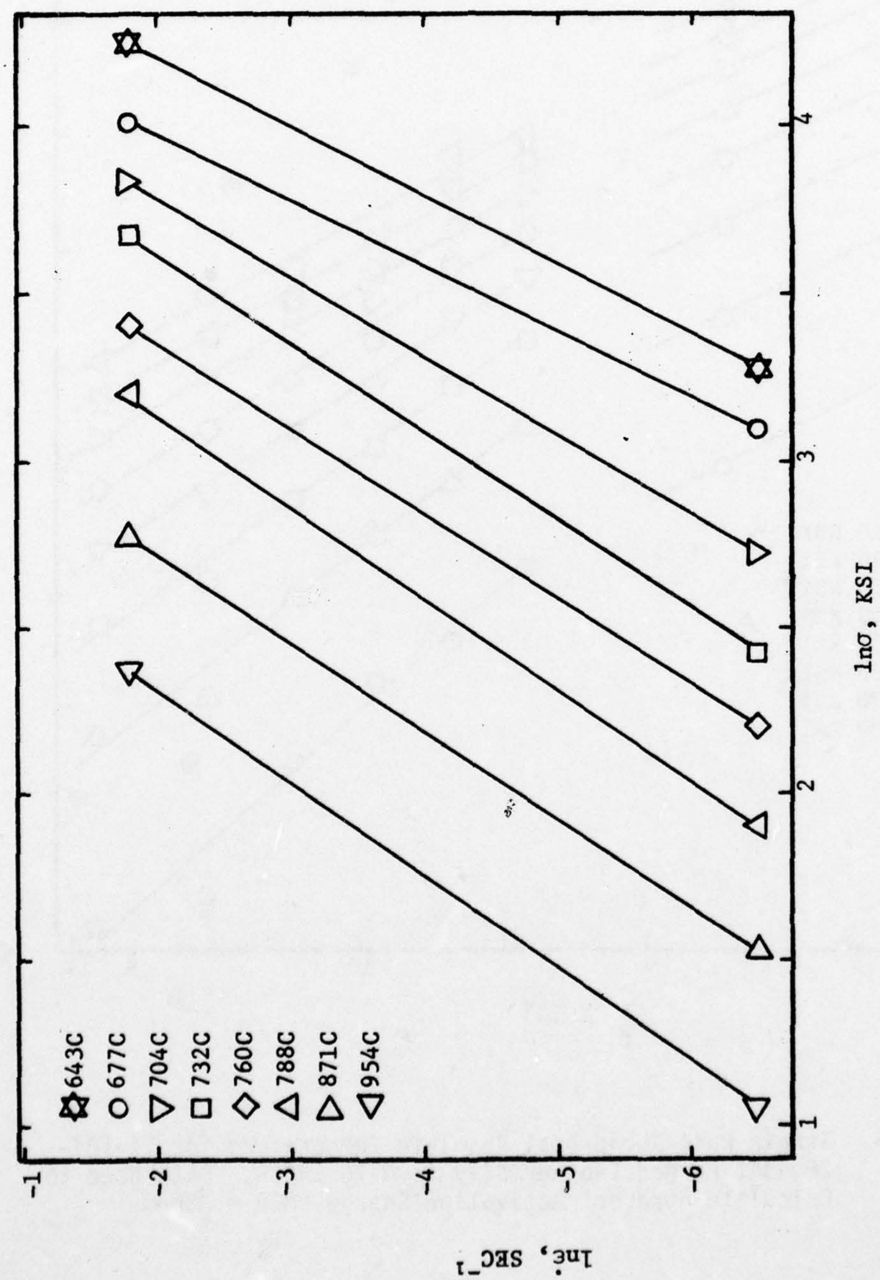

Figure D.2a. Strain Rate-Stress Relation for Ti-10V-2Fe-3Al Forged Isothermally to 0.20 In/In, MGD = 255μm

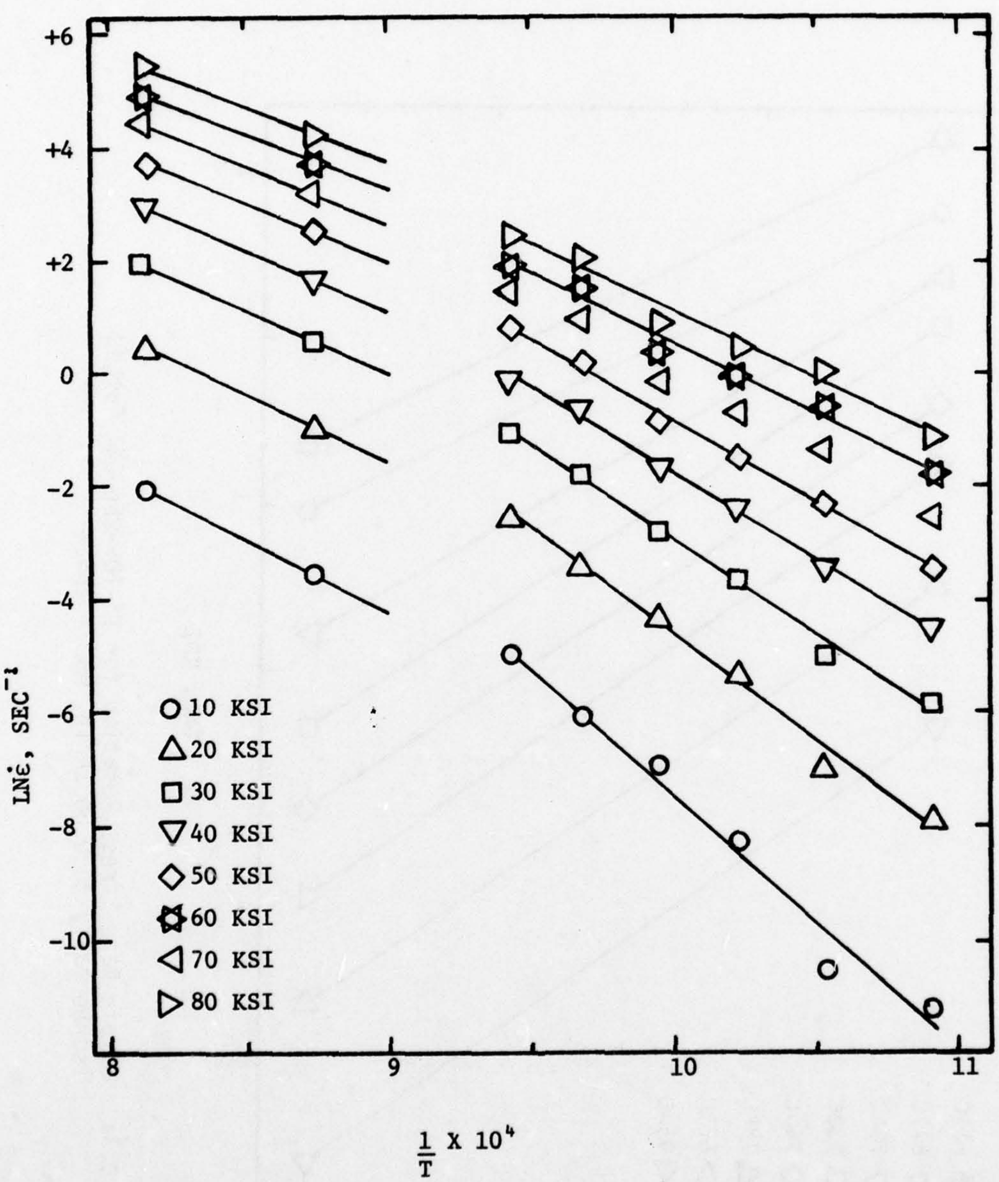

Figure D.2b. Strain Rate-Reciprocal Absolute Temperature for Ti-10V-2Fe-3Al Forged Isothermally to 0.20 In/In. Data Used to Calculate Apparent Activation Energy, MGD = 255μm

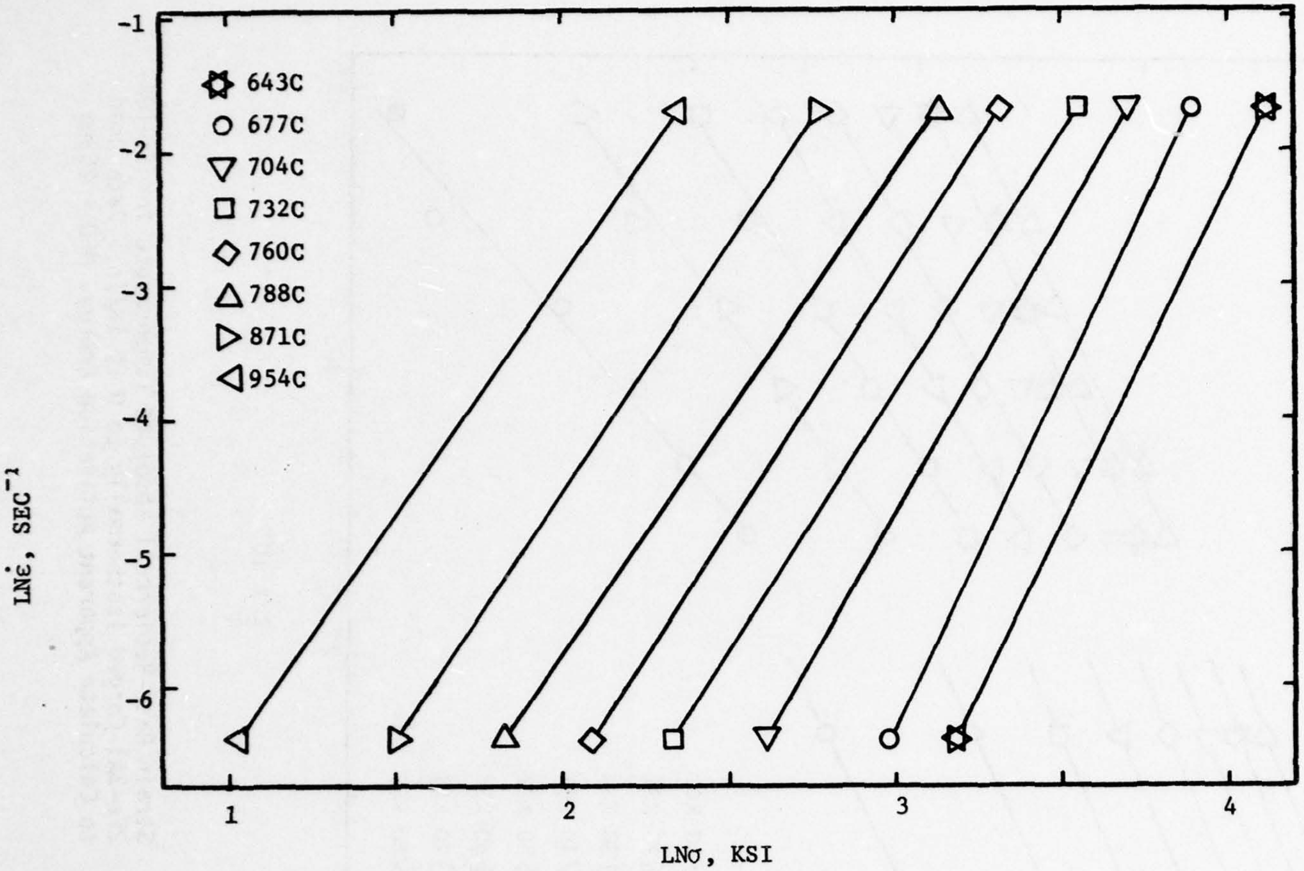

Figure D.3a. Strain Rate-Stress Relation for Ti-10V-2Fe-3Al Forged Isothermally to 0.30 In/In, MGD = 255μm

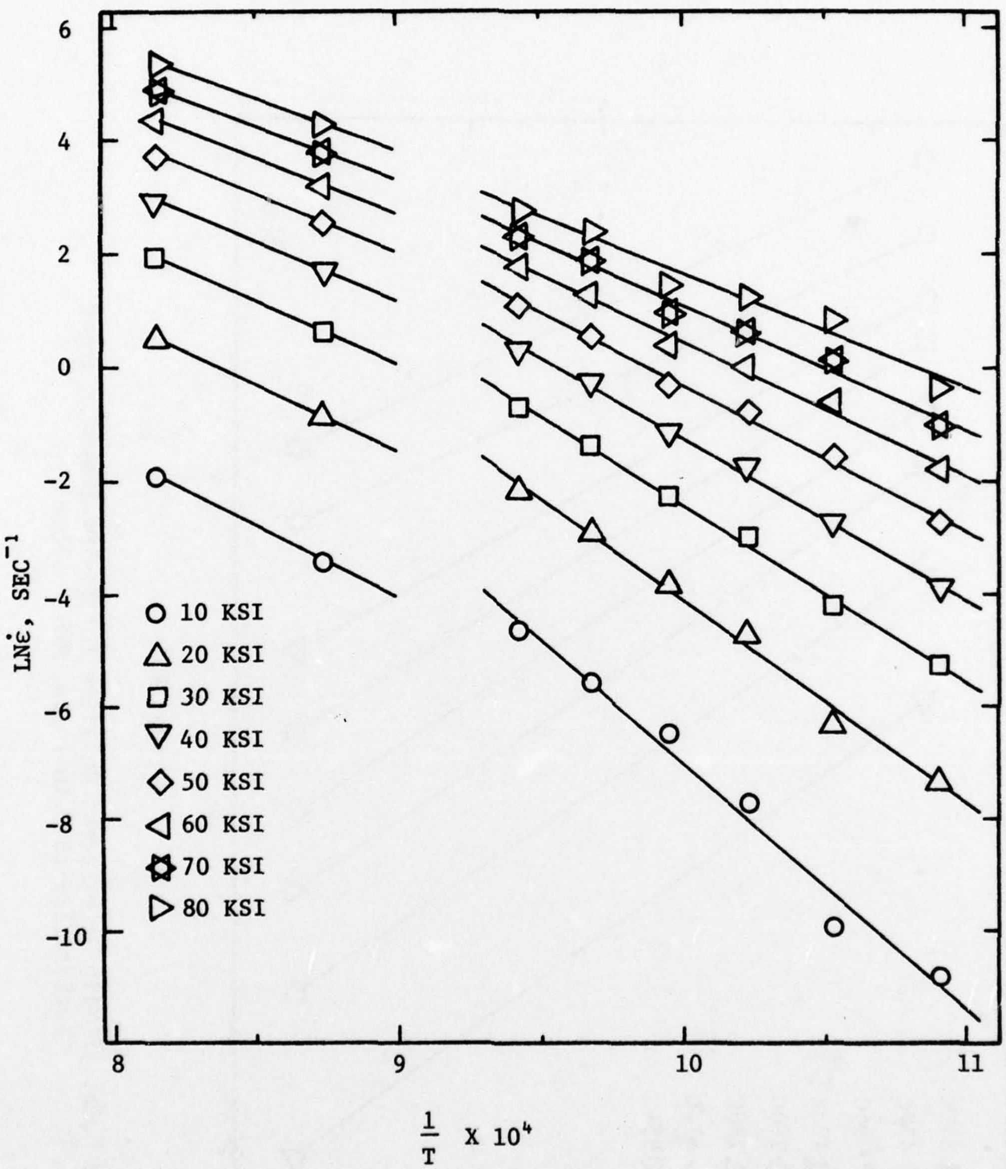

Figure D.3b. Strain Rate-Reciprocal Absolute Temperature for Ti-10V-2Fe-3Al Forged Isothermally to 0.30 In/In. Data Used to Calculate Apparent Activation Energy, MGD = 255μm

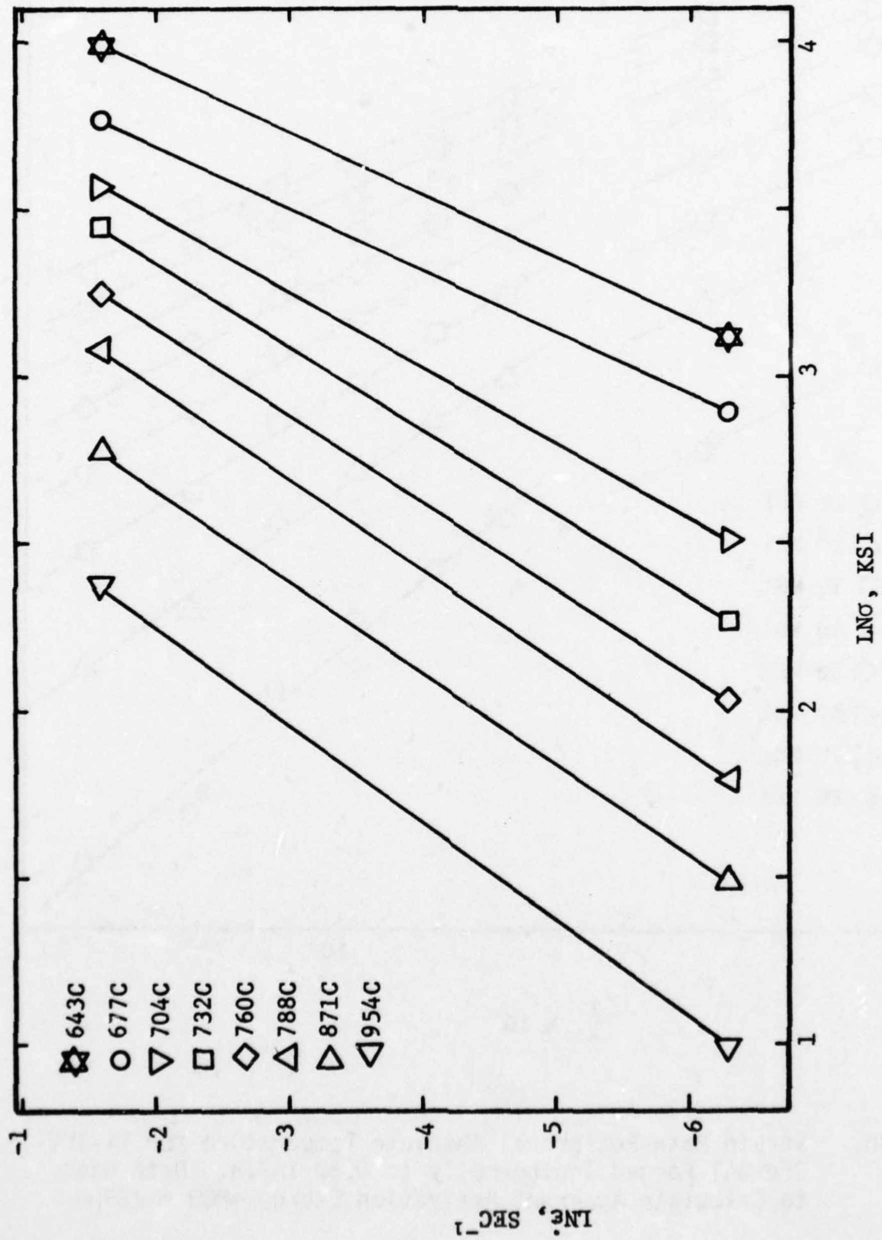

Figure D.4a. Strain Rate-Stress Relation for Ti-10V-2Fe-3Al Forged Isothermally to 0.40 In/In, MGD = 255μm

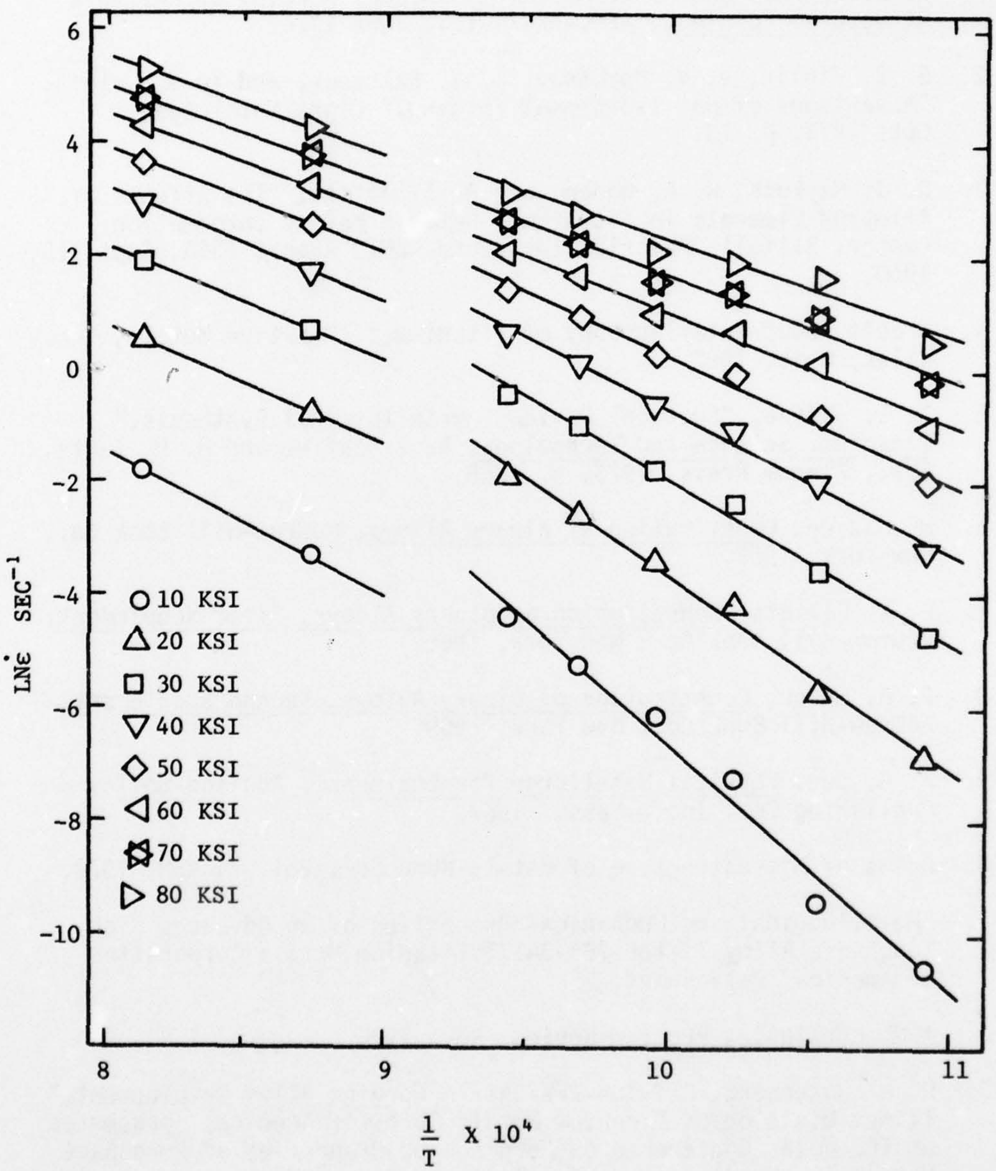

Figure D.4b. Strain Rate-Reciprocal Absolute Temperature for Ti-10V-2Fe-3Al Forged Isothermally to 0.40 In/In. Data Used to Calculate Apparent Activation Energy, MGD = 255μm

AD-A066 062 AIR FORCE MATERIALS LAB WRIGHT-PATTERSON AFB OHIO F/G 11/6
EFFECTS OF ISOTHERMAL FORGING CONDITIONS ON THE PROPERTIES AND --ETC(U)
DEC 78 I A MARTORELL

UNCLASSIFIED AFML-TR-78-114 NL

3 OF 3
AD
A066062

END
DATE
FILMED
5-79
DDC

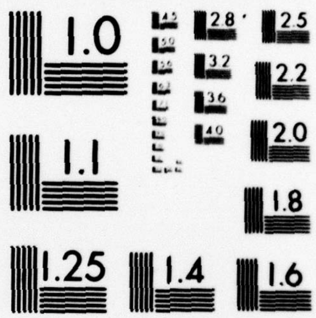
1.0
2.8
2.5
3.2
2.2
3.6
4.0
2.0
1.1
1.8
1.25
1.4
1.6

REFERENCES

1. A. J. Vazquez and A. F. Hayes, Isothermal Forging of Reliable Structural Forgings, AFML-TR-74-123, June 1974.

2. S. Z. Figlin, V. V. Boyutsov, A. V. Bakharev, and Yu G. Kalpin, "Advantages of Hot Isothermal Forging," Light Metal Age, Oct. 1973, p. 13.

3. D. J. Maykuth, H. R. Ogden, and R. I. Jaffee, "The Effects of Alloying Elements in Titanium," Defense Metals Information Center, Battelle Memorial Institute, DMIC Report 136A, Sept. 15, 1960.

4. "Facts About Metallography of Titanium," Reactive Metals, Inc., Niles, Ohio, 1967.

5. R. I. Jaffee, "Critical Review: Metallurgical Synthesis," Titanium, Science and Technology, R. I. Jaffee and H. M. Burte, Eds., Plenum Press, 1973, p. 1665.

6. M. Hansen, Constitution of Binary Alloys, McGraw-Hill Book Co., New York, 1958.

7. R. P. Elliott, Constitution of Binary Alloys, First Supplement, McGraw-Hill Book Co., New York, 1965.

8. F. A. Shunk, Constitution of Binary Alloys, Second Supplement, McGraw-Hill Book Co., New York, 1969.

9. A. G. Guy, Physical Metallurgy for Engineers, Addison-Wesley Publishing Co., Inc., Mass., 1962.

10. Atlas of Microstructure of Metals Handbook, Vol. 7, ASM, 1972.

11. "Metallurgical and Mechanical Properties of an Advanced High Toughness Alloy Ti-10V-2Fe-3Al," Titanium Metals Corporation of America, Data Sheet.

12. AFML Continuing Program Review, Nov. 1976.

13. H. W. Rosenberg, "Ti-10V-2Fe-3Al: A Forging Alloy Development," (Timet Division of Titanium Metals Corp. of America), presented at The Joint Conference on Forging and Properties of Aerospace Materials, Leeds University, England, Jan. 1977.

14. E. Bohanek, "Potential of Ti-10V-2Fe-3Al for Heavy Section Applications," Project 99-5, Technical Report 55, Titanium Metals Corp. of America, May 1972.

REFERENCES (CONTINUED)

15. J. R. Becker, F. W. Boulger, and M. L. Rhoten, Forging-Fundamentals and Practices, Vol. 2., Materials and Practices, Chapters 4, 5, 7, AFML-TR-73-55, May 1973.

16. K. M. Kulkarni, N. M. Parikh, and T. Watmough, "Isothermal Hot Die Forging of Complex Parts in a Titanium Alloy," Journal of the Institute of Metals, Vol. 100, 1972, p. 146.

17. G. H. Heitman, J. E. Coyne, and R. P., Galipeau, "Effect of Alpha + Beta and Beta Forging on the Fracture Toughness of Several High Strength Titanium Alloys," Metals Engineering Quarterly, Vol. 8, (3), Aug. 1968, p. 15.

18. T. E. Green and C. D. T. Minton, "The Effects of Beta Processing on the Properties of Titanium Alloys," The Science, Technology and Application of Titanium, R. I. Jaffee and N. E. Promisel, Eds., Pergamon Press, Oxford, 1970, p. 111.

19. J. Broichhausen and H. Van Kann, "Influence of Forging Conditions on The Fatigue Behaviour of Ti-6Al-4V," Titanium, Science and Technology, R. I. Jaffee and H. M. Burte, Eds., Plenum Press, New York, 1973, p. 1785.

20. G. J. Petrak, "Mechanical Property Evaluation of Beta Forged Ti-6Al-4V," AFML-TR-70-291, Jan. 1971.

21. J. E. Coyne, "The Beta Forging of Titanium Alloys," The Science, Technology and Application of Titanium, R. I. Jaffee and N. E. Promisel, Eds., Pergamon Press, Oxford, 1970, p. 97.

22. C. C. Chen and C. P. Gure, "Forgeability, Structures and Properties of Hot-Die Processed Ti-10V-2Fe-3Al Thin Section Forgings," Wyman-Gordon Co., Report No. RD 74-120.

23. C. C. Chen, "The Forgeability of Hot-Die Processed Ti-10V-2Fe-3Al Alloy Rib and Web Forgings," Wyman-Gordon Co., Report No. RD 75-118, Nov. 1975.

24. J. A. Hall, C. M. Pierce, D. L. Ruckle, and R. A. Sprague, Property-Microstructure Relationships in Titanium Alloy Ti-6Al-2Sn-4Zr-6Mo, AFML-TR-71-206, Nov. 1971.

25. E. Bohanek, "Deep Hardenable Titanium Alloys for Large Air-Frame Elements," Titanium, Science and Technology, R. I. Jaffee and H. M. Burte, Eds., Plenum Press, New York, 1973, p. 1993.

26. O. H. Cook and S. W. McClaren, "Beta Forging Titanium," Technical Memo No. 2-59210/8 TM-2, Feb. 9, 1968.

REFERENCES (CONTINUED)

27. D. H. Rogers, "The Effects of Microstructure and Composition on the Fracture Toughness of Titanium Alloys," Titanium Science and Technology, R. I. Jaffee and H. M. Burte, Eds., Plenum Press, New York, 1973, p. 1719.

28. M. A. Greenfield and H. Margolin, "The Interrelation of Fracture Toughness and Microstructure in a Ti-5.25Al-5.5V-0.9Fe-0.5Cu Alloy," Met. Trans., Vol. 2, March 1971, p. 841.

29. P. J. Fopiano and C. F. Hickey, Jr., "The Effects of Heat Treatment on the Mechanical Properties of the Alloy Ti-8Al-1Mo-1V," Titanium, Science and Technology, R. I. Jaffee and H. M. Burte, Eds., Plenum Press, New York, 1973, p. 2009.

30. D. Eylon, J. A. Hall, C. M. Pierce, and D. L. Ruckle, "Microstructure and Mechanical Properties Relationships in Ti-11 Alloy at Room and Elevated Temperatures," Met. Trans., Vol. 7A, Dec. 1976, p. 1817.

31. C. Hammond and J. Nutting, "The Physical Metallurgy of Superalloys and Titanium Alloys," Metal Science, Oct. 1977, p. 474.

32. F. J. Gurney and A. T. Male, "Effects of Extrusion Process Variables on the Structure and Properties of Titanium Alloys," Titanium Science and Technology, R. I. Jaffee and H. M. Burte, Eds., Plenum Press, New York, 1973, p. 1769.

33. S. J. Ashton and L. H. Chambers, "The Influence of Microstructure on the Mechanical Properties of Forged Alpha/Beta Titanium Alloys," The Science, Technology and Application of Titanium, R. I. Jaffee and N. E. Promisel, Eds., Pergamon Press, Oxford, 1970, p. 879.

34. J. C. M. Li, Dislocation Dynamics, McGraw Hill, 1968.

35. W. Kauzmann, "Flow of Solid Metals from the Standpoint of the Chemical-Rate Theory," Trans. AIME, Vol. 143, 1943, p. 57.

36. H. Conrad, "Thermally Activated Deformation of Metals," Journal of Metals, July 1954, p. 582.

37. G. B. Gibbs, "The Thermodynamics of Creep Deformation," Phys. Stat. Sol., 5, 1964, p. 693.

37a. G. B. Gibbs, "The Thermodynamics of Thermally-Activated Dislocation Glide," Phys. Stat. Sol., 10, 1965, p. 507.

38. J. B. Jones and G. A. Hawkins, Engineering Thermodynamics, John Wiley and Sons, New York, 1960.

REFERENCES (CONTINUED)

39. F. Garofalo, Fundamentals of Creep and Creep Fracture in Metals, Macmillan Co., New York, 1965.

40. J. A. Bailey and A. R. E. Singer, "Effect of Strain Rate and Temperature on the Resistance to Deformation of Aluminum, Two Aluminum Alloys and Lead,", Journal Inst. of the Metals, Vol. 92, No. 64, 1963, p. 404.

41. J. F. Alder and V. A. Phillips, "The Effect of Strain Rate and Temperature on the Resistance of Aluminum, Copper and Steel to Compression," Journal Inst. of the Metals, Vol. 83, No. 55, 1954, p. 80.

42. W. A. Wong and J. J. Jonas, "Aluminum Extrusion as a Thermally Activated Process," Trans Met. Soc. AIME, Vol. 242, No. 11, 1968, p. 2271.

43. J. E. Hockett, "On Relating the Flow Stress of Aluminum to Strain, Strain Rate, and Temperature," Trans. Met. Soc. AIME, Vol. 239, No. 7, 1967.

44. W. J. McG.Tegart, "Activation Energies for High Temperature Creep of Polycrystalline Magnesium," Acta Met., Vol. 9, No. 6, 1961, p. 614.

45. O. D. Sherby, T. A. Trozera, and J. E. Dorn, "Effect of Creep Stress History at High Temperatures on the Creep of Aluminum Alloys," Trans. ASTM, Vol. 56, 1956, p. 789.

46. E. M. Howard, W. L. Barmore, J. D. Mote, and J. E. Dorn, "On the Thermally Activated Mechanism of Prismatic Slip in the Silver-Aluminum Hexagonal Intermediate Phase," Trans. Met. Soc. AIME, Vol. 227, No. 10, 1963, p. 1061.

47. A. Lawley, J. A. Coll, and R. W. Cahn, "Influence of Crystallographic Order on Creep of Iron-Aluminum Solid Solutions," Trans. Met. Soc. AIME, Vol. 218, No. 2, 1960, p. 166.

48. O. D. Sherby, "Creep of Polycrystalline Alpha and Beta Thallium," Trans. Met. Soc. AIME, Oct. 1958, p. 708.

49. F. Garofalo, "An Empirical Relation Defining the Stress Dependency of Minimum Creep Rate in Metals," Trans. Met. Soc. AIME, Vol. 227, No. 4, 1963, p. 351.

50. J. Weertman, "Dislocation Climb Theory of Steady-State Creep," Trans. ASM, 61, 1968, p. 681.

51. F. Keith, Principles of Heat Transfer, International Textbook Co., Pa., 1965.

REFERENCES (CONTINUED)

52. J. Weertman, "High Temperature Creep Produced by Dislocation Motion," Proceedings of the John E. Dorn Symposium, Rate Processes in Plastic Deformation of Materials, ASM, 1975, p. 315.

53. C. R. Barrett and W. D. Nix, "A Model for Steady State Creep Based on the Motion of Jogged Screw Dislocations," Acta Met., Vol. 13, No. 12, 1965, p. 1247.

54. J. P. Hirth and J. Lothe, Theory of Dislocations, McGraw-Hill Book Co., New York, 1968.

55. ASTM E112-74, Standard Methods for Estimating the Average Grain Size of Metals.

56. B. Avitzur, Metal Forming: Processes and Analysis, McGraw-Hill, New York, 1968.

57. B. Avitzur, Bulge in Hollow Disk Forging, AFML-TR-69-261, Nov. 1969.

58. V. DePierre and F. J. Gurney, A Method for Determination of Constant and Varying Friction Factors During Ring Compression Test, AFML-TR-72-135.

59. J. J. Jonas and M. J. Luton, "Flow Softening at Elevated Temperatures," in Advances in Deformation Processing, J. J. Burke and V. Weiss, Eds., Syracuse University Press, Syracuse, New York, 1975.

60. ASTM E8-399-72, Standard Methods for Plain Fracture Toughness of Metallic Materials.

61. ASTM E8-69, Standard Methods of Tension Testing of Metallic Materials.

62. I. A. Martorell and F. S. Gurney, High Sensitivity - Low Capacity Cell with Overload Protection, AFML-TR-78- , June 1978.

☆U.S.Government Printing Office: 1979 — 657-002/404